Use of InSAR data for building deformation monitoring

J.P. de Jong

TUDelft

Use of InSAR data for building deformation monitoring

by

J.P. de Jong

to obtain the degree of Master of Science
at the Delft University of Technology,
to be defended publicly on Monday December 17, 2018 at 15:00 PM.

Student number:	4280695	
Project duration:	March 19, 2018 – December 17, 2018	
Thesis committee:	Dr. Ir. M. Korff	TU Delft (Chair)
	Prof. Dr. K.G. Gavin	TU Delft
	Prof. Dr. Ir. R.F. Hanssen	TU Delft
	Ir. A. Venmans	Deltares
	Ir. M. op de Kelder	Ingenieursbureau Gemeente Amsterdam

TUDelft

Preface

This thesis is the final product of the master programme Geo-Engineering at Delft University of Technology. This research has been carried out at Deltares, in collaboration with Ingenieursbureau Gemeente Amsterdam.

First of all, I would like to thank my thesis committee: Mandy Korff, Ramon Hanssen, Ken Gavin, Arjen Venmans and Martin op de Kelder, for the guidance, feedback and discussion. Especially, I would like to thank my main supervisor, Mandy Korff, for her support and the opportunity to work on this topic. For this opportunity I also would like to thank Deltares.

Next, I would like to thank SkyGeo for providing the InSAR data and Gemeente Amsterdam for providing the necessary monitoring data and background information.

Finally, I would like to thank my family for their support and encouragement.

J.P. de Jong
December 2018

Abstract

This thesis explores the use of InSAR data for building monitoring. The area of main interest is the city centre of Amsterdam, where quay wall replacements are necessary on a large scale. In Amsterdam, the foundation quality needs to be checked before construction activities nearby are performed, such as a quay wall replacement. Levelling benchmarks are usually installed to determine building deformation. In case large deformation rates are observed, additional measures are taken to ensure no building damage occurs during construction. Interferometric Synthetic Aperture Radar (InSAR) measures deformations from space and provides multiple years of deformation measurements. This can therefore reduce required monitoring time before construction.

In this thesis, the use of InSAR for building deformation monitoring is investigated by analysis of occurring deformations of three areas in the city of Amsterdam. Furthermore, deformation in the Spoorsingel area in Delft is analyzed since large deformations are observed here. In all cases, levelling benchmarks are available for comparison of deformations.

The results from the Amsterdam cases indicate similar building deformation behaviour by InSAR and levelling. For linear deformation in time, deformation rates are calculated for both monitoring techniques. For buildings along the Herengracht, Recht Boomssloot and Krom Boomssloot an average difference of 0.68 millimeter/year and 0.35 millimeter/year was found between the levelling and InSAR deformation rates. Several buildings along the Oudezijds Achterburgwal show abrupt change in deformation due to quay wall replacement activities. This is visible in the InSAR time series as a deformation shift. Due to the repetitive characteristic of the InSAR phase measurements, this shift can show up as an upward or a downward deformation. Therefore this deformation shift indicates the presence of large deformation but does not provide the amount of deformation. For buildings in this area with linear deformation, an average difference of 0.79 mm/y is calculated between the InSAR and levelling deformation rates. Differences between InSAR and levelling are suggested to be the result of the measurement location and non-uniform building movement.

A first indication of the building foundation quality is mainly derived from the deformation rate. In the city centre of Amsterdam, buildings with more than 2 mm/y deformation require additional measures or investigation. A probabilistic approach is proposed with regard to the deformation rate. The probability of exceeding the 2 mm/y threshold is calculated by combining the calculated deformation rate with the variance of this estimate. This method is not only useful for InSAR displacement time series but also for other monitoring methods such as levelling, where the amount of measurements is often limited.

The InSAR data enables the identification of building deformation mechanisms such as rotation, as is observed for the Spoorsingel in Delft. To identify this movement, rigid building behaviour is assumed. For buildings in plane-strain situation a method is devised to calculate the three dimensional deformation, using the ascending and descending track of a Synthetic Aperture Radar.

Furthermore, it was investigated whether the building deformation, as observed in the InSAR data, had caused building damage for buildings along the Spoorsingel. The large building deformations were caused by the underground parking facility construction along the Spoorsingel. A building survey of five buildings along the Spoorsingel did not provide convincing results that the damage is caused by the underground parking facility construction.

The InSAR data is of added value to determine the building deformation behaviour. For this, the location precision, the quality of the time series, the line-of-sight measurement and the variance of the deformation rate estimate should be taken into consideration. A flow chart is proposed which describes the use of InSAR for building monitoring.

Contents

1

Introduction

In the Netherlands, quay walls have been built in an urban environment for centuries and have become characteristic for many historic city centres. The first urban quay walls date back to the 13th century [40]. The city centre of Amsterdam has about 200 kilometres of quay walls [4]. A large part of these urban quay walls is more than 60 years old [4]. Over time, the functional requirements of the quay walls have changed [40]. For example, higher traffic loads are present nowadays compared to 100 years ago. The current loading conditions are often way beyond their original design loads [40]. Upgrading or replacement of the quay walls is required [4].

1.1   Problem description

In the past few years several calamities related to quay walls have occurred in the municipality of Amsterdam [14]. Large deformations of the quay wall along the Singel were observed in horizontal and vertical direction [34]. A sinkhole formed next to the Marnixkade due to a broken water pipe [37] and part of the Nassaukade collapsed after a water pipe burst [24]. This has shown the urgency for replacement of urban quay walls on a large scale. At present, the rate at which the quay wall replacement task is carried out is insufficient [3]. The current preparation and replacement procedure for quay walls is costly and time-consuming [4]. The replacement task is slowed down by monitoring of nearby buildings, as prescribed by the building protocol. The building protocol in Amsterdam [10] requires up to five years of monitoring of nearby buildings before replacing a quay wall. It should indicate the current state and damage sensitivity of the nearby buildings and is part of the proactive risk managements [10]. The historic buildings in the city centre require close attention due to their old foundations [4]. To monitor the vertical deformation, levelling benchmarks need to be installed on the walls of these buildings.

The development of Interferometric Synthetic Aperture Radar (InSAR) allows for accurate deformation measurements from space [36]. The last generation of high resolution SAR sensors, TerraSAR-X and COSMO-SkyMed, has further improved the monitoring of deformations in urban areas[36]. The use of InSAR for building monitoring in combination with conventional geodetic monitoring techniques, such as levelling, could reduce preparation time in quay wall replacement projects necessary for monitoring of the nearby buildings. InSAR allows for looking back in time. It provides a large amount of data points and could be a cost-efficient deformation measurement technique. However, the InSAR data is obtained opportunistically. The observation times are determined by the satellite orbits and the locations of the observations points are dictated by the scattering characteristics [12]. Thus InSAR does not enable the specification of monitoring locations. In particular, the opportunistic nature of the measurement technique results in the impossibility to draw generic conclusions on applicability based on singular case studies [43]. In contrast to traditional geodetic techniques, where the terms of reference can be defined beforehand, and the survey network is designed accordingly, for InSAR a 'network of opportunity' [21] is given, and it needs to be evaluated on a case-by-case basis whether the data have value for a particular application. In case the InSAR deformation mea-

surement performance is satisfactory for a particular application, it could replace levelling or provide deformation data complementary to levelling.

1.2 Research questions

The research will be focused on monitoring of buildings and the management of urban quay walls using InSAR. It aims to reduce the required monitoring time for replacement of quay walls. The main research question is therefore:

How and under what conditions can the InSAR data contribute to monitoring of buildings adjacent to quay walls?

To be able to answer this question, the following sub-questions have been formulated:

1. How are quay walls in an urban environment managed and replaced?
The main construction types and asset management of urban quay walls in general will be discussed. Also, common replacement techniques will be described shortly.

2. How can deformation measurements be obtained using the InSAR technique?
The theoretical background with respect to Synthetic Aperture Radar and interferometric methods will be discussed. The combination of measurements from different satellite viewing geometries will be discussed.

3. To which extent can the displacements observed by InSAR be explained from actual physical driving mechanisms?
Can the deformations be explained based on information of a specific site, such as construction activity.

4. To which extent does the estimated displacement time series from the SAR data depend on the applied processing methodology?
The processing of the InSAR data plays an important role in obtaining deformations. How does it affect the resulting deformation time series.

1.3 Reading Guide

Literature review
Chapters 2, 3 and 4 will provide the required background information for the research. First, the general design of quay walls will be discussed in chapter 2. This includes an explanation of common replacements techniques for quay walls and the current building protocol in Amsterdam. In chapter 3, the current techniques for measuring building deformations are described. The theory behind Interferometric Synthetic-Aperture Radar (InSAR) will be covered in chapter 4. This chapter also describes the quality and gives an overview of available research related to InSAR deformation monitoring.

Cases Amsterdam
In chapter 5, the building deformations for several quay wall projects in Amsterdam will be analysed using levelling and InSAR data. The results of the different monitoring techniques will be compared and differences will be discussed.

Case Spoorsingel Delft
The monitoring data of the Spoorsingel in Delft will be analysed in chapter 6. The Spoorsingel area is subjected to large deformations due to construction activity. Using available data from levelling, monitoring prisms and InSAR, the performance of InSAR is investigated. The deformation behaviour obtained from the monitoring data is explained based on known information of this area.

Conclusion and Recommendations
In the last chapter the main results will be described and the research questions will be answered. Based on the results, the usability of the InSAR data for building monitoring can be assessed.

<div style="text-align: right; font-size: 3em;">2</div>

Urban quay walls

2.1 Types of quay walls

The first quay walls were already constructed in the 13th century [40]. The development of urban quay walls is shown in figure 2.1. In time, the construction methods and construction materials have changed.
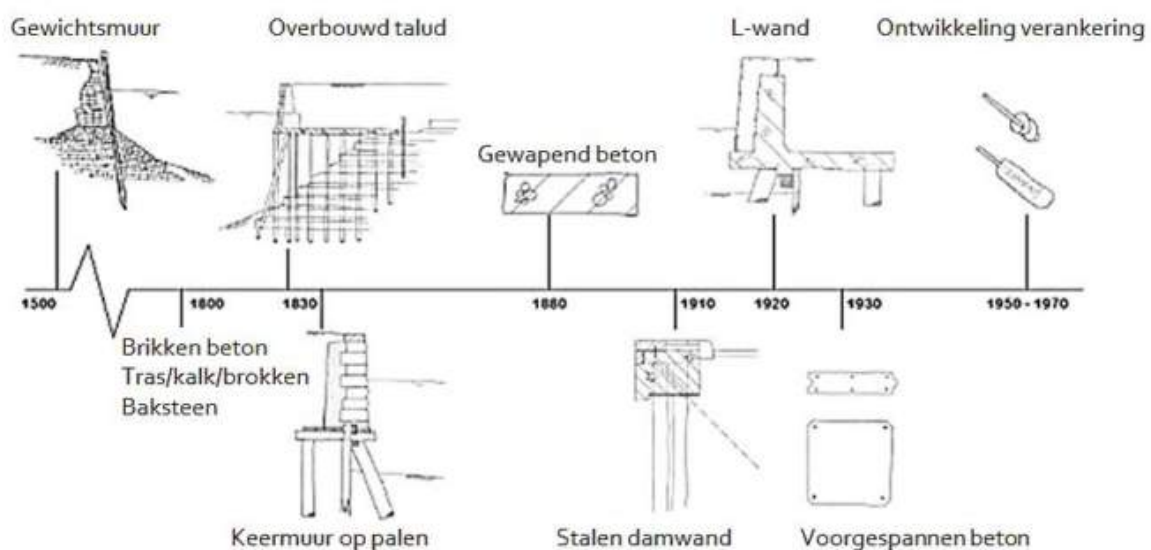
Figure 2.1: Development of quay walls [40]

Several types of urban quay walls can be distinguished based on the construction method. The basic types are [15]:

- Gravity walls
- Sheet pile walls
- Structures with relieving platform
- Open berth quays

The description of the various construction methods is based on the Handbook Quay Walls [15]. The gravity wall obtains its retaining function from the self-weight of the structure. This creates enough shearing resistance in the soil. A firm subsoil is required with enough bearing capacity for the high loads of the wall. Due to the soft subsoil, gravity wall are usually founded on piles in the Netherlands.

Usually, prefabricated elements are used for this type of quay wall. This can be an efficient method when long quays needs to be constructed.

A sheet pile wall derives its retaining function from the soil pressures and bending resistance of the sheet pile. They are installed when the subsoil has low bearing capacity and is easily penetrable. Sheet piles are often combined with anchors to decrease the displacement of the sheet pile wall.

Using structures with relieving platforms, the loads on the retaining structure are transferred to the soil by means of a horizontal connection with tension or bearing piles. Relieving platforms are mainly used for high retaining heights and small allowable displacements of the retaining structure.

For open berth quays, slopes are used to overcome the height difference. A horizontal deck founded on vertical or inclined piles is used for mooring and looks like a jetty. This method can be used when enough space is available in the waterway and relatively poor subsoil is present.

2.2 Functional requirements

To assess the quality of a quay wall, the functional requirements should be determined first. These requirements often change in time. A change in functional requirements often leads to an unfavourable load condition of the quay wall [40]. The most important requirements of an urban quay wall are described in this section.

Retaining function
The construction needs to resist the acting horizontal loads from both soil and water. The loads depend, amongst others, on the retaining height and the water level of the quay wall.

Bearing function
The quay wall is required to transfer vertical forces from traffic and storage, to the ground.

Mooring function
An urban quay wall should provide mooring possibilities for ships. Nowadays, the channels have a recreational use mainly and only small ships are moored along the quay walls [40].

Traffic function
Many roads and parking spots are located close to quays. Heavy traffic such as trucks and cranes can form a significant load for a nearby quay wall.

Storage function
Quays can be used for storage and shipment of goods.

Historical and recreational function
Quay walls can be, together with the monumental buildings in the city center, of historical value.

2.3 Management and Maintenance

Municipalities have developed their own policy concerning the management and maintenance of urban quay walls [40]. At the moment, the management of quay walls in the municipality of Amsterdam is mainly reactive; monitoring of quay walls starts when the quality of a quay wall is visibly declining or when sudden large deformations of a quay wall are observed. The municipality is moving towards a more proactive management of quay walls. Due to damages occurring to nearby assets in construction projects, a building protocol has been composed in the municipality of Amsterdam. The process of quay walls replacement is determined by this protocol.

Building protocol
The following section is based on the Bouwprotocol [10].

The building protocol was first introduced in 2007 in the municipality of Amsterdam. In the last decade the protocol has proven to reduce hindrance and claims from owners of nearby buildings of construction projects. As a result, construction projects can be insured with better terms and conditions. Furthermore, the building protocol serves a political and social purpose. It ensures a decent preparation, design and execution of a construction project.

The building protocol describes how damage to nearby objects can be reduced using a proactive risk management approach. It is based on experience with large construction projects such as the North South Line subway, the Rijksmuseum and several sewer construction works in Amsterdam.

Possible damage resulting from construction works needs to be investigated before construction starts. The constructor needs to exercise due diligence in predicting the damage. Too large risks must be mitigated by taking additional measures. The building protocol specifies how this investigation should be conducted.

The investigation into possible damages of construction works is considered to be the first phase in a construction project. After this, the construction is realized in the design phase (phase 2) and the construction phase (phase 3).

2.3.0.1   Phase 1

The first phase is summarized in the flow chart shown in figure 2.2. First, it needs to be determined whether the building protocol needs to be applied for a certain project. Application of the protocol is necessary when nearby objects are within the influence zone of the construction. As a rule of thumb, objects within 20 m of the construction are considered to be influenced by the construction activities. Extra care should be taken in case of special geotechnical circumstances such as excavations near pile foundations and shallow foundations, earth retaining structures and a decrease of the groundwater table. In addition, construction projects in historic city centres are always considered to be of influence on objects close by.

Phase 1: Investigation

Is the building protocol applicable?

Map the quality and damage sensitivity of nearby objects

Nearby buildings

Other nearby objects

Deformation measurements (3 measurements per year for at least 2 years)

Request quality, damage sensitvity and requirements with respect to deformations and vibrations at object manager

Moderate to large deformations >2 mm/year

Small deformations <2 mm/year

>3 mm/year

Foundation inspection (CFO)

2 - 3 mm/year

Negative result

Positive result

Foundation repairs

No foundation repairs

No fast agreement

Postpone construction project

Implement strict requirements in design, construction method, monitoring and building inspections

Agreement with owners

Communicate about consequences of poor foundation with owners

Perform repairs

Phase 2: Design

Figure 2.2: Flow chart of phase 1 of the building protocol [10]

For all objects within the influence zone, the quality and damage sensitivity need to be determined. For buildings, this means deformations measurements need to done for two to five years. The required monitoring time depends on the type of quay wall replacement. For combi walls two years of monitoring is required as this is considered to be a robuste replacement method. For the traditional replacement five years of monitoring is required. To monitor the deformations, levelling benchmarks need to be installed with a center-to-center distance of 6 meter with at least one benchmark for each building. The measurements need to be referenced to multiple stable reference points to achieve an accuracy of +- 0.5 millimetre.

Additionally, before construction works start, the current condition of a building is established in a building survey which includes both the interior and exterior of a building. The building surveys are often used for the claims of damage related to the construction and is thus useful for juridical purposes.

The next step in the investigation phase is based on the results of the deformation measurements. Buildings with less than 2 millimetre deformation per year are considered to be of low risk with regard to damage. Moderate deformations, i.e. 2 3 millimetre per year, require adjustments in the design, execution and monitoring of a construction project. Where large deformations are measured, i.e. more than 3 millimetre per year, a foundation inspection needs to be carried out. The inspection should provide detailed information about the current condition of the building. When the condition of the foundation is unsatisfactory according to the inspection, foundation repairs are necessary.

The repairs can sometimes lead to delay of the construction. In consultation with the insurer and depending on cooperation of the building owners, construction can nevertheless start if appropriate measures are taken.

Other nearby objects, including cables and pipes, roads and civil structures such as bridges, should be mapped as well. The quality and damage sensitivity of these objects can be of influence on the design as well.

2.3.0.2 Phase 2

In the second phase, the design is made. This includes, amongst others, a risk analysis and monitoring plan. A distinction is made between damage caused by deformations and by vibrations.

Deformations should be calculated using a numerical model, taking into account the construction method, ground water table fluctuations, excavations and loading conditions. Subsequently, strain in a building resulting from differential settlement is calculated and is related to a damage level.

The effects of vibrations on nearby objects is based on limit values described in the guidelines. The limit values depend on quality and type of construction, the vibration, the foundation type and the frequency.

The damage predictions and the results from the investigation phase are used to reach a design with acceptable damage risks. A monitoring plan is made based on the design and risks. During monitoring the development of deformations during construction are registered. Required measures can be implemented once certain deformations are reached. To this goal, the limit values of deformations must be determined beforehand.

2.3.0.3 Phase 3

In the construction phase, the contractor should follow the design as precisely as possible to keep the risks manageable. The owner of the project is responsible for monitoring during construction and often instructs an independent party to perform the monitoring. A decent communication is required between contractor and monitoring party to be able to perform the measurements on time. For example, measurements should be conducted before the next phase in the construction starts. Also, a clear line of communication must be established in case unexpected large deformations are observed.

2.4 Replacement methods

In a densely populated urban area, quay wall construction is restricted by the amount of space. About fifty percent of the quay walls in the city center of Amsterdam is estimated to be outdated. Most of these quay walls are brick gravity walls on a wooden pile foundation. The quay wall is usually founded on three wooden piles with a center-to-center distance of 1.5 to 2.0 meter, this is shown in figure 2.3. The two outer piles are often inclined although this is not shown in the figure. [4]

Not only have these quay walls reached their designed life time, the wooden foundation has also been affected by dry rot caused by bacteria. Besides, old quay walls are frequently affected by seepage of groundwater. Often no seepage screens were installed during construction. This has led to excessive flow of groundwater beneath the quay wall. [4]
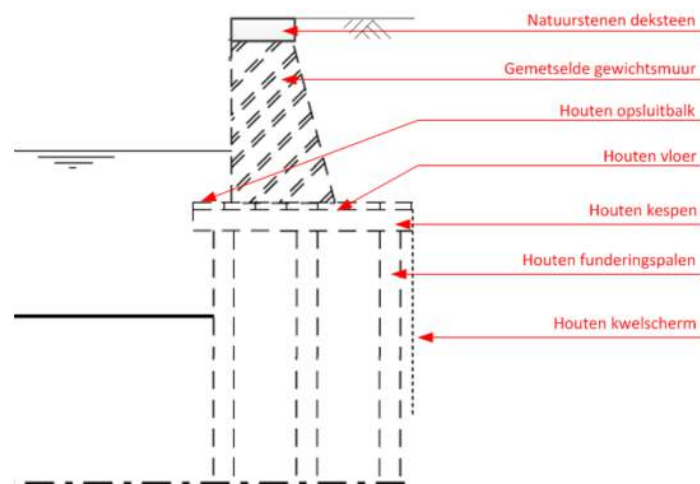
Figure 2.3: Brick gravity wall with a wooden pile foundation [4]

In recent years, some of the quays have been replaced in Amsterdam. The two main construction methods for replacement are: a concrete L-wall and a combi-wall.These construction methods are described here.

For the construction of a concrete L-wall, first two temporary sheet pile walls need to be installed for a dry building pit. One sheet pile wall is placed on the land side while the other sheet pile is placed in the canal. After removing the old quay wall concrete piles are installed by screwing or vibrating them into the soil. Subsequently, an L-shaped concrete structure is casted on top of the piles. Also a sheet pile wall is installed on the land side as seepage screen [4]. This method is the traditional way of replacement and is considered the cheapest of the two options.

The second option is a combined wall (combi-wall). The combi-wall is a combination of steel pipe piles and steel sheet piles. An advantage of this method is that no building pit is required which results in less hindrance. This method also requires less space compared to the traditional method of replacement. Due to the installation method and high stiffness of a combi-wall, this method is considered to be a robust method. The execution of this method is faster as well.

3

Deformation monitoring systems

In deformation monitoring, the determination of ground and structure movements is pursued by repeated measuring. Three types of deformation monitoring can be distinguished: a stability analysis, a kinematic analysis and a dynamic analysis. In a stability analysis, it is investigated whether the object of interest is stable. A kinematic analysis aims to determine the deformation behaviour as a function of time from which deformation velocities can be derived. In a dynamic analysis, the driving mechanisms causing the deformation are determined as well.

The monitoring data can be used for decision-making in the construction or management phase of a certain asset [33]. During construction, loads are constantly changing. To guarantee a safe construction phase and prevent undesirable events, deformations need to be monitored continuously during construction. It can also serve as a confirmation of the design [23]. Several assumptions are made in the design process. By analysing the deformations during and after construction, it can be checked if the behaviour of the structure is in accordance with the design predictions. During the use phase of a structure, monitoring systems can detect high deformations and dangerous deformation mechanisms in an early phase. This way, assets can be effectively managed by monitoring.

Next to monitoring of the constructed asset itself, e.g. a bridge or a parking garage, it is important to monitor deformations of the subsoil and structures in the surroundings during and after construction. This also serves as design check and ensures a safe situation for the surroundings. As mentioned earlier, the deformation data can indicate the causes of deformation. Also, the monitoring of deformations can be used for liability issues. For example, it forms an important source of information in case of damage claims. The deformations can be used to determine if causality exists between the observed damage in the surroundings and the construction activities.

In case of construction in a densely populated area, the monitoring also has a social purpose. For example, monitoring of buildings near a construction site allows for better communication with building owners about consequences of the construction activity and shows commitment of the construction party [33].

The next sections provide a short description of the most common deformation monitoring techniques.

3.1 Total stations

In this technique, total stations measure the positions of prisms attached to the object of interest. Each total station measures multiple prisms. It is important that the prisms are visible from the total station point of view. Generally, this intensive way of monitoring is only used during the construction stage.

The total station contains Automatic Target Recognition; It sends out an infra-red beam in the direction of the last known position of the prism [13]. The exact position of the prism is based on the

reflection characteristics. Subsequently the theodolite function is used to measure the direction, and the electronic distance measurement is used to measure the distance to the prism REF RTS. With this information the new position of the prism can be determined and the deformation in x, y and z direction can be derived. Using robotic total station, measurements can be conducted continuously for intensive monitoring. Generally, measurements are made every few hours. It can also be decided to measure the prisms manually for weekly/monthly measurements or at specific moments during the construction.

According to Cooke, measurement precision up to +-0.6 mm can be achieved in optimal conditions and +- 1.5 mm precision can be achieved in non-optimal conditions for sighting distances less than 60 m [13].

3.2 Levelling

In levelling, an optical instrument is used to manually measure the height difference between two points with levelling rods. Only the vertical heights are measured in levelling. By repeated measurements the vertical deformation with respect to the reference point can be monitored in time. Levelling benchmarks (bolts) are often installed on the walls of buildings for long-term monitoring of settlements. Figure 3.1 shows such a benchmark. In an extensive monitoring project, the manual measurements of levelling benchmarks are often used as a backup for the total stations [33]. These measurements are conducted every few weeks or months. For Leica levelling equipment a standard deviation of 0.3 mm/km can be achieved [18].

Figure 3.1: levelling benchmarks on a building of the Spoorsingel in Delft

3.3 GPS

Another method for deformation measurements is GPS monitoring. GPS receivers can be installed on a structure at specified locations where significant deformations are likely to occur. GPS receivers can measure 3-D deformations. The use of GPS allows for fast and easy automation of monitoring. The deformations measurements can be sent to central processing system. This allows for near real-time monitoring. Lepadatu and Tiberius [30] investigated the performance of the GPS technique for bridge displacements and concluded the results were satisfying for measuring centimeter scale deformations.

3.4   3D-laserscan

The distance to an object is measured using a laser and the two way travel time. The highest accuracy can be achieved using a laser scanner from the ground surface. A large amount of closely spaced measurements is collected in a short period of time. The same measurement can be repeated at a later time. By comparing the two scans, the global deformation behaviour can be determined. This technique gives millimetre accuracy measurements in x, y and z direction and provides high detail [33]. However, the repeatability of measurements is low due to the unknown measurement location.

3.5   In-situ sensors

Sensors such as strain gauges, accelerometers, tilt meters and displacement transducers can also be installed on buildings. Strain gauges can be used to determine the stress and strain in an object. Accelerometers detect structural vibrations and tiltmeters measure the deviation from the horizontal plane of a structure. Displacement transducers can measure the displacement of objects.

<div align="right">

4

</div>
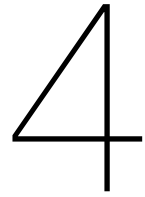
InSAR

This chapter describes the basic concepts of InSAR for deformation monitoring. The quality of deformation monitoring using InSAR is also described using precision and reliability. Finally, several applications of InSAR data are shortly discussed.

4.1 Basics of Remote Sensing

Remote sensing can be defined as the collection of information about the earths surface and atmosphere, from a distance using electromagnetic radiation [38]. Remote sensing systems can be subdivided into active and passive systems. Passive systems detect naturally occurring radiation while active systems emit radiation and analyse the backscattered signal. The radiance of energy onto the earths surface results in backscattering of the signal. The amount of energy backscattered towards the sensor depends on the chemical composition and the roughness of the scatterers[1].

When electromagnetic radiation hits an object on the surface, the radiation is scattered. The amount of scattering primarily depends on the roughness of the surface[38]. Some of the radiation will reflect back towards the remote sensing system. The sensor receives the amount of radiation towards the system. This will indicate the reflectivity of the target and, in combination with the required time, the range to the target. In case of very smooth surfaces, the reflection can be specular. The surface acts like a mirror. No energy will be send back towards the system for this type of surfaces.

The propagation of an electromagnetic waves through the atmosphere will change the characteristics. Upon hitting a particle in the atmosphere the radiation can be scattered or absorbed. Transmittance of the earths atmosphere limits the types of remote sensing which can be used for remote sensing. Therefore three main windows of the electromagnetic spectrum can be distinguished. These include the visible and near-infrared region (VNIR), the thermal infrared region (TIR) and the microwave region. [38]

4.2 Synthetic Aperture Radar

Synthetic Aperture Radar (SAR) is a radar imaging system transmitting microwaves towards the earth. A continuous strip image is generated by processing the backscattered energy of the radiated surface. SARs belong to the group of side-looking radars, transmitting energy pulses only to one side of the radar.

The geometry of a SAR system is shown in figure 4.1. The slant-range refers to the distance between the SAR antenna and the surface of the earth. The direction of the orbit is often referred to as the azimuth while the direction perpendicular to the orbit is called the range. The nadir is the line from the satellite pointing towards the earth. The off nadir angle ψ refers to the angle between the nadir and the direction of the antenna while the incidence angle θ is the angle at which the rays hit the earths surface. The incidence angle differs from the off-nadir angle due to the curvature of the earth.
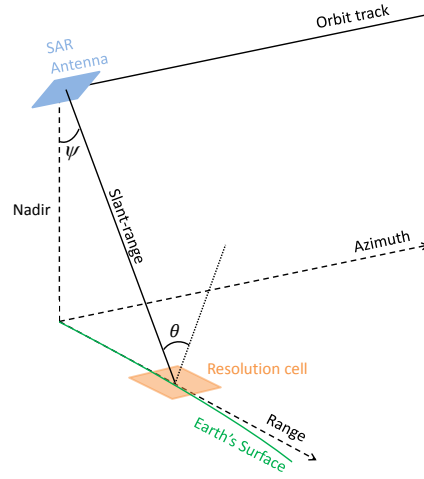
Figure 4.1: Geometry of a SAR system

The resolution of a radar system can be defined as the minimum distance to distinguish two targets [20]. The resolution in the along-track or azimuth direction r_a is related to the antenna beamwidth β_a which in turn is governed by the diffraction limit [38]

$$r_a = \beta_a R = \frac{\lambda}{L_a} R = \frac{\lambda \cdot H}{L_a \cos\theta}, \tag{4.1}$$

where R is the slant-range, λ is the wavelength, H is the height of the SAR system and θ is the incidence angle. In earlier versions of the side-looking radar the along-track resolution was limited by the physical length of the antenna L_a. A SAR system increases the length of the antenna synthetically by using the motion of the system. A time interval T after a signal is transmitted, the system has covered a distance vT. The signal received after a time interval T, can subsequently be reconstructed as a signal collected from an antenna with length vT. [38]

The azimuth resolution is further enhanced by using the Doppler bandwidth, i.e. the variation of the frequency during passage of the scatterer through the beam [21].

The slant-range resolution r_s is related to the pulse duration t_p [38], by

$$r_s = \frac{ct_p}{2}, \tag{4.2}$$

where c is the speed of light. The factor 2 in equation 4.2 accounts for the two-way travel time. Subsequently the resolution in the across-track or range direction r_r can easily be derived from trigonometry, using the incidence angle θ:

$$r_r = \frac{ct_p}{2sin\theta}, \tag{4.3}$$

A higher slant-range and range resolution is achieved by pulse compression of the signal [21].

The range and azimuth resolution determine the resolution cell size of a SAR system. The resolution cell is the area responsible for the reflection data mapped to a single pixel [21]. Therefore the reflection data of a single pixel contains all the reflections of the scatterers within the resolution cell. A pixel does not have a physical size, although this is suggested by the representation of a grid of pixels as an image [21]. A pixel contains the data representing a resolution cell. Due to oversampling during signal processing, the resolution cell size will differ from the pixel spacing [21].

4.3   Radar Interferometry

With the time observations of a signal returning to the SAR sensor, the line-of-sight distance can be calculated. The accuracy of this distance is in the order of several meters [38]. The measurement of small deformations by SAR sensors is enabled by using interferometry.

Interferometry uses two SAR images to obtain the phase differences between two observations. In principle, if the same target is acquired from the same point in space at different times, the change in phase between the two observations is directly proportional to the change in range of the target [39]. In practice, two observations are never exactly from the same point in space. The difference in geometry of the two observations should be accounted for in processing of the two images.

To obtain an interferogram, the two images need to be aligned and resampled to the same grid. Then, by multiplication of the two images, a complex interferogram is obtained which contains both the phase difference and the amplitude multiplication of the two datasets [21]. With information of the phase difference extremely high resolution can be achieved, considering that SAR systems typically use wavelengths of a few centimeters [38].

The interferometric phase ϕ^{ms} is the difference between the phase of the master and slave image and can be considered as the sum of the following terms [29]:

$$\phi^{ms} = \phi^m - \phi^s = -2\pi a + \phi_{flat} + \phi_{topo} + \phi_{def} + \phi_{atm} + \phi_{orb} + \phi_{scat} + \phi_{noise} \tag{4.4}$$

One of the contributions is the atmospheric delay ϕ_{atm} which is due to different atmospheric conditions between the two acquisitions. The atmospheric delay is variable in both time and space. The phase difference due to the error in the information of the orbits is defined as ϕ_{orb}. This can result in a trend in the interferogram [21]. One particular source of noise is the changing scattering profile from a resolution cell. The phase difference caused by this is the term ϕ_{scat}. Other sources of noise are collected in the term ϕ_{noise} [29].

The term ϕ_{flat} accounts for the difference in range due to the position of the satellite of the master and slave image. It can be calculated by:

$$\phi_{flat} = \frac{-4\pi}{\lambda} B_\parallel \tag{4.5}$$

In this equation $B_\parallel$ is the parallel baseline as shown in figure 4.2. The phase shift due to the topography is accounted for by the term ϕ_{topo} and can be calculated using:

$$\phi_{topo} = \frac{-4\pi R}{\lambda} \tag{4.6}$$

The slant range R can be rewritten using figure 4.2 to end up with:

$$\phi_{topo} = \frac{-4\pi B_\perp}{\lambda R \sin\theta} H, \tag{4.7}$$

where $B_\perp$ is the perpendicular baseline as shown in figure 4.2. From equation 4.7 it can be seen that the topographic phase shift depends on the distance between the satellite positions of the acquired images, expressed as perpendicular baseline $B_\perp$.

The contribution due to deformation of the surface ϕ_{def} is often what we are interested in. This phase shift depends on the deformation occurring between the acquisitions of the two images. Due to the right-looking geometry of SAR, the measured deformation is in the line of sight and can consist of both horizontal and vertical deformation. This phase shift is

$$\phi_{def} = \frac{-4\pi}{\lambda} d_{los}. \tag{4.8}$$

In this equation d_{los} is the line of sight deformation.
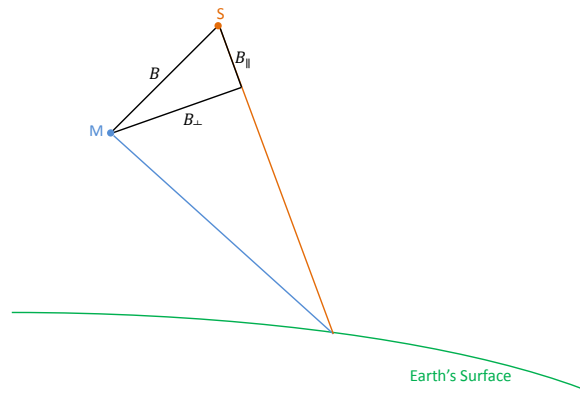
Figure 4.2: Geometry of acquisition of master and slave image

Mathematical Model

The interferometric phases are the observations and form the input to determine the deformations. The relation between the measurements and the unknown parameters of interest is described in a functional model [29]. The statistical properties of the observations are described in a stochastical model [29]. The functional and stochastical model together form the mathematical model. The mathematical model can be described using a Gauss-Markov model

$$E\{\phi\} = Ax; D\{\phi\} = Q_\phi. \tag{4.9}$$

In this equation is E the expectation operator, ϕ the phase observations, A the design matrix, x the unknown parameters, D the dispersion operator and Q_ϕ the covariance matrix of the phase observations. In the covariance matrix the contributions of noise and model imperfections are quantified [29]. Assuming the observations are uncorrelated, a diagonal covariance matrix is obtained with variance $\sigma^2_{phi,i}$ of each observation i on the diagonal. The functional model is the first part of equation 4.9 and the stochastic model is the second part.

4.4 Time Series and Phase Unwrapping

The use of InSAR is limited by temporal and geometric decorrelation and atmospheric delay [29]. Temporal decorrelation is the result of the change of the reflection properties in time and geometric decorrelation is due to the different viewing geometry of the two SAR systems. In a time series analysis, a stack of interferograms of the same area acquired over time, is used. This allows for a better identification of the phase contributors. The reliability of a time series largely depends on the phase unwrapping of the images [29]. Phase unwrapping is the process of adding the correct integer multiple of 2π to the interferometric fringes [1], as indicated by $2\pi a$ in equation 4.4. This is the result of the repetitive nature of the interferometric phase in an interferogram. Several methods for phase unwrapping are available. Usually phase unwrapping does not provide a unique solution and is based on various assumptions [1]. One of the assumptions is the deformation model, as specified in the functional model. The deformation model is used for phase unwrapping. Crucial factors influencing the correctness of the phase unwrapping are [29]:

- The amount of decorrelation
  The presence of noise negatively affects the phase unwrapping process.

- The spatio-temporal variability of the atmospheric signal delay
  Variations in the phase contribution of the atmosphere over time hinders the phase unwrapping.

- The spatio-temporal smoothness of the actual deformation signal
  Abrupt changes in time or space of the deformation can prevent a proper phase unwrapping due to the required assumptions about the deformation behaviour.

4.5   Persistent Scatterers

The reflection from a resolution cell is the contribution of all individual scatterers in that cell. If the resolution cell contains one prominent scatterer, the phase of the returned signal is largely determined by that scatterer. This means that movement of other scatterers in this pixel doesnt have a significant impact on the returned signal of this pixel. The temporal decorrelation is significantly reduced in case of persistent scatterers [29]. On the contrary, when no prominent scatterer is present, the phase of the pixel is determined by several scatterers. This is characteristic for a distributed scatterer. The two situations are depicted in figure 4.3.

The detection and deformation estimation of persistent scatterers in a time series stack is called persistent scatterer interferometry (PSI) [29]. Reliable deformation measurements can be obtained for urban areas using persistent scatterers because man-made structures often provide strong reflections [22].

In Persistent Scatterer Interferometry the quality of the data is assessed beforehand. Amplitude information is used to determine the phase stability of a pixel. A large part of the available data can be disregarded based on this information. This way only the most promising scatterers are left.[29]
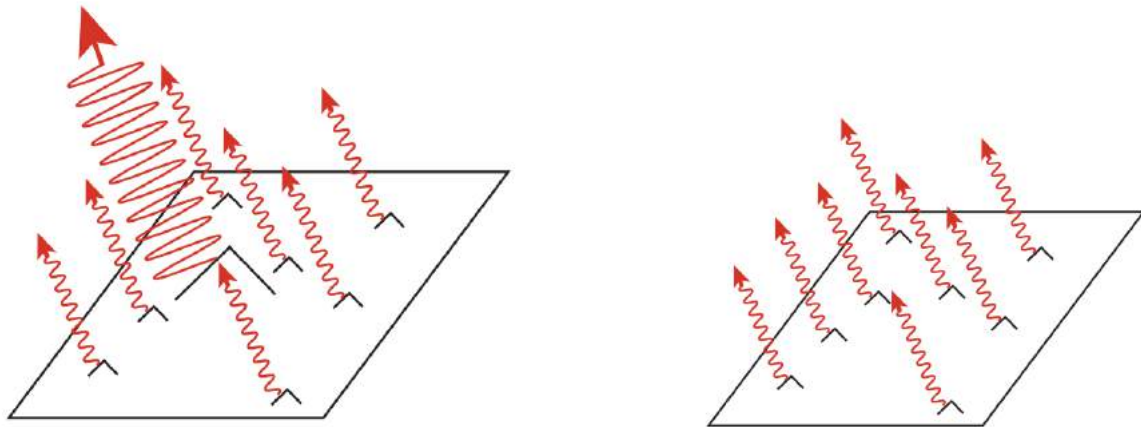
Figure 4.3: Scattering characteristics of of persistent scatterering resolution cell (left) and a distributed scattering resolution cell (right) [22]

4.6   Line-of-sight vector decomposition

As mentioned before, the right-looking geometry of the satellite results in a deformation measurement in the line-of-sight. Therefore the deformation vector d_{los} in the line-of-sight represents a three-dimensional displacement and can contain both horizontal and vertical components. The deformation vector d_{los} can be represented by three components, namely d_n, d_e and d_u, in North, East and Up direction respectively [21]. Projection of these vector components onto the line-of-sight results in [21]:

$$d_{los} = d_u cos(\theta) - \sin\theta)(d_n \cos(\alpha) - 3\pi/2) + d_e]sin(\alpha - 3\pi/2)$$
$$= d_u \cos\theta) - \sin\theta)(-d_n \sin\alpha + d_e \cos\alpha)$$

(4.10)

In this equation α represents the heading of the satellite and $\alpha - 3\pi/2$ is the angle of the azimuth with respect to the north, for a right-looking satellite. The vector decomposition is depicted in figure 4.4.
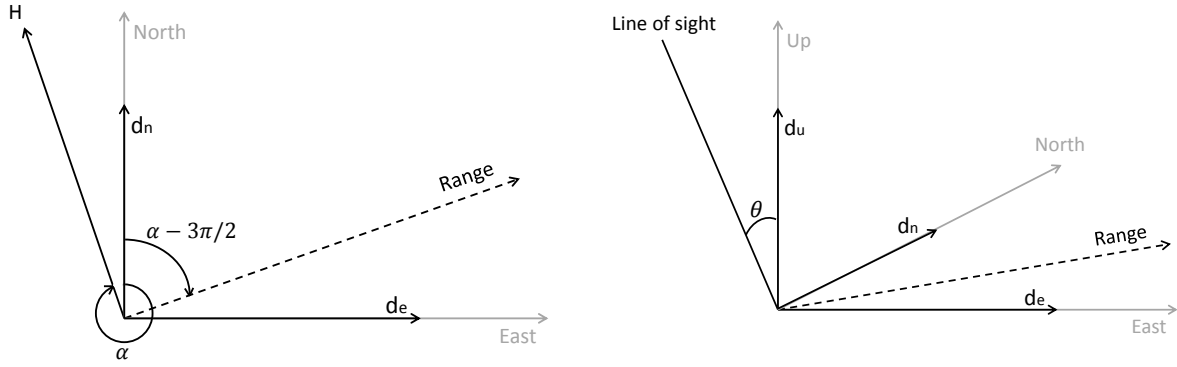
Figure 4.4: Top-view (left) and 3D view (right) of the line-of-sight vector decomposition [21]

Equation 4.10 shows the estimation of the three vector components is based on d_{los} [29]. The components can not be estimated based on a single measurement. By combining the deformation vector of an ascending and descending track, and an assumption on the direction of the deformation, the three components can be estimated. This often means an assumption for the direction of the horizontal deformation. For example, for 3D deformation estimates near a quay wall, the horizontal deformation can be assumed to be restricted to the direction perpendicular to the quay wall.

To distinguish the assumed direction of horizontal deformation, the vector components d_n and d_e need to be transformed to a local (x,y) coordinate system in the horizontal (North-East) plane [29]. This can be achieved using a rotation matrix [29]:

$$\begin{bmatrix} d_e \\ d_n \end{bmatrix} = \begin{bmatrix} sin\gamma & -cos\gamma \\ cos\gamma & sin\gamma \end{bmatrix} \begin{bmatrix} d_x \\ d_y \end{bmatrix} \tag{4.11}$$

In this equation, *x* is the direction of the assumed horizontal deformation and gamma is the angle of the assumed horizontal deformation with respect to the north. This equation simplifies due to the assumption that the deformation is zero in the y-direction:

$$\begin{bmatrix} d_e \\ d_n \end{bmatrix} = \begin{bmatrix} \sin\gamma \\ \cos\gamma \end{bmatrix} d_x \tag{4.12}$$

Substitution into equation 4.10 results in [29]:

$$d_{los} = d_u cos(\theta) - d_x sin(\theta) sin(\alpha - \gamma) \tag{4.13}$$

4.7 Precision

Ketelaar [26] defines precision as the dispersion of the deformation estimates around their expectation value. Precision is often quantified using a standard deviation.

A corner reflector experiment has been performed to validate the InSAR quality of deformations obtained from the Envisat and ERS-2 satellite [26]. Corner reflectors provide a strong and stable reflection and a well-known scattering centre. Hence corner reflectors are used to validate InSAR data. For a period of five years, between 2003 and 2007, levelling of the corner reflectors was performed within 24 hours after a satellite passed the corner reflectors [26].

To be able to compare the independent levelling and InSAR observations, the observations have been converted to double-differences using a corner reflector as common reference point. The levelling data provides a height difference between the point of interest and the reference point at a certain time. The PSI measurement is an interferometric difference between a master and slave image acquired at different times. A double-difference is a difference in both time and space and is the first

interpretable observation from InSAR data [31]. Thus, the spatial difference between a certain corner reflector and the reference corner reflector should be the same for the InSAR data and the levelling data. Furthermore, the temporal difference should be the same as well due to the (almost) identical acquisition times of the InSAR data and levelling data.

The InSAR double-differences are corrected for sub-pixel position. The sub-pixel position is the position of the persistent scatterer in the resolution cell [26]. The InSAR displacements are also converted to vertical displacements assuming the corner reflectors dont displace in a horizontal direction. The results show that double difference displacements from levelling, ERS-2 and Envisat are very comparable [26]. The double-difference displacements are shown in a plot in figure 4.5. The calculated correlation between levelling and ERS-2 and Envisat is 79% and 94% respectively. After outlier removal, which is applied when the standard deviation of the double difference is exceeded, the correlation between levelling and ERS-2 increases to 84%. The calculated double-difference displacement precision for ERS-2 and Envisat is 3.0 mm and 1.6 mm respectively.
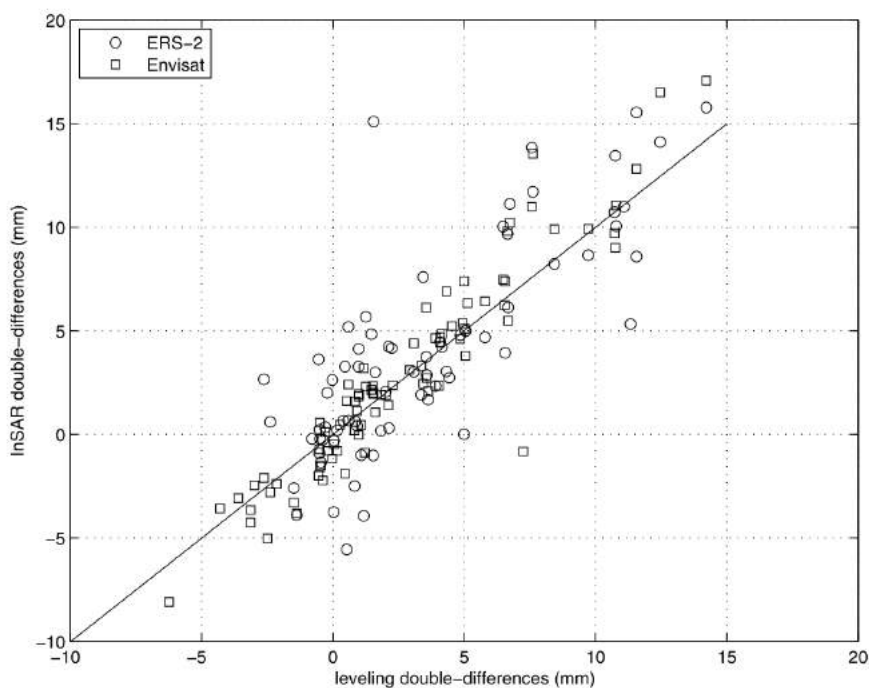
Figure 4.5: Plot of levelling and InSAR double-differences [26]. A correlation of 94% was found between levelling and Envisat and a correlation of 79% and 84% was found between levelling and ERS-2 before and after outlier removal respectively [26]

Van Leijen elaborates on the quality using a 3 mm standard deviation of a LOS measurement, based on the results of Marinkovic et al. on the same corner reflector experiment [31]. For an Envisat satellite with a 23ř look angle, a precision of 3 mm in the line of sight translates to a precision of 3.3 mm in vertical direction and a precision of 7.7 mm in horizontal direction [29]. This is visualized in figure 4.6. Deformations in the direction perpendicular to the line of sight cannot be measured.

Additionally, the horizontal precision in other directions as the direction perpendicular to the orbit track is shown in figure 4.7. Again an Envisat satellite with a 23ř look angle and a 3 mm precision in the line of sight is used. Also, an orbit heading of 193ř used [29]. As can be expected, the precision degrades towards the direction of the orbit track which is almost north-south. From these results it can be concluded that horizontal deformations can only be measured accurately in a roughly east-west direction [29].
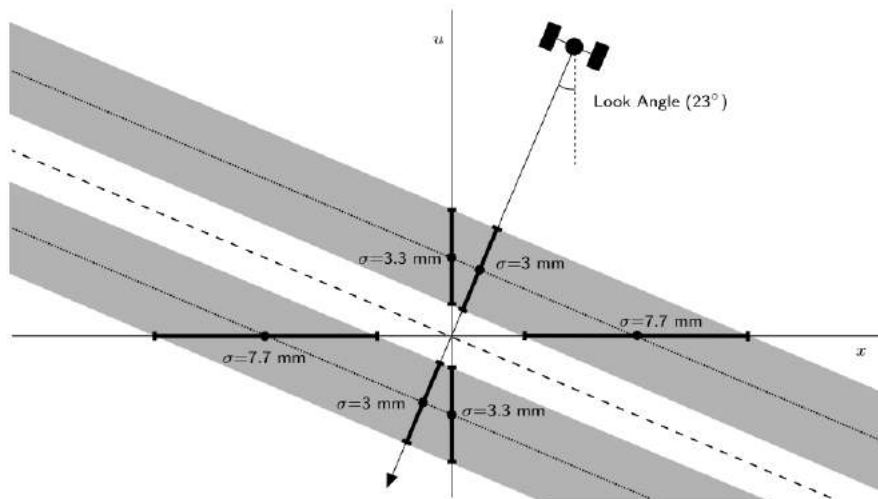
Figure 4.6: Figure indicating the deformation precision in horizontal and vertical direction based on a 3 mm precision in the line of sight [29]
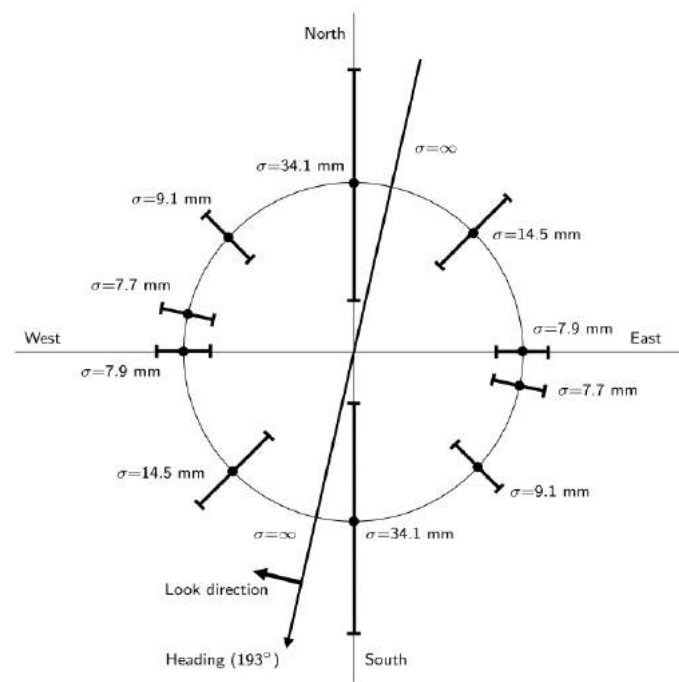
Figure 4.7: Figure indicating the horizontal deformation precision in all directions based on a 3 mm precision in the line of sight and an Envisat satellite with 193ř orbit heading [29]

Ferretti et al.[19] also performed a validation experiment to determine the precision in both horizontal and vertical direction of displacement time series estimation. Two pairs of dihedral reflectors were set up on top of a building, less than 50 m apart. Each pair has a reflector visible in the ascending track of the satellite and a reflector visible in the descending track of the satellite, as shown in figure 4.8. One pair is fixed in place and used as a reference point, the other pair can be displaced in horizontal and vertical direction with submillimeter accuracy. The mobile reflector was displaced only in the vertical direction and the east-west direction due to the low precision in north-south direction. An ascending and descending dataset of Radarsat were used to estimate the horizontal and vertical components of deformation. The applied displacements on the mobile reflector were not known to the processing

team. The results show a standard deviation of the error of 0.75 mm and 0.58 mm for vertical and horizontal deformation respectively. It should be noted that the measurements are obtained under favourable conditions. The atmospheric delay is hardly present due to the short distance between the two reflectors. Also, the artificial reflectors provide very stable and strong reflections.

Figure 4.8: Assembly of mobile reflectors [19]

Yang et al. [46] focussed on the validation of InSAR data with regard to building deformation. TerraSAR-X images obtained between May and December 2014, were used to monitor the vertical deformation of two large buildings in Tianjin in China; the Bohai Building and the China Theater. Levelling points were installed on these buildings and monitored using optical levelling. The InSAR data was converted to vertical displacements assuming no horizontal deformation occurred. The positions of the PS and the levelling points of the Bohai Building are shown in figure 4.9. For comparison, the PS displacements are interpolated to determine the PS displacement at the location of the levelling points. Inverse distance interpolation was used for this purpose. Subsequently, the difference between the two measurement techniques was calculated at every levelling point. The standard deviation of the error was found to be 1.11 mm and 1.14 mm for the Bohai Building and the China Theater respectively.

Figure 4.9: Location of PS (left) and location of levelling points (right) on the Bohai Building

4.8   Reliability

Teunissen (cited in Ketelaar [26]) defines reliability as the sensitivity for and detectability of model imperfections. Important model imperfections are sub-pixel position and orbital inaccuracies. Unmodeled deformation such as the deformation related to the position of the persistent scatterer in the resolution cell, i.e. the sub-pixel position, results in an error in the PS height [26]. The sub-pixel position is often not modelled to reduce the lack of redundancy in the functional model. Inaccuracies in the satellite orbits can lead to errors in the velocity and height estimates.

While for other deformation measurement techniques multiple observations can be used to estimate the precision and reliability, this is not the case for InSAR measurements; Only one observation is acquired at a certain time [29]. Therefore a different approach is required to determine the reliability and the precision of the InSAR measurements. As equation 4.4 shows, for each observation several unknown parameters have to be estimated to obtain the deformation. The radar phase observations have a lack of redundancy.

To evaluate the reliability, Ketelaar combines multiple ascending and descending tracks of the Groningen area in the Netherlands [25] [26] [27]. The Groningen area is subjected to subsidence as a result of gas extraction. A large area of 30 kilometers extent is affected with vertical deformations up to 7 mm/year. Due to the latitude of this area, more than 50% of the adjacent tracks are overlapping. This way redundancy is introduced. The different tracks provide independent measurements of the same area and the same deformation mechanism. The PSI measurements of the different tracks have their own coordinate system (datum) and reference. The tracks need to have a common coordinate system. One of the tracks is defined to be the master track. The datum of the other tracks, i.e. the slave tracks, is transformed to the master track datum using a polynomial. This results in a common datum which is based on the viewing geometry of the master track. Subsequently, physically identical and nearby PS of different tracks are grouped in clusters. The mutual distance between the PS is at most 500 meters. It is assumed that the displacements of nearby PS refer to the same deformation signal. Then, the PS clusters are used for decomposition into vertical and horizontal displacements. Figure 4.10 shows the standard deviation of the vertical velocities per cluster of the whole area. It was found that about 70% of the velocities in a PS cluster had a standard deviation lower than 1 mm/year. Figure 4.11 shows the displacements of a single cluster in time; Observations of four tracks show similar displacements. This shows that the results of the independent tracks are consistent. The obtained displacements or velocities of PS in the same cluster should only differ because of a different reference PS. However, the observations of the different tracks are acquired at different times, distributed over 35 days.
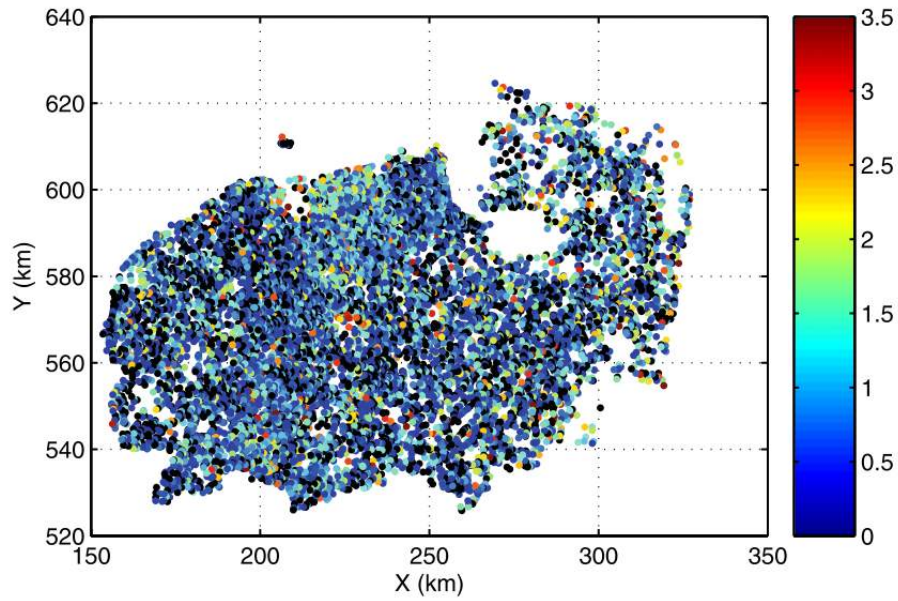
Figure 4.10: Standard deviation of vertical PS velocity of each cluster in mm/year [26]
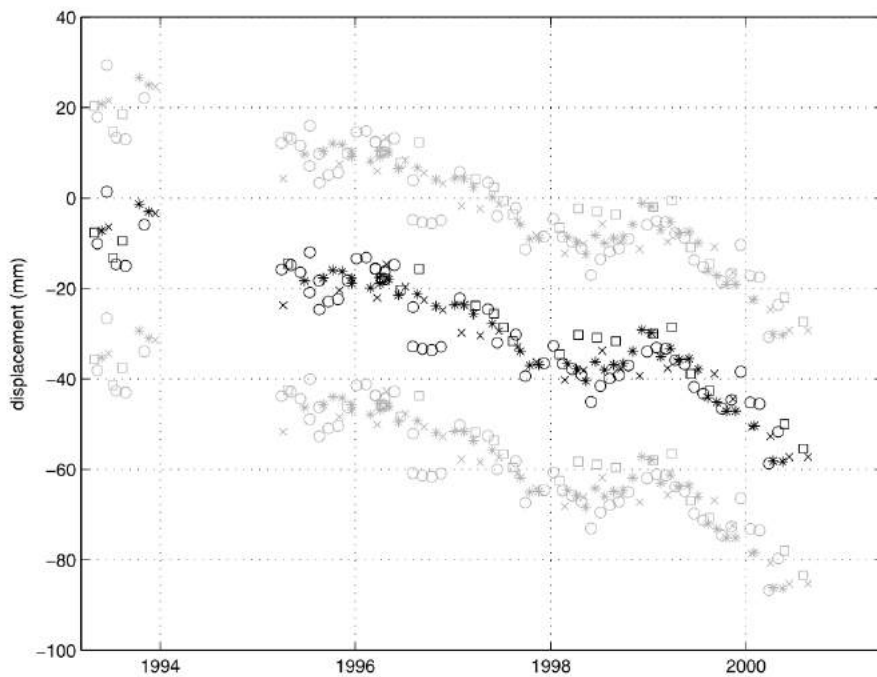
Figure 4.11: Displacements in time of a cluster containing four different tracks, after transformation to a common datum. Ambiguity in displacements are shown in grey [26]

5

Cases Amsterdam

Following the building protocol as described in section 2.3, the building deformation behaviour of several areas in Amsterdam has been measured in recent years. It allows or has allowed for the replacement of the nearby quay walls. For this, levelling benchmarks have been used. This is considered to be a reliable method for measuring the deformations on millimeter scale. In this chapter, the deformation based on installed levelling benchmarks and available InSAR data of several areas is analysed. Three areas are selected where levelling benchmarks have been installed and which provide monitoring data over a significant period of time. The three selected areas in Amsterdam are: Herengracht 1-103, Oudezijds Achterburgwal 41-149 and Recht Boomssloot 81-101 together with Krom Boomssloot 1-69. The buildings deformations in these areas will be discussed in section 5.1, 5.3 and 5.2 respectively.

5.1 Herengracht

The quay wall on the even numbered side of the Herengracht between the Blauwburgwal and the Brouwersgracht needs to be replaced, due to the bad condition of the quay wall [7]. As preparation, the buildings near this quay wall have been monitored in advance using levelling benchmarks.

5.1.1 Methodology

This section describes the available deformation measurements input and the methodology to process this data. First, the available levelling and InSAR data is described in section 5.1.1.1 and 5.1.1.2. The main interest in this research is the movement of buildings. Therefore the deformation data is analyzed per building. The selection of deformation data of each building is described in section 5.1.1.4. Lastly, a deformation model is fitted to the deformation measurements in section 5.1.1.3.

5.1.1.1 Levelling data

Between Herengracht 1 and Herengracht 103, 38 buildings have been equipped with levelling benchmarks. In total 90 levelling benchmarks have been installed. The deformations of the levelling benchmarks have been measured five times. The measurement dates are 15-9-2016, 20-01-2017, 12-05-2017, 12-09-2017, 22-11-2017.

5.1.1.2 InSAR data

The InSAR data contains TerraSAR-X measurements covering Amsterdam. The TerraSAR-X satellite has a repeat time of 11 days. Three datasets are available. One dataset of the ascending track provides observations between February 2009 and January 2018 of Amsterdam. It thus provides almost nine years of observations. Additionally, two shorter datasets are provided: a dataset of the ascending track with observations between January 2016 and January 2018 and a dataset of the descending track with observations between March 2016 and December 2017. The specifications of the datasets are shown

in table 5.1. For all datasets, the line of sight deformations are converted to vertical deformations using the incidence angle and assuming no horizontal deformations.

Each dataset consists of four subsets: PS high points, PS low points, DS high points and DS low points. PS and DS stand for persistant scatterer and distributed scatterer respectively, and indicate the type of scatterers that are used. The difference between persistant and distributed scatterers is already discussed in section 4.5. The distinction between high and low points is made using a digital terrain model (DTM). All measurement points elevated more than 2 meter above the earths surface are called high points, and all points located within 2 meter of the earths surface level are low points. Because the research is focused on the monitoring of buildings, only the PS high points subset is used.

Table 5.1: Specifications of the available InSAR datasets

Name	Acquisition period	Number of observations	Heading angle	Incidence angle
asc_9y	05-02-2009 05-01-2018	219	349°	31.1°
asc_2y	19-09-2016 03-12-2017	57	349°	31.1°
dsc_2y	18-03-2016 27-12-2017	54	191°	35.4°

The levelling data of the Herengracht contains measurements between September 2016 and December 2017. Thus all three available InSAR datasets can be used, as these datasets all cover this time span. For the analysis, only the asc_2y and asc_9y InSAR datasets are used. For the asc_2y dataset, it is decided to use same time span as the levelling data , that is, between September 2016 and December 2017. For the asc_9y dataset all available observations are used, between February 2009 and January 2018.

5.1.1.3 Deformation model fit

To obtain a deformation rate from the deformation measurements, it is assumed that the deformation in time is linear for both the levelling and the InSAR data. The overall deformation pattern is expected to be similar for levelling and InSAR data. A linear deformation model is fitted to the data using least-squares. For this end, the functional model can be written as:

$$\underbrace{\begin{bmatrix} h_0 \\ h_1 \\ h_2 \\ . \\ . \\ h_m \end{bmatrix}}_{y} = \underbrace{\begin{bmatrix} 1 & 0 \\ 1 & t_1 - t_0 \\ 1 & t_2 - t_0 \\ 1 & . \\ 1 & . \\ 1 & t_m - t_0 \end{bmatrix}}_{A} \underbrace{\begin{bmatrix} b \\ r \end{bmatrix}}_{x}, \tag{5.1}$$

where y is the vector of observations, A is the design matrix, x is the vector of unknown parameters, m is the number of observations, $h_0, h_1, h_2, ..., h_m$ are the height observations at time $t_0, t_1, t_2, ..., t_m$, b is interception of the linear line with the y-axis and r is the slope of the line. The least-squares solution of x is then obtained using:

$$\hat{x} = (A^T Q_{y,a-priori}^{-1} A)^{-1} A^T Q_{y,a-priori}^{-1} y, \tag{5.2}$$

where $\hat{x}$ is the estimator of the unknowns, A is the design matrix, $Q_{y,a-priori}$ is the predefined covariance matrix and y are the observations.
The a-priori covariance matrix $Q_{y,a-priori}$ can be estimated using:

$$Q_{y,a-priori} = \sigma_{y,a-priori}^2 I_m, \tag{5.3}$$

where $\sigma^2_{y,a-priori}$ is the predefined measurement variance and I_m is an identity matrix with dimension m.

Using the estimator of the unknowns $\hat{x}$, the estimator of the observations $\hat{y}$ and the corresponding residuals $\hat{e}$ can be calculated by

$$\hat{y} = A\hat{x}, \tag{5.4}$$

$$\hat{e} = y - \hat{y}. \tag{5.5}$$

To determine if the linear deformation model is significant, an overall model test is used. In the overall model test, the linear deformation model forms the null hypothesis. To decide whether the null hypothesis needs to be rejected, the test statistic T is calculated with:

$$T = \hat{e}^T Q^{-1}_{y,a-priori} \hat{e}. \tag{5.6}$$

The test statistic T contains both the residuals and the measurement precision. The test statistic T follows a chi-squared distribution with q degrees of freedom [29]:

$$T \sim \chi^2(q,0) \tag{5.7}$$

with

$$q = m - n, \tag{5.8}$$

where q the degrees of freedom, n is the number of unknowns and m is the number of observations. Once the distribution of the test statistic T is known, we can determine a critical value K based on a level of significance α. This is indicated in figure 5.1. Choosing a low value for α ensures that it is unlikely that the test statistic T will be larger than the critical value. Therefore the criterion to reject the null hypothesis of linear deformation in time is:

if $T > K$, then reject H_0 ,

In other words, when $T < K$, the deformation model explains a significant portion of the variation in deformation and the null hypothesis does not need to be rejected. In case $T > K$, the deformation model is rejected and an error is suspected. This means an error is present in the observations or the wrong deformation model is used. When the deformation model is rejected, the deformation time series is disregarded in this analysis.
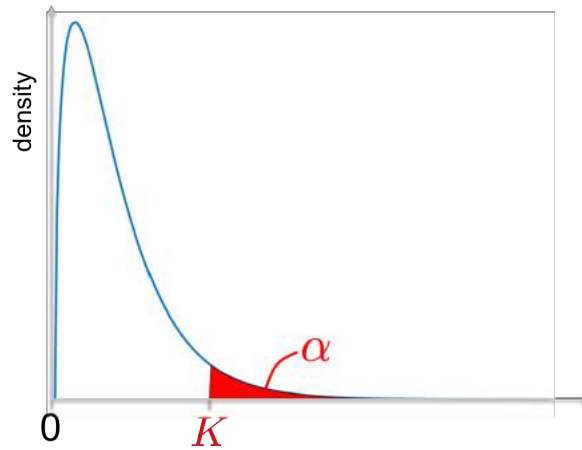
Figure 5.1: A χ^2-distribution with a critical value K corresponding to a level of significance α [42]

Once the overall model test is performed and only the deformation time series with a correct deformation model are left, the posterior measurement variance $\sigma_{y,a-posteriori}$ can be calculated with:

$$\sigma^2_{y,a-posteriori} = \frac{\hat{e}^T Q^{-1}_{y,a-priori} \hat{e}}{m - n} \sigma^2_{y,a-priori}. \tag{5.9}$$

where $\sigma_{y,a-priori}$ is the predefined measurement variance. The precision of the parameters $Q_{\hat{x}}$ can be calculated with:

$$Q_{\hat{x}} = (A^T Q_{y,a-posteriori}^{-1} A)^{-1}$$
$$= \begin{bmatrix} \sigma_b^2 & 0 \\ 0 & \sigma_r^2 \end{bmatrix} \tag{5.10}$$

with

$$Q_{y,a-posteriori} = \sigma_{y,a-posteriori}^2 I_m, \tag{5.11}$$

where $Q_{y,a-posteriori}$ is the covariance matrix of the observations after determining the measurement variance $\sigma_{y,a-posteriori}$, σ_b^2 is the variance of the intersection of the line with the y-axis, σ_r^2 is the variance of the slope of the line and m is the number of observations. This way, a unique measurement variance $\sigma_{y,a-posteriori}$ and covariance matrix of the parameters $Q_{\hat{x}}$ is obtained for each deformation time series.

Using the abovementioned methodology a linear model can be fitted to the deformations, the correctness of the deformation model can be assessed and the deformation rate and corresponding variance of the deformation rate estimate can be calculated. The slope of the linear model represents the average deformation rate of the measured object in millimeter/year.

5.1.1.4 Selection of building deformation data

To analyze the deformation behaviour of the observed buildings, buildings with levelling benchmarks installed, are also inspected for available InSAR data. As the location precision of the InSAR points is given to be 1-2 meters [41], all points located within 2 meters of the buildings are selected. Because only high points are selected, it is likely that these points originate from the buildings as well. This is depicted in figure 5.2. Points located outside any building but within 2 meter distance, are allocated to the nearest building.
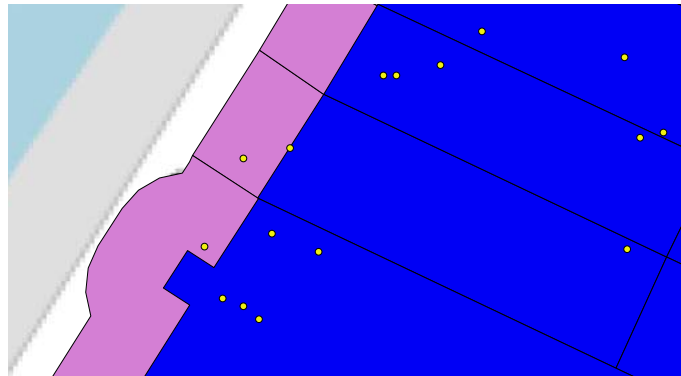
Figure 5.2: InSAR points (yellow) and 2 meter buffer area (pink) around several buildings (blue) to account for the location precision of the InSAR data

5.1.1.5 Probability of deformation rate

For the use of InSAR data in asset management, one might not be interested so much in an absolute deformation, but specifically in deformation rates above a certain threshold. Often, a certain deformation rate is stipulated above which deformations are considered to be alarming. This way, the management of assets is streamlined. For example, the building protocol in Amsterdam, as described in section 2.3, sets a deformation rate of 2 mm/y as a threshold for moderate building deformation. A deformation rate larger than 2 mm/y requires additional measures to be taken with respect to construction activities nearby.

Using the calculated deformation rate and its variance, we can determine the probability of a deformation rate larger than a specific value, for each deformation time series. This is depicted in figure 5.3 for a deformation rate of 2 mm/y. For a calculated deformation rate r, we assume a normal distribution with standard deviation σ_r. This way, the probability that the true deformation is more than -2 mm/y can be estimated. Subsequently, by specifying a confidence level, we can determine whether a significant chance exists the deformation rate exceeds the threshold (-2 mm/y).
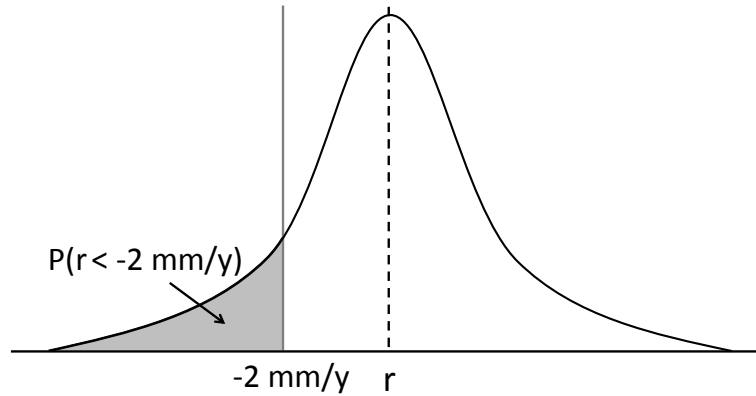
Figure 5.3: Probability of a deformation rate larger than -2 mm/y for a calculated deformation rate r

5.1.2 Results

First, the deformation time series from levelling and InSAR of several buildings in this area are shown in section 5.1.2.1. This gives an impression of the results. Subsequently, the results from the overall model test are presented in section 5.1.2.2. After applying the overall model test, the precision of the InSAR data is analyzed in section 5.1.2.3. Next, in section 5.1.2.4, the deformation rates are presented for each building in a building deformation map. Finally, the deformation rate estimate is combined with the variance of this estimate in a probability map in section 5.1.2.5.

5.1.2.1 Deformation time series of several buildings

To analyze the observed deformations, a selection of deformation time series from levelling and InSAR of several buildings is shown first. The calculated deformation rate r_{lev} or r_{InSAR}, the standard deviation of the deformation rate σ_r, the test statistic T and the critical value K corresponding to a 95% confidence level are displayed for each time series as well. For this, a conservative measurement variance is used of 0.5^2mm^2 and 3^2mm^2 for the levelling measurement variance $\sigma_{y,lev}$ and the InSAR measurement variance $\sigma_{y,InSAR}$ respectively.

Herengracht 7

Some of the deformation time series on Herengracht 7 from levelling and the 2 year and 9 year InSAR datasets are shown in figure 5.4. The only levelling benchmark present on this building provides high deformations between September 2016 and November 2017, resulting in a deformation rate of -4.4 mm/year. However, the test statistic of the linear deformation is higher than the critical value indicating the observations can not be explained by the measurement variance and the deformation model. The deformation rates from the 2 year InSAR dataset are lower, although the deformation rate standard deviation is higher. The 9 year InSAR points give lowest deformation rates with large deformation variance.

(a)

(b)   (c)

(d)   (e)
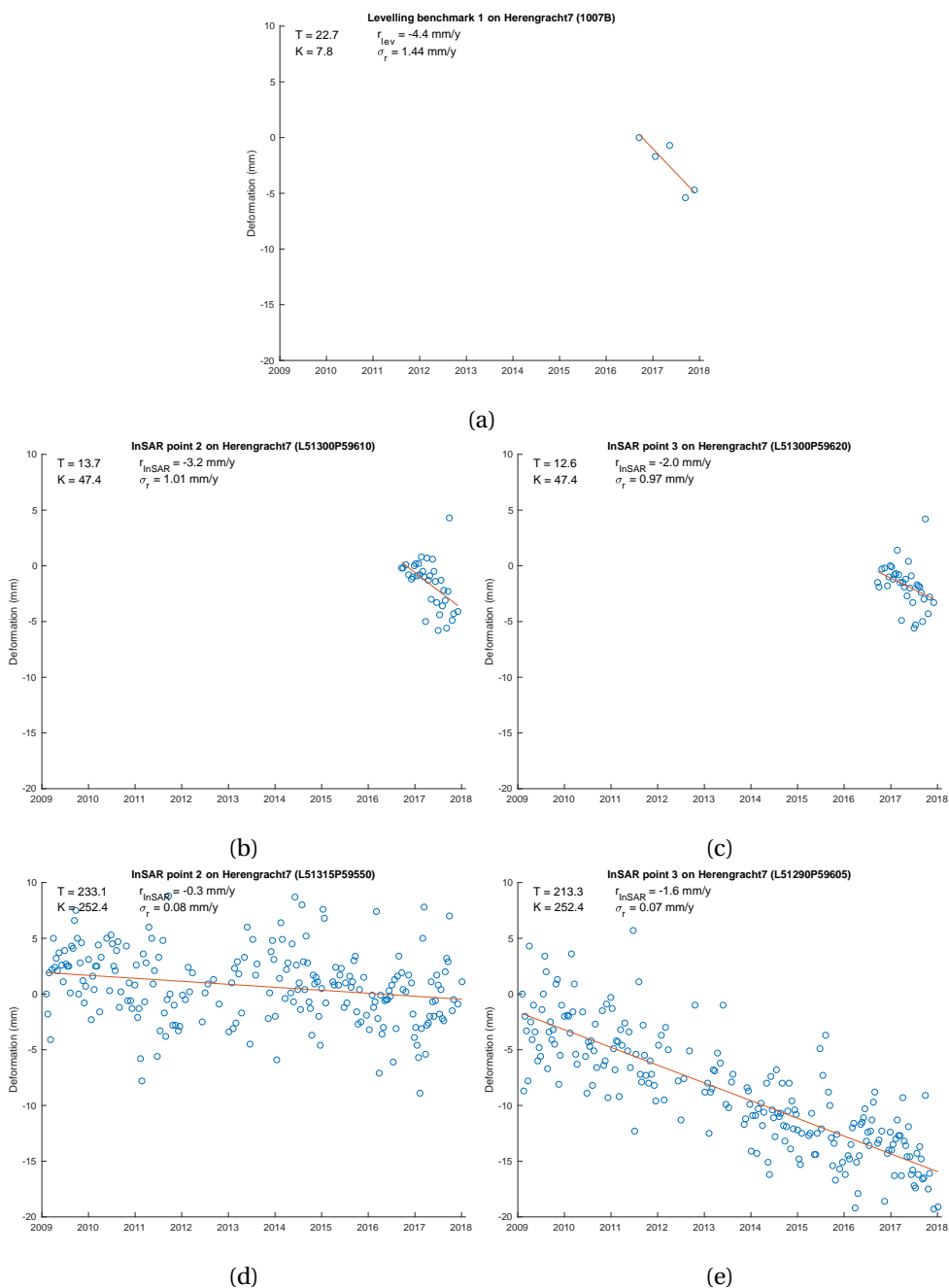
Figure 5.4: Deformations of a levelling benchmark (top), two InSAR points from the asc_2y dataset (middle) and two InSAR points from the asc_9y dataset (bottom) located on Herengracht 7

Herengracht 43

Several deformation time series from the different datasets are shown in figure 5.5. The levelling benchmarks provide low deformations. A deformation rate of -0.4 and -0.8 mm/year is calculated. However, the hypothesis of linear deformation in time for the levelling benchmarks needs to be rejected according to the overall model test. It is hard to distinguish a linear trend in the time series from the 2 year InSAR dataset, where deformation rates of -2.2 and 1.2 mm/year are calculated. The two InSAR points from the 9 year InSAR dataset both give a deformation rate of -0.3 mm/year. However, InSAR point 2 must be disregarded as the overall model test suggests errors in the observations or in the deformation model.
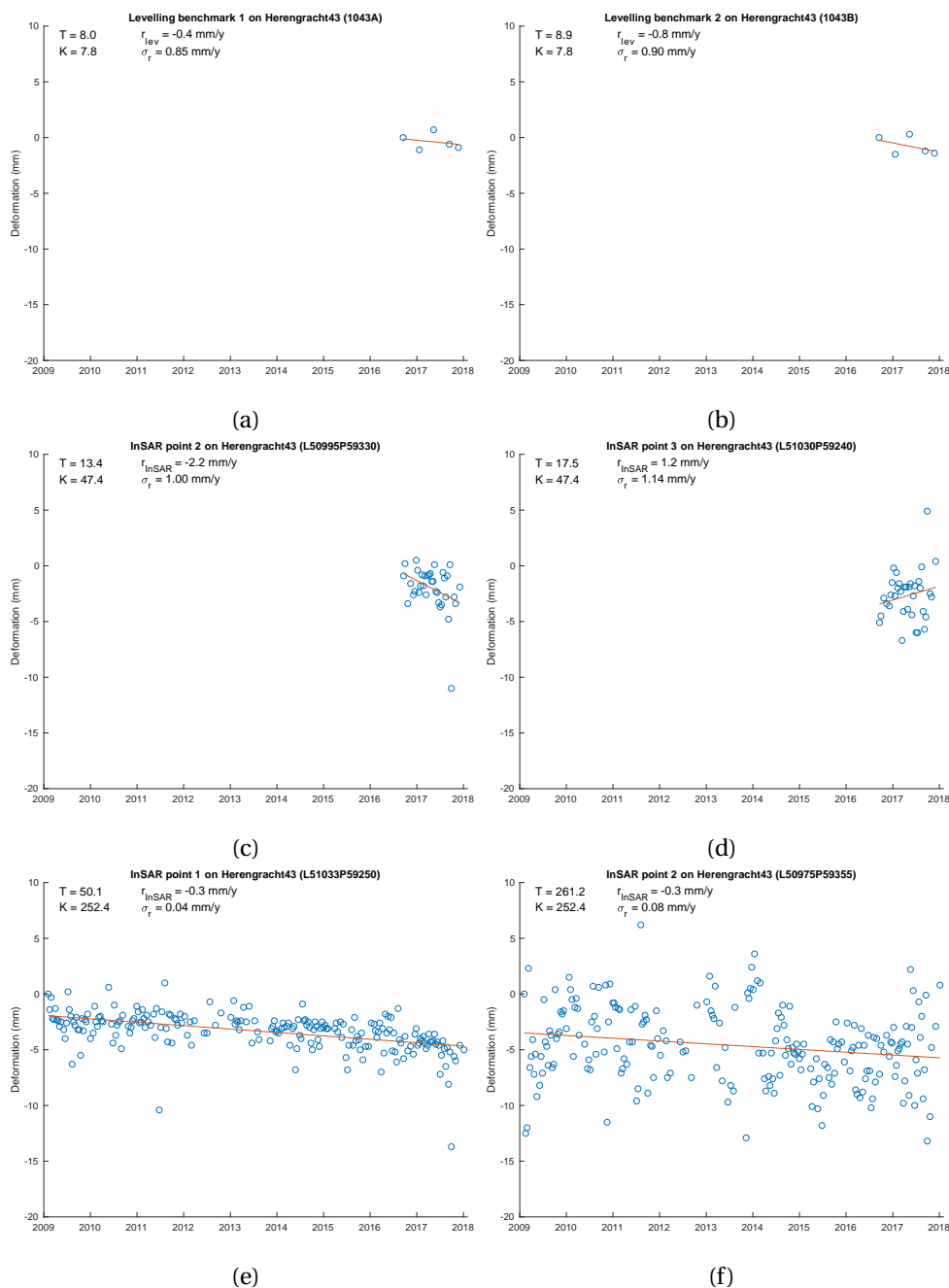
Figure 5.5: Deformations of two levelling benchmark (top), two InSAR points from the asc_2y dataset (middle) and two InSAR points from the asc_9y dataset (bottom) located on Herengracht 43

Herengracht 63

The levelling benchmarks give deformation rates of -2.3 and -1 mm/year but the null hypothesis of linear deformation must be rejected for the first levelling benchmark. Although a linear trend can hardly be observed in the 2 year dataset, a deformation rate of -2.5 mm/year is found. For the 9 year InSAR dataset, rates of -1.2 and -1.3 are calculated. The difference in quality of these two InSAR point is obvious. Based on the test statistic T, the deformation model of InSAR point 2 needs to be rejected.
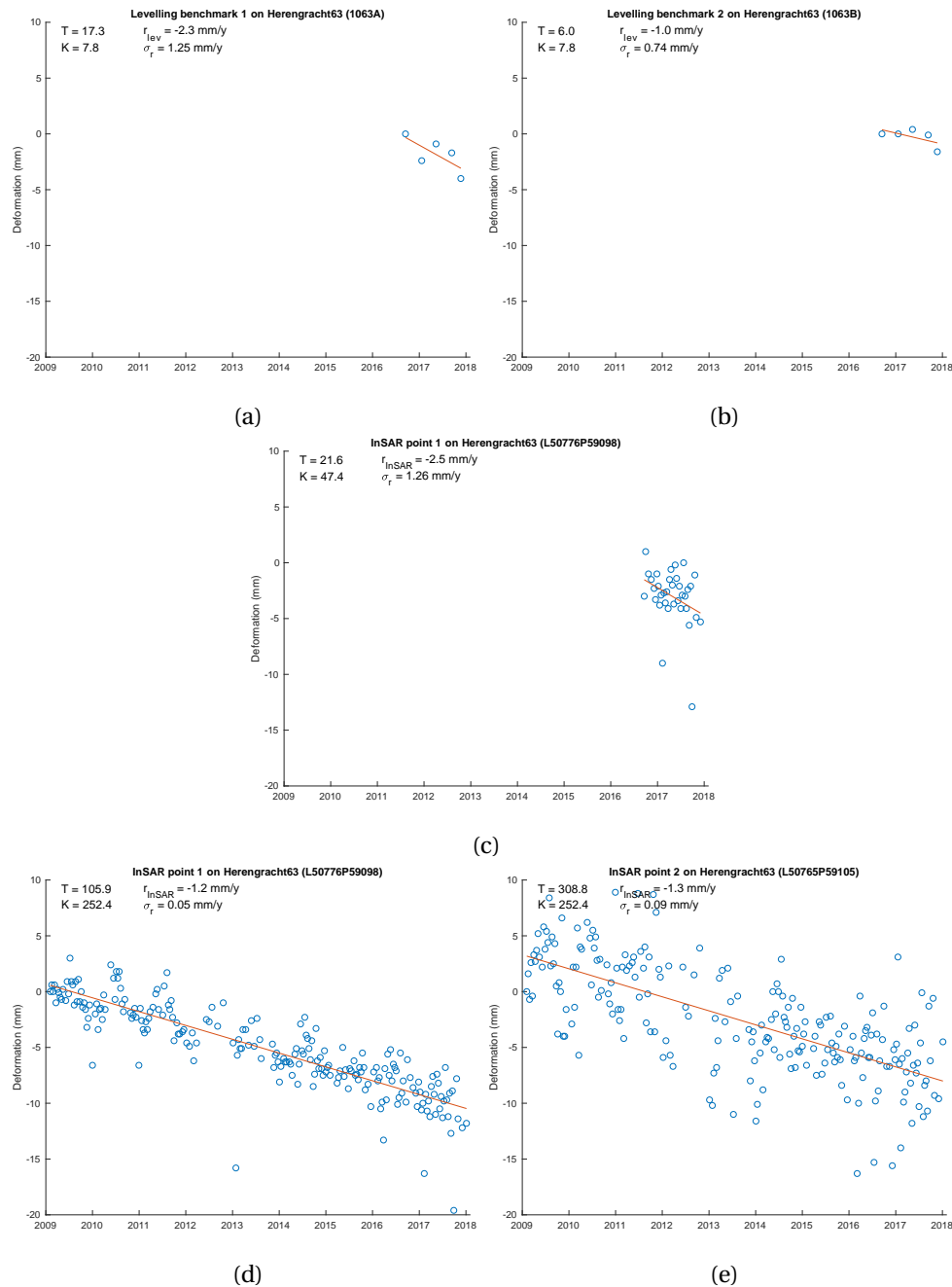
Figure 5.6: Deformations of two levelling benchmark (top), one InSAR point from the asc_2y dataset (middle) and two InSAR points from the asc_9y dataset (bottom) located on Herengracht 63

5.1.2.2 Overall model test

To test whether the deformation model fits the observations, the test statistic T is calculated. The time series in the results shown above indicate that the null hypothesis of linear deformation in time needs to be rejected in several cases. The results of the overall model test for the levelling and InSAR datasets are shown in table 5.2. As mentioned in section 5.1.1, a conservative measurement variance $\sigma^2_{y,a-priori}$ of 0.5^2 and 3^2 is used for the levelling and InSAR data respectively. Furthermore, a critical value K corresponding to a confidence level of 95%, is used.

The results show that 29% of the present levelling benchmarks reject the null hypothesis of linear deformation in time. The 9 year InSAR dataset shows 23% of the points is rejected based on the overall model test. For the 2 year InSAR dataset the null hypothesis is sustained for almost all InSAR points, only 3% of the points is rejected.

Table 5.2: Results of the overall model test for the Herengracht

Dataset	Measurement variance $\sigma^2_{y,a-priori}$	Total number of points	Number of points rejected	Percentage of points rejected
Levelling	0.5^2	66	19	29%
InSAR asc_9y	3^2	151	35	23%
InSAR asc_2y	3^2	104	3	3%

5.1.2.3 A-posteriori precision analysis

When the deformation model is accepted according to the overall model test, the deformation time series are analyzed for their measurement variance. This is calculated as described in section 5.1.1.3. The results are shown in figure 5.7a and 5.7b, for the 2 year dataset and the 9 year dataset respectively. The measurement variance is lowest for the 2 year dataset with an average measurement variance of 2.15^2 millimeter, while the 9 year dataset gives an average variance of 2.53^2 millimeter.

(a)   (b)
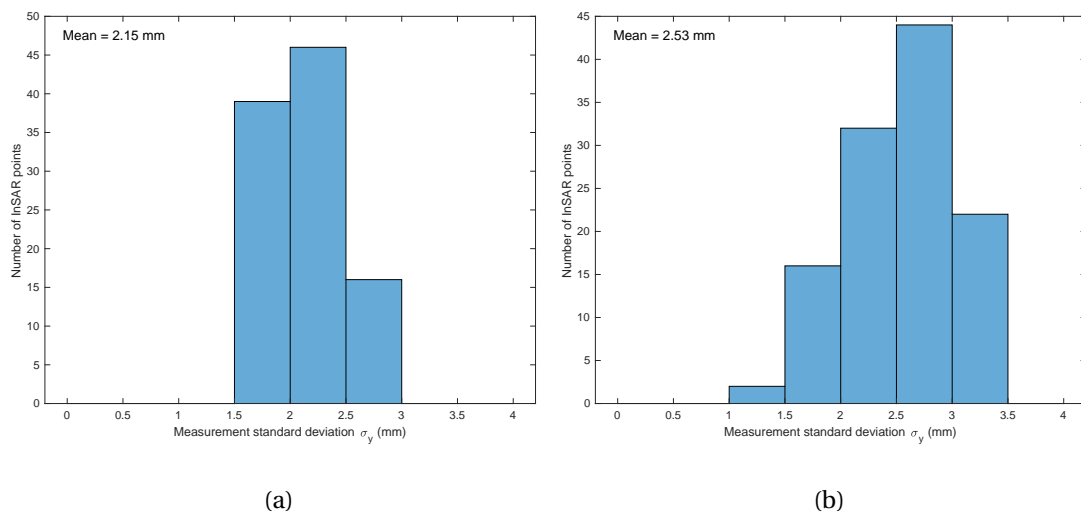
Figure 5.7: Histograms of the measurement variance of the InSAR points on the considered Herengracht buildings, from the asc_2y dataset using deformations between September 2016 and November 2017 (left) and from the asc_9y dataset using deformations between February 2009 and January 2018 (right)

5.1.2.4 Building deformation map

After performing the overall model test, only deformation time series are left for which the linear deformation model fits reasonably well. Instead of showing individual InSAR points, in this section the average building deformation is presented. The InSAR points of each building are selected as described in section 5.1.1.4. To obtain an overall deformation rate per building, the deformation rates obtained from InSAR points or levelling benchmarks on the same building are averaged. To compare the determined deformation rates from levelling data and InSAR data, the mean absolute error (MAE) is calculated. This value provides a measure of the average magnitude of the difference between the calculated values. It is calculated by

$$MAE = \frac{1}{n} \sum_{j=1}^{n} |r_{InSAR,average,j} - r_{lev,average,j}|, \tag{5.12}$$

where n is the number of buildings and $r_{InSAR,average}$ and $r_{lev,average}$ are the average deformation rates of each building derived from InSAR data and levelling data respectively.

First, building deformations are calculated using the observations of the levelling and InSAR data over the same period of time. Figure 5.8a depicts the deformation rates of the buildings along the Herengracht based on the levelling data obtained between September 2016 and November 2017. All considered buildings show low settlement rates, i.e. less than 3 millimeter settlement per year. Due to the rejection of the null hypothesis for several levelling benchmarks, the deformation rate of six of the 38 buildings is not calculated.

Figure 5.8b depicts the deformation rates of the buildings along the Herengracht based on the InSAR data of the asc_2y dataset. The deformation rates are based on deformation measurements obtained between September 2016 and November 2017, using the asc_2y dataset. In general, slightly higher deformation rates are obtained from this InSAR dataset. For five of the 38 buildings the linear deformation in time of present InSAR points is rejected or no InSAR points are located on the building.

For comparison between the levelling and InSAR results, the deformation rates are plotted in figure 5.9 with a 1:1 reference line. The lines through the points indicate the variation of the found deformation rates on each building. The lines extend to the minimum and maximum deformation rate found for the particular building. The blue and red lines represent the variation in deformation rate of the InSAR data and levelling data respectively, for each building. The figure shows that in most cases higher InSAR deformation rates are found. The variation in the determined deformation rates tends to be larger for the InSAR points. Note that points without a line in this figure, indicate that the specific building only has one levelling point and InSAR point. The mean absolute difference between the InSAR and levelling deformation rates is 1.00 millimeter/year.
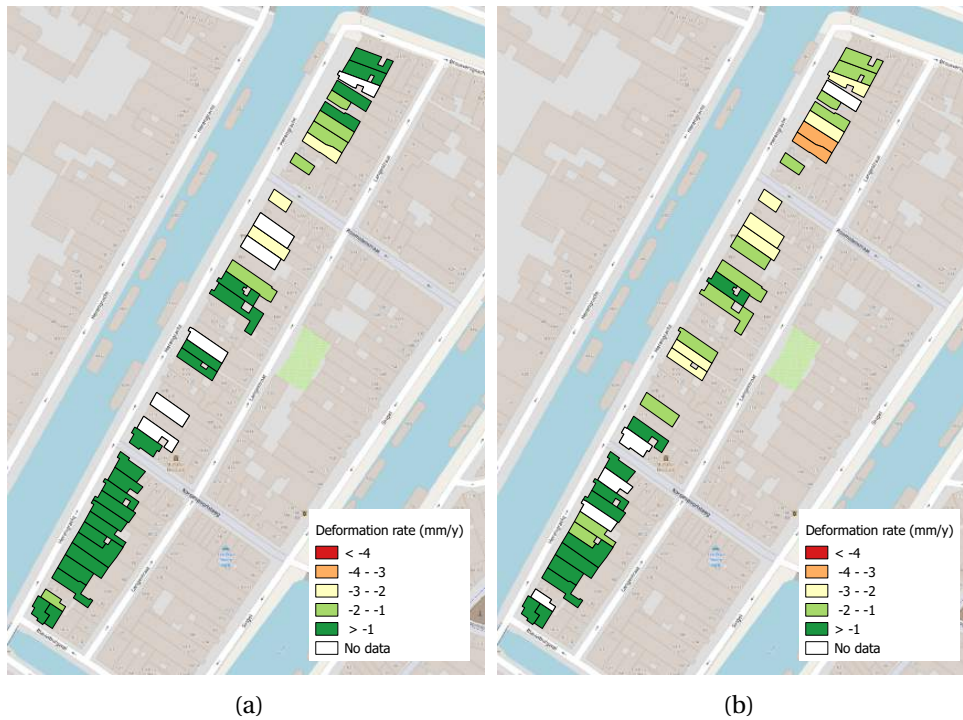
Figure 5.8: Average building deformation rate along Herengracht from levelling data (left) and InSAR data (asc_2y)(right) between September 2016 and November 2017
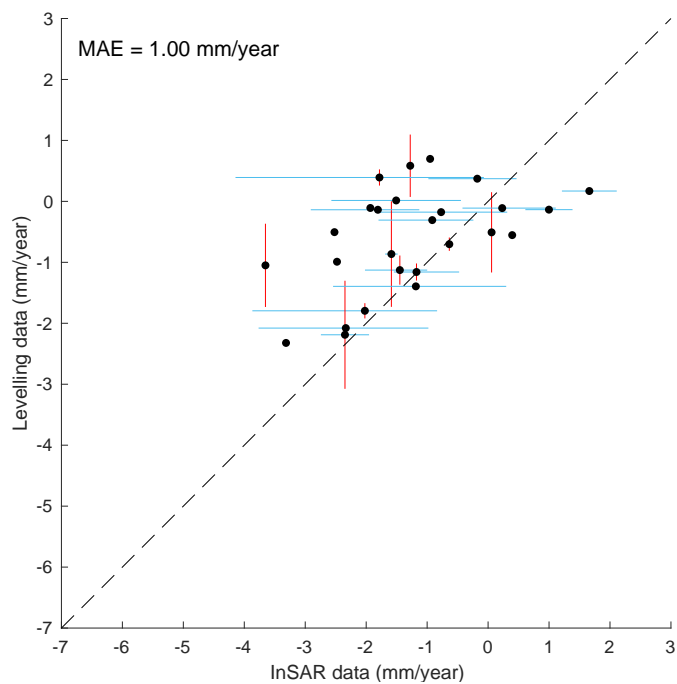
Figure 5.9: Graph of calculated deformation rates from the levelling data and the InSAR data (asc_2y) using deformations between September 2016 and November 2017

The InSAR enables the use of deformation data over a longer period of time. In this case, nine years of InSAR data is available. It is therefore interesting to see what results are obtained from the nine year ascending dataset (asc_9y). This way, the capabilities of InSAR are used to their full extent. In this comparison however, the linear deformation behaviour in the 9 year dataset is assumed to be similar as the linear deformation between September 2016 and November 2017 from in the levelling data. Figure 5.10b shows deformation rates obtained from InSAR data between February 2009 and January 2018. For easy comparison, the deformation rates from levelling are depicted again in figure 5.10a. Figure 5.10b clearly shows that lower deformation rates are obtained using this large time span. All buildings show low deformation rates of less than -2 mm/year. Due to the rejection of linear deformation in time of present InSAR points or the absence of InSAR points, no deformation rate can be calculated for two of the 38 buildings.

To evaluate the differences, the levelling and InSAR deformation rates are again plotted in figure 5.11. Compared to figure 5.9, the resemblance in this figure seems to be larger. The mean absolute difference between the InSAR and levelling data is 0.64 millimeter/year. Also, the variation in InSAR deformation rates is significantly smaller using nine years of InSAR data instead of two years.
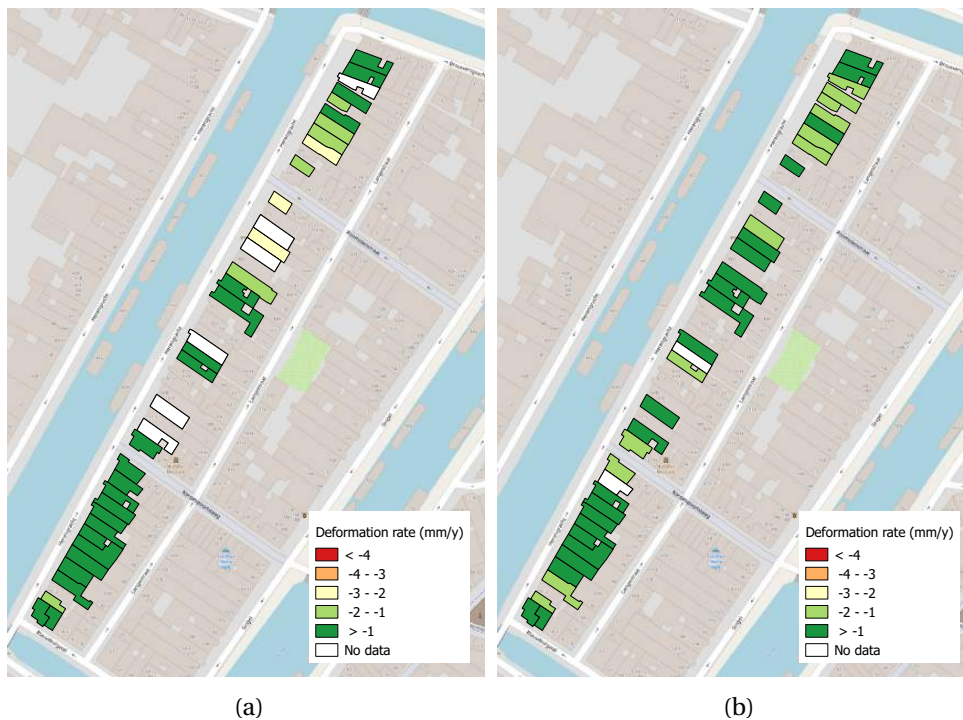
Figure 5.10: Average building deformation rate along Herengracht from levelling data (left), between September 2016 and November 2017, and InSAR data (asc_9y)(right), between February 2009 and January 2018
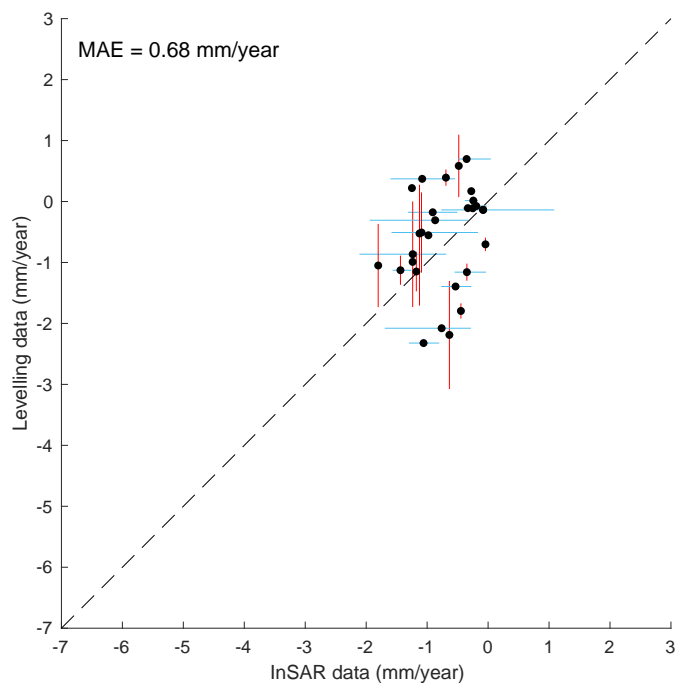
Figure 5.11: Graph of calculated deformation rates from the levelling data, between September 2016 and November 2017, and the InSAR data (asc_9y), between February 2009 and January 2018

5.1.2.5 Probability Map

Usually, the calculated deformation rates from InSAR data are presented. In this section, an alternative InSAR product is presented which gives the probability of a deformation rate above a threshold. The method to obtain this probability from the deformation time series is described in section 5.1.1.5. The result is presented in a probability map where the probability of this specified deformation rate occurring, is presented. The probability is calculated for a deformation rate of -2 mm/y, which is used as threshold for moderate building movement in the building protocol, as described in 2.3.

The probability map of the asc_2y dataset with observations between September 2016 and December 2017, is depicted in figure 5.12a. The probability map of the asc_9y dataset with observations between February 2009 and January 2018, is shown in figure 5.12b. Deformation time series with a probability smaller than 5% are indicated in green and time series with a probability larger than 5% are indicated in red. As can be seen in the figure 5.12a, the 2 year dataset does not provide high confidence regarding exceedance of the -2 mm/y deformation rate threshold. On the other hand, the 9 year dataset in figure 5.12b gives much certainty about a deformation rate of -2 mm/y.

(a)   (b)
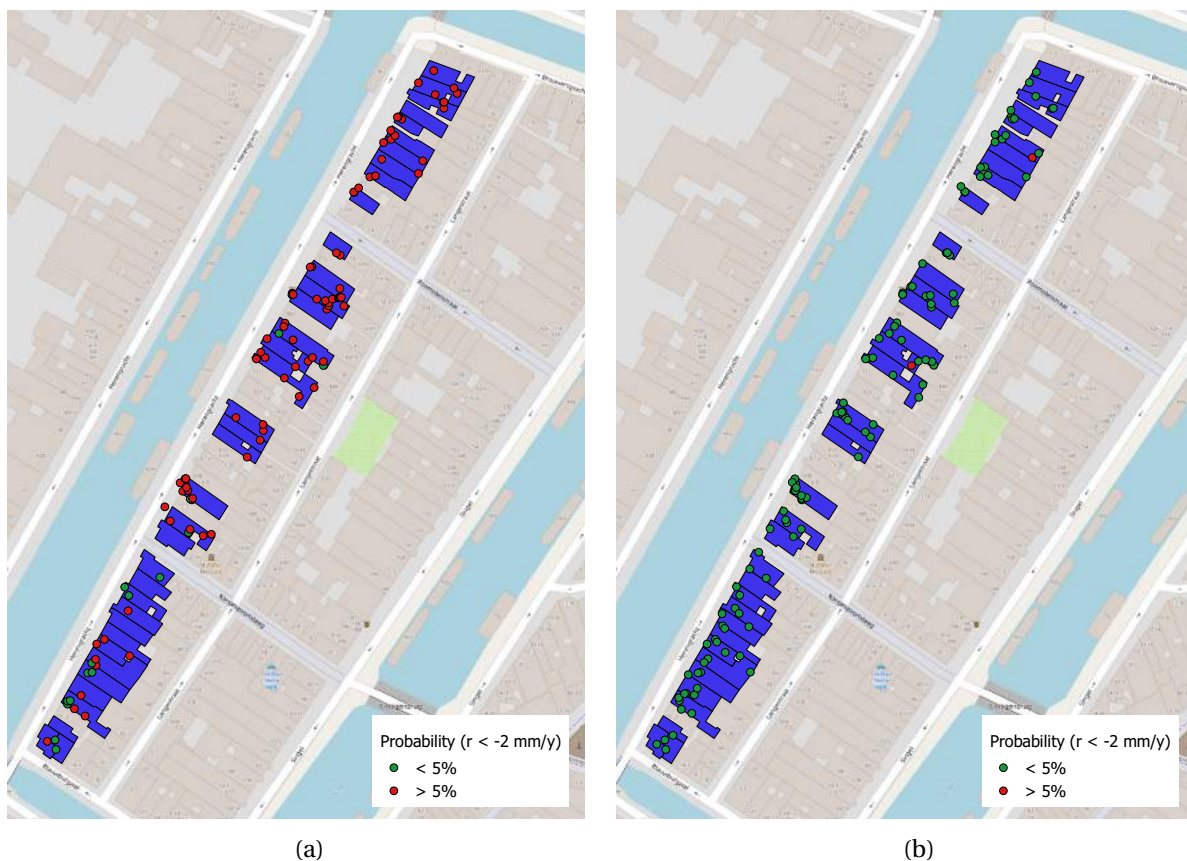
Figure 5.12: Probability of a deformation rate of more than -2 mm/y based on the calculated σ_r of each InSAR point for InSAR data between September 2016 and November 2017 (left) and InSAR data between February 2009 and January 2018 (right)

5.1.3 Discussion and Conclusion

The availability of levelling data of the Herengracht allows for comparison of deformations with InSAR data. Due to the levelling data between September 2016 and November 2017, the InSAR data with the same time span is selected from a 2 year dataset. Also, to use the capabilities of the InSAR data to its full extent, a 9 year InSAR dataset with deformations between February 2009 and January 2018 is used for the analysis. For this, it is assumed the linear deformation pattern in the levelling between September 2016 and November 2017, is the same between February 2009 and January 2018.

The levelling data seems to show linear deformation in time for the Herengracht buildings. The overall model test allows for the assessment of the fitted deformation model in combination with the measurement variance. The linear model fitted through the levelling data is rejected for 29% of the present levelling benchmarks, according to an overall model test with a 5% significance level and a measurement variance of 0.5^2. The null hypothesis of linear deformation in time is rejected in the 2 year InSAR dataset and the 9 year InSAR dataset for 3% and 23% of the points, respectively. For the InSAR data a conservative measurement variance of 3^2 was used. This shows a linear deformation model is likely to be present for the Herengracht buildings. The low amount of points rejected in the 2 year InSAR dataset is expected to be related to the relatively large measurement variance with respect to the amount of deformation in this short time span. Because of this, a linear deformation model is more likely to fit the observations.

After performing the overall model test, in a precision analysis an average measurement standard deviation of 2.15 millimeter and 2.53 millimeter is calculated, for the 2 year and 9 year InSAR dataset respectively.

The building deformation map depicts the average building movement derived from the deformation data. The average difference between the levelling and 2 year InSAR building deformation rates is 1.00 millimeter/year. One of the reasons for this difference is visible in the deformation time series of Herengracht 7, 43 and 63 from the 2 year InSAR dataset. The short analysed time period (one year and two months) can make the InSAR less suited to determine a deformation rate from, due to the variance in InSAR deformations. This results in a large standard deviation of the estimated deformation rate σ_r compared to the 9 year InSAR dataset. For the 2 year dataset a σ_r in the order of 1 mm/y is calculated while the 9 year dataset has a σ_r of less than 0.1 mm/y.

The average difference between the 9 year InSAR deformation rates and levelling rates is 0.68 mm/year. In this case, differences can be explained by the different time period of the measurements. Although the null hypothesis of linear deformation in time is rejected for the levelling benchmark on Herengracht 7, this benchmark shows much larger deformation than the InSAR 9 year data of this building suggests. For this particular building, the resemblance with the 2 year InSAR deformations is better. This might be caused by increased settlement in 2016 and 2017. The better resemblance of the levelling data with the 9 year dataset is expected to be related to the variance of the estimated deformation rate, as mentioned earlier. This is also expected to be the reason of the smaller variation in estimated deformation rates for each building (blue lines) in the 9 year dataset, shown in figure 5.11, compared to the 2 year dataset, shown in figure 5.9.

Any differences between the levelling rates and InSAR rates can also be caused by non-uniform building settlement. This is, for example, visible for the levelling benchmarks on Herengracht 63. The deformation rates of the two benchmarks are -2.3 and -1 mm/year. The different location of the levelling benchmarks and the InSAR points, can result in different deformations.

In the presented probability ma p, the calculated deformation rate is combined with the variance of this estimated deformation rate. Using this information, the probability of a certain deformation rate occurring, can be calculated. The probabilistic approach to the deformation measurements can prove to be valuable for asset management. The probability map can be used in decision-making regarding the monitoring and quality of building foundations.

In this case, the probability of a -2 mm/y deformation rate is calculated, which is set as threshold for moderate to high building deformation. The high probability of a -2 mm/y deformation rate occurring in the 2 year dataset is caused by the high deformation rate variance. This high variance is the result of the use of only one year and two months of InSAR data in combination with the InSAR measurement variance. On the other hand, the 9 year InSAR data provides much more confidence with respect to this deformation rate threshold. This means that short time series of InSAR deformations are less suited to draw conclusions from, based on the calculated deformation rate.

5.2   Recht Boomssloot and Krom Boomssloot

The quay walls on part of the Recht Boomssloot and the Krom Boomssloot are in the process of being replaced. This is due to the bad condition of the current quay wall [45]. Several buildings on the Recht Boomssloot and Krom Boomssloot are therefore monitored with levelling benchmarks.

5.2.1   Methodology

The methodology to process the levelling and InSAR data is similar to the methodology of the Herengracht as described in section 5.1.1. Therefore only the available deformation measurements are described in this section. The available levelling data is described in section 5.2.1.1, and the available InSAR data is described in section 5.2.1.2.

5.2.1.1   Levelling data

A total of 31 buildings have been equipped with levelling benchmarks. This includes 12 buildings on the Recht Boomssloot and 19 buildings on the Krom Boomssloot. In total 59 levelling benchmarks have been installed. The deformations of the levelling benchmarks have been measured five times. The measurement dates are 25-01-2013, 19-03-2015, 26-06-2015, 28-10-2015, 17-03-2016 and 06-12-2016.

5.2.1.2   InSAR data

The same InSAR data is available as for the Herengracht, as described in section 5.1.1.2. Because levelling data between January 2013 and December 2016 is available, only the asc_9y dataset will be used for the analysis of the Recht Boomssloot and the Krom Boomssloot. The levelling data almost spans 4 years. That's why it is decided to select the InSAR data from the same time span. This means only InSAR data between January 2013 and December 2016 is used of the available asc_9y dataset.

5.2.2   Results

First, the deformation time series from levelling and InSAR of several buildings in this area are shown in section 5.2.2.1. This gives an impression of the results. Subsequently, the results from the overall model test are presented in section 5.2.2.2. After applying the overall model test, the precision of the InSAR data is analyzed in section 5.2.2.3. Next, in section 5.2.2.4, the deformation rates are presented for each building in a building deformation map. Finally, the deformation rate estimate is combined with the variance of this estimate in a probability map in section 5.2.2.5.

5.2.2.1   Deformation time series of several buildings

To analyze the observed deformations, a selection of deformation time series from levelling and InSAR of several buildings is shown first. The calculated deformation rate r_{lev} or r_{InSAR}, the standard deviation of the deformation rate σ_r, the test statistic T and the critical value K corresponding to a 95% confidence level are displayed for each time series as well. For this, a conservative measurement variance is used of 0.5^2mm^2 and 3^2mm^2 for the levelling measurement variance $\sigma_{y,\text{lev}}$ and the InSAR measurement variance $\sigma_{y,\text{InSAR}}$ respectively.

Recht Boomssloot 99
Some of the results of Recht Boomssloot 99 are given in figure 5.13. Both the levelling and InSAR give small deformations between 2013 and 2016. The deformation variance is larger for InSAR point 3 compared to InSAR point 1. Nevertheless InSAR point 3 still satisfies the overall model test due to the specified measurement variance.
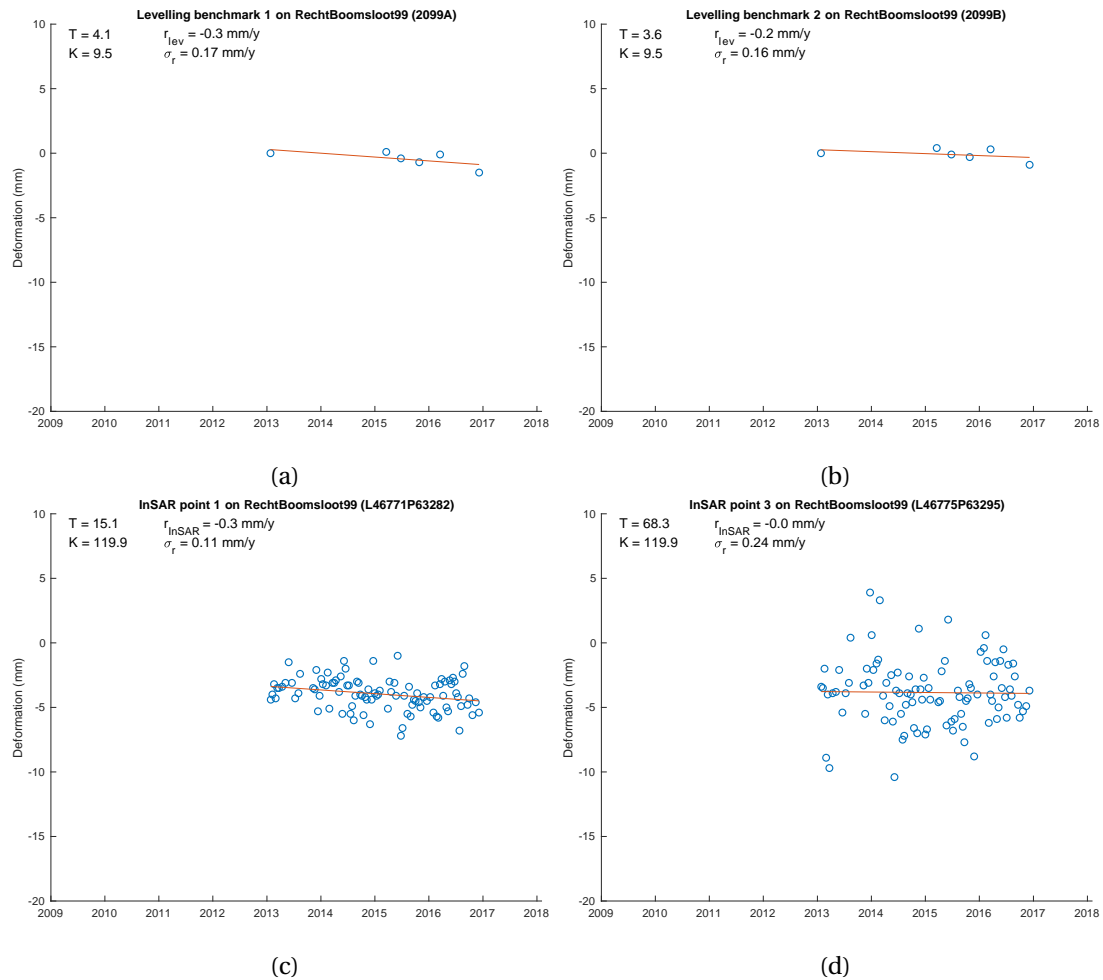
Figure 5.13: Deformations of two levelling benchmark (top) and two InSAR points from the asc_9y dataset (bottom) located on Recht Boomssloot 99

Krom Boomssloot 67

Figure 5.14 shows the deformations from levelling and InSAR for Krom Boomssloot 67. A difference of roughly 5 millimeter between the two levelling benchmarks is present in roughly four years. The two InSAR points show similar deformation rates as levelling benchmark 1. Both InSAR points sustain the linear deformation in time according to the overall model test.
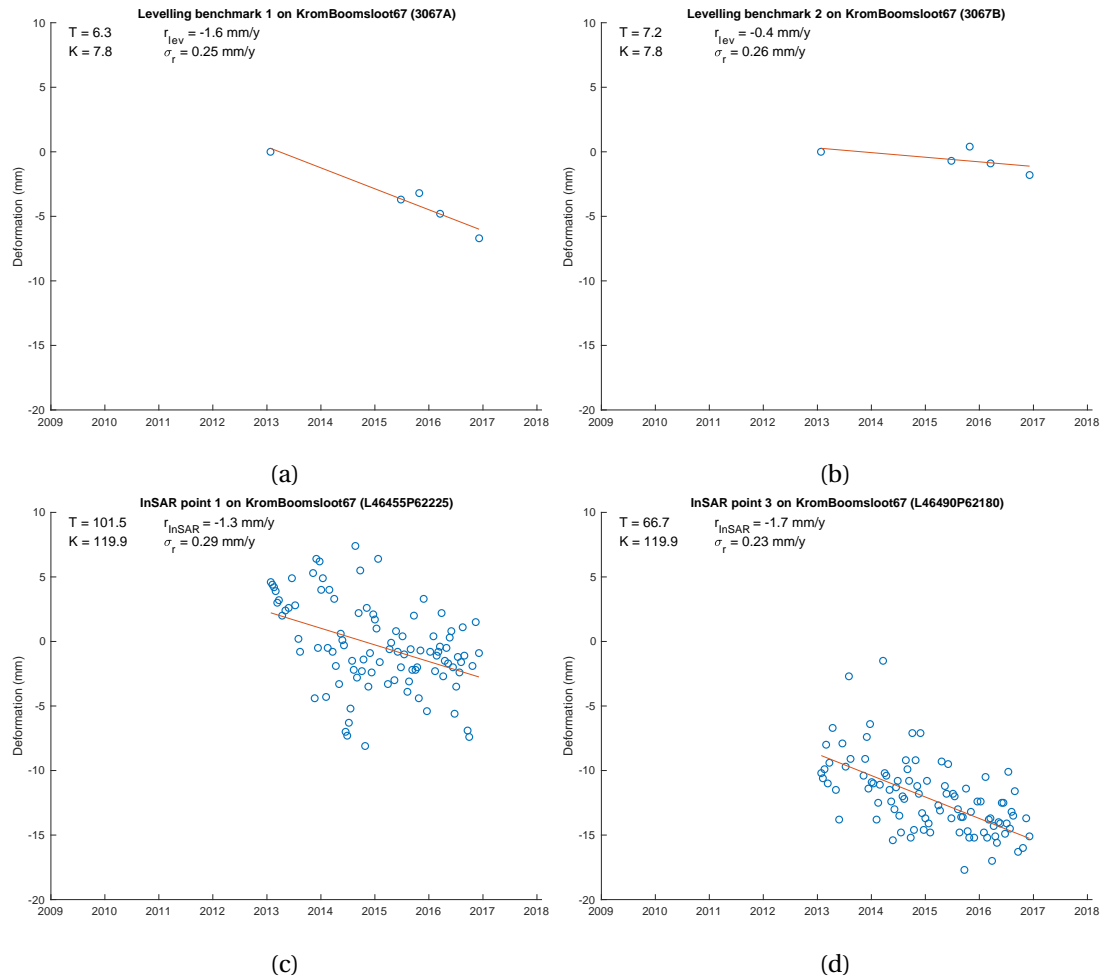
Figure 5.14: Deformations of two levelling benchmark (top) and two InSAR points from the asc_9y dataset (bottom) located on Krom Boomssloot 67

Krom Boomssloot 1

The deformation time series found for Krom Boomssloot 1, are given in figure 5.15. No clear deformation pattern can be observed for levelling benchmark 1 while benchmark 2 seems to follow a linear deformation in time. Nevertheless, the linear deformation model is rejected for both levelling benchmarks due to the defined measurement variance of 0.5^2. The InSAR point shows large variance in deformation. A positive deformation rate of 0.9 mm/year as a result.

(a)

(b)

(c)
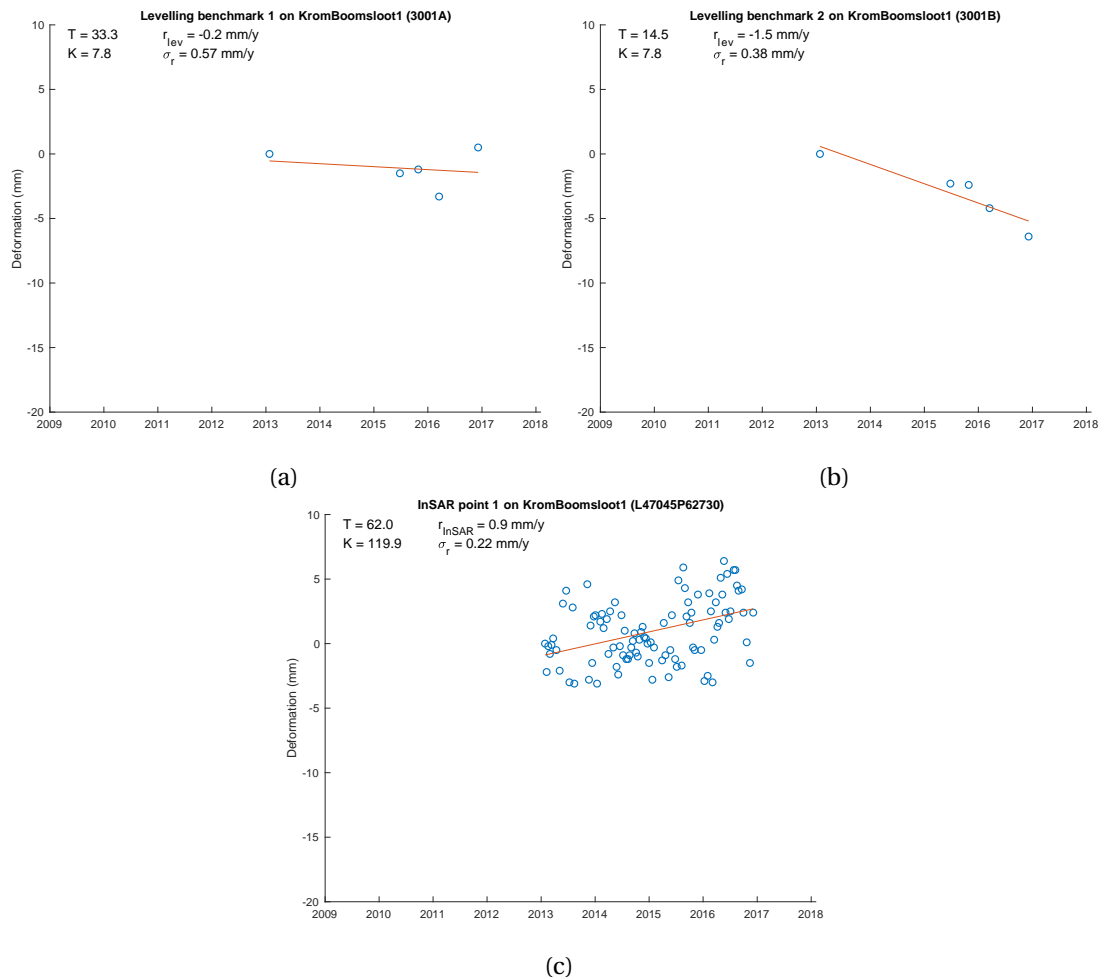
Figure 5.15: Deformations of the two levelling benchmark (top) and one InSAR points from the asc_9y dataset (bottom) located on Krom Boomssloot 1

5.2.2.2   Overall model test

To test whether the deformation model fits the observations, the test statistic T is calculated. The time series in the results shown above indicate that the null hypothesis of linear deformation in time needs to be rejected in several cases. The results of the overall model test for the levelling and InSAR datasets are shown in table 5.3. A conservative measurement variance $\sigma^2_{y,a-priori}$ of 0.5^2 and 3^2 is used for the levelling and InSAR data respectively. Furthermore, a critical value K corresponding to a confidence level of 95%, is used.

The results show that 32% of the present levelling benchmarks reject the null hypothesis of linear deformation in time. The InSAR dataset shows 15% of the points is rejected based on the overall model test.

Table 5.3: Results of the overall model test for the Recht Boomssloot and Krom Boomssloot

Dataset	Measurement variance $\sigma^2_{y,a-priori}$	Total number of points	Number of points rejected	Percentage of points rejected
Levelling	0.5^2	59	19	32%
InSAR asc_9y	3^2	96	14	15%

5.2.2.3   A-posteriori precision analysis

When the deformation model is accepted according to the overall model test, the deformation time series are analyzed for their measurement variance. This is calculated as described in section 5.1.1.3. The result is shown in figure 5.16a. An average measurement variance of 2.09^2 millimeter is found.
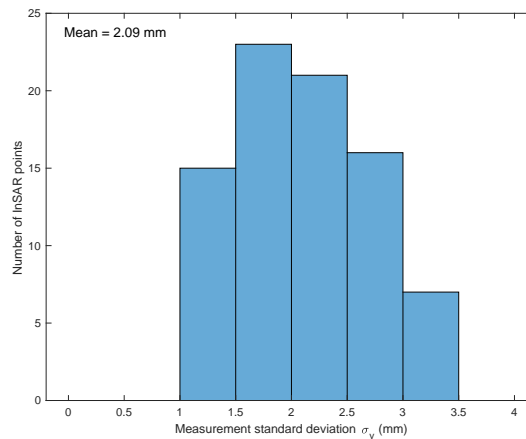
(a)

Figure 5.16: Histogram of the measurement variance of the InSAR points on the considered Recht Boomssloot and Krom Boomssloot buildings, from the asc_9y dataset using deformations between January 2013 and December 2016

5.2.2.4   Building deformation map

The application of the overall model test has left only the deformation time series for which the linear deformation in time is reasonable. Subsequently, to obtain an overall deformation rate per building, the deformation rates obtained from InSAR points or levelling benchmarks on the same building are averaged. Then, to compare the average deformation rate per building from levelling data and InSAR data, the mean absolute error (MAE) is calculated. This value provides a measure of the average magnitude of the difference between the calculated values. It is calculated by

$$MAE = \frac{1}{n} \sum_{j=1}^{n} |r_{InSAR,average,j} - r_{lev,average,j}| \tag{5.13}$$

Where n is the number of buildings and $r_{InSAR,average}$ and $r_{lev,average}$ are the average deformation rates per building derived from InSAR and levelling respectively.

Figure 5.17a depicts the deformation rates of the buildings along the Recht Boomssloot and Krom Boomssloot based on the levelling data obtained between January 2013 and December 2016. All buildings show small settlements of less than -2 mm/year. With the overall model test, the linear deformation model is rejected for the levelling benchmarks of six buildings. Small deformation rates are also observed in the InSAR data, depicted in figure 5.17b. For four of the 31 buildings, no InSAR points are present or the linear deformation model is rejected, based on the overall model test, for the present InSAR points. As a result, no deformation rate is calculated for these buildings.

The deformation rates results are also depicted in the graph in figure 5.18. The dotted line indicates a 1:1 reference line. The lines extend to the minimum and maximum deformation rate found for the particular building. The blue and red lines represent the variation in deformation rate of the InSAR data and levelling data respectively. The graph again indicates the resemblance between the deformation rates obtained with InSAR and levelling. A mean absolute difference between the InSAR and levelling rates of 0.35 millimeter/year is calculated.
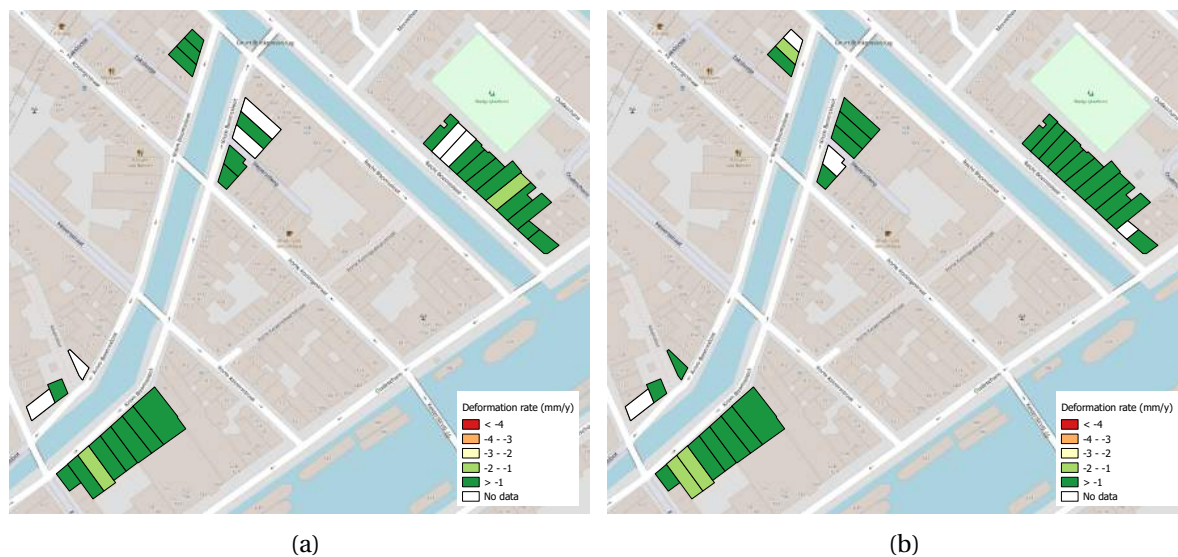
Figure 5.17: Average building deformation rate along the Recht Boomssloot and Krom Boomssloot from levelling data (left) and InSAR data (asc_9y)(right) between January 2013 and December 2016
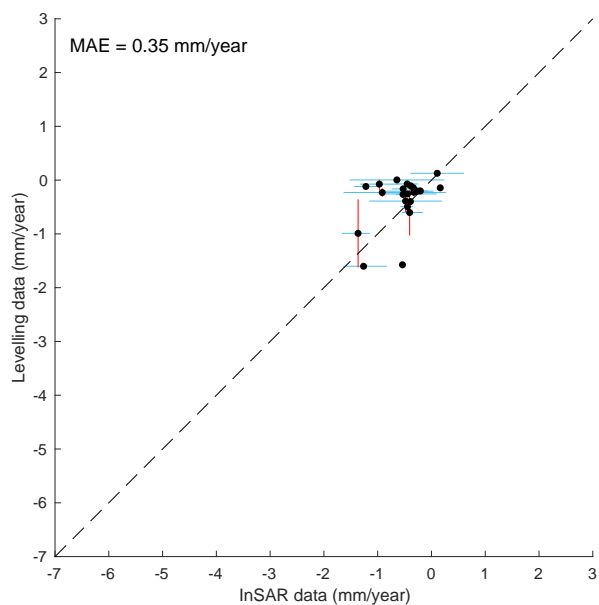
Figure 5.18: Graph of calculated deformation rates from the levelling data and the InSAR data (asc_9y) using deformations between January 2013 and December 2016

5.2.2.5   Probability Map

In figure 5.19 a probability map is presented of the InSAR points located on the considered buildings of Recht Boomssloot and Krom Boomssloot. The map indicates whether the probability of a -2 mm/y deformation rate is more or less than 5%. The method to obtain this probability from the deformation time series is described in section 5.1.1.5. Only two InSAR points provide deformations which could indicate a deformation rate of more than 2 mm/y.

Figure 5.19: Probability of a deformation rate of more than -2 mm/y based on the calculated σ_r of each InSAR point for InSAR data between January 2013 and December 2016

5.2.3   Discussion and Conclusion

For 31 buildings, the deformation is measured for almost four years, between January 2013 and December 2016. To analyze the deformations from InSAR data, the deformations are selected from the 9 year InSAR dataset between January 2013 and December 2016.

A linear deformation model is fitted through the deformation data. With the overall model test, it is tested whether the defined variance and the deformation model can explain the present noise in the deformation time series. For the levelling data with a predefined measurement variance of 0.5^2, 32% of the present levelling benchmarks is rejected according to the overall model test. For the InSAR data, with a measurement variance of 3^2, 15% of the present InSAR points is rejected. A linear deformation between January 2013 and December 2016 is therefore reasonable. After the overall model test, the measurement variance is calculated for the remaining InSAR points. An average measurement variance of 2.09^2mm^2 is calculated.

The deformations of the buildings along the Recht Boomssloot and Krom Boomssloot show very small deformations in the period from January 2013 to December 2016. This is observed in both the InSAR data and the levelling data. The difference in linear deformation rates between the two monitoring methods is minimal, mostly less than 1 mm/year. As the deformation time series of Krom Boomssloot 1 show, the small difference can be caused by the variance in InSAR deformations. Also, the amount of levelling observations is limited and can affect the calculated levelling rates. Besides, the levelling benchmarks of Krom Boomssloot 67 and 1 indicate differential settlement of single buildings. This can also explain differences found between InSAR and levelling. The results of the Recht Boomssloot and Krom Boomssloot proves the application of InSAR for detecting small deformation rates.

The probability map of the InSAR points located on the considered buildings, show a possible larger deformation rate of more than 2 mm/y for only two InSAR points. Thus, the settlement of these buildings could be significant. However, several other InSAR points on these buildings provide probabili-

ties of less than 5% for a -2 mm/y deformation rate. Therefore, a large deformation of these buildings is unlikely. Nonetheless, the levelling data of these buildings should be analyzed with extra attention.

5.3   Oudezijds Achterburgwal

In February 2011 the quay wall replacement started on the odd numbered side of the Oudezijds Achterburgwal between the Molensteeg and the Oude Hoogstraat [6]. It had been recognised that the quay wall was in a poor condition. Due to the ageing of the quay wall, root growth of the trees next to the quay wall and the increased traffic load, cracks had appeared in the quay wall and the quay wall had deformed horizontally on some locations [5]. For the quay wall replacement, the project was subdivided into two phases. Phase 1 consists of the area between the Molensteeg and the Barndesteeg, i.e. Oudezijds Achterburgwal 4191 [6]. The second phase concerns the area between the Barndesteeg and the Oude Hoogstraat, i.e. Oudezijds Achterburgwal 93-149 [6]. This is shown in figure 5.20.

Figure 5.20: Map of the project area of the Oudezijds Achterburgwal with the two construction phases

During the first phase of the project, a large deformation was observed for some of the buildings in this area. One of the suggested reasons for this large deformation was leakage of the building pit [6]. After foundation inspection, some buildings turned out to have a shallow foundation [6]. Also, large settlements for buildings in phase 2 of the project were observed, even before any construction activities were undertaken in this area. Phase 1 was finalized in March 2013 [2]. It was decided to postpone phase 2 of the replacement project to allow for further foundation inspection and repairs of the affected buildings [6]. Due to the bad conditions of the quay wall in phase 2, a temporary sheet pile construction was installed in June and July 2013 [44]. This construction is still present in October 2018, as shown in figure 5.21. Phase 2 of the replacement will be executed on short notice.

Figure 5.21: Temporary sheet pile construction at the Oudezijds Achterburgwal

Available monitoring data and the approach to process the data, will be described in 5.3.1. The results will be shown in section 5.3.2 and the conclusion will be given in section 5.3.3.

5.3.1 Methodology

The methodology to process the levelling and InSAR data is similar to the methodology of the Herengracht as described in section 5.1.1. Therefore only the available deformation measurements are described in this section. The available levelling data is described in section 5.2.1.1, and the available InSAR data is described in section 5.2.1.2.

5.3.1.1 Levelling data

Between Oudezijds Achterburgwal 41 and 149, 43 buildings have been monitored using 69 levelling benchmarks. Due to the occurring problems related to this replacement project, a large amount of levelling data is available. The levelling period varies between the buildings in phase 1 and phase 2. This is indicated in table 5.4. For buildings in phase 1, Oudezijds Achterburgwal 4191, levelling measurements are available between February 2011 and April 2014. For buildings in phase 2, Oudezijds Achterburgwal 93-149, levelling measurements are available between February 2011 and December 2017. The amount of measurements varies among the benchmarks. At least 18 measurements have been taken on each benchmark. Some levelling benchmarks contain more than 60 measurements.

Table 5.4: Available levelling data for the buildings along the Oudezijds Achterburgwal

Area	Start levelling	End levelling
Phase 1	14-02-2011	07-04-2014
Phase 2	14-02-2011	14-12-2017

5.3.1.2 InSAR data

The same InSAR data is available as for the Herengracht, as described in section 5.1.1.2. Only the asc_9y dataset will be useful for the analysis of the Oudezijds Achterburgwal because levelling measurements are conducted between 2011 and 2017. It is decided to use InSAR data covering the same time span as the levelling data. For InSAR points located on buildings in phase 1, this means three

years of InSAR data will used. For InSAR points located on buildings in phase 2, almost eight years of InSAR data will be used.

5.3.2 Results

First, the deformation time series from levelling and InSAR of several buildings in this area are shown in section 5.3.2.1. Subsequently, the results from the overall model test are presented in section 5.3.2.2. After applying the overall model test, the precision of the InSAR data is analyzed in section 5.3.2.3. Next, in section 5.3.2.4, the deformation rates are presented for each building in a building deformation map. Finally, the deformation rate estimate is combined with the variance of this estimate in a probability map in section 5.3.2.5.

5.3.2.1 Deformation time series of several buildings

To analyze the observed deformations, the levelling and InSAR deformations of four buildings, located in phase 1 and phase 2, are shown. These buildings are selected because they provide valuable insight into the observed deformation from levelling and InSAR data. The calculated deformation rate r_{lev} or r_{InSAR}, the standard deviation of the deformation rate σ_r, the test statistic T and the critical value K corresponding to a 95% confidence level are displayed for each time series as well. For this, a conservative measurement variance is used of 0.5^2mm^2 and 3^2mm^2 for the levelling measurement variance $\sigma_{y,lev}$ and the InSAR measurement variance $\sigma_{y,InSAR}$ respectively.

Oudezijds Achterburgwal 65 (Phase 1)
The levelling benchmark in figure 5.22a shows a deformation of about 45 millimeter in 2011 and 2012. The linear deformation model fitted through the measurements is clearly rejected. Therefore the shown deformation rate and variance, r_{lev} and σ_r, should be neglected. The only InSAR point located on this building, figure 5.22b, shows a large amount of noise between 2011 and halfway 2012. Less noise is present from 2012 onwards. No large deformations are observed for the InSAR point. According to the overall model test, the linear deformation model is accepted.

(a)

(b)
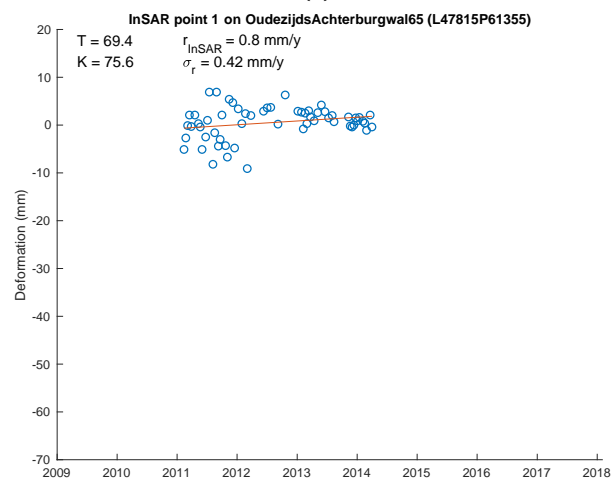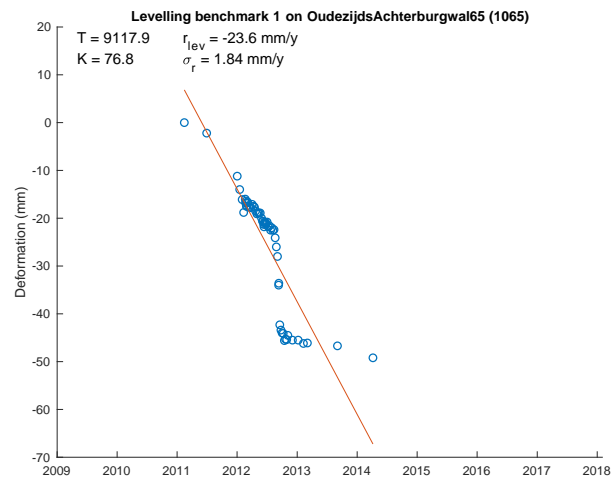
Figure 5.22: Deformations of the levelling benchmark (top) and the InSAR point (bottom) located on Oudezijds Achterburgwal 65

Oudezijds Achterburgwal 91 (Phase 1)

The levelling benchmark on this building indicates large settlements between 2011 and 2014, as shown in figure 5.23a. The linear deformation model is accepted and a deformation rate of -3.9 mm/y is calculated. Compared to the levelling benchmark, a similar deformation rate of -4.5 mm/y is observed for InSAR point 1 in figure 5.23b. However this InSAR point is rejected as the calculated test statistic T is higher than the critical value K. In figure 5.23c, a slightly larger rate of -6.1 mm/y is found for InSAR point 3. The linear deformation model for this point is accepted according to the overall model test.

(a)

(b)

(c)
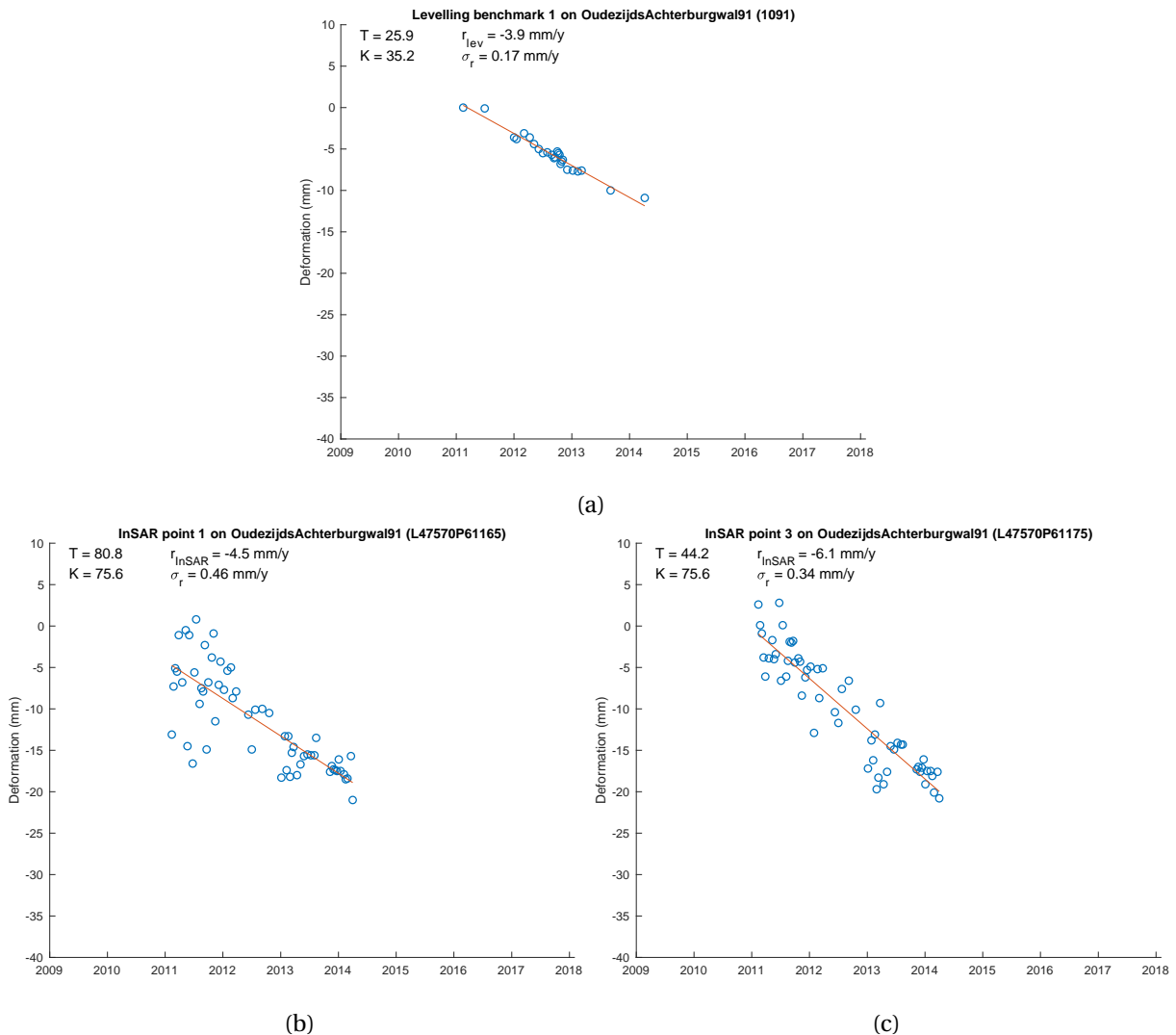
Figure 5.23: Deformations of the levelling benchmark (top) and two InSAR points (bottom left and right) located on Oudezijds Achterburgwal 91

Oudezijds Achterburgwal 133 (Phase 2)

The two levelling benchmarks in figure 5.24a and 5.24b both show a large settlement in 2013. After this, the deformation rate seems to be lower. The deformation of benchmark 1 is significantly larger as benchmark 2. Clearly, a linear deformation model is not applicable for this building, as also indicated by the test statistic T in combination with the critical value K.

Eleven InSAR points are located on this building. Several of these points show an upward deformation in 2013, as shown for InSAR point 4 in figure 5.24d. Other InSAR points, such as InSAR point 2 in figure 5.24c, show a downward deformation in 2013. The deformation rate of the InSAR points seem to be lower as well after 2013. Despite the presence of a deformation shift for both InSAR points, the linear deformation model is accepted according to the overall model test.

(a)

(b)

(c)

(d)
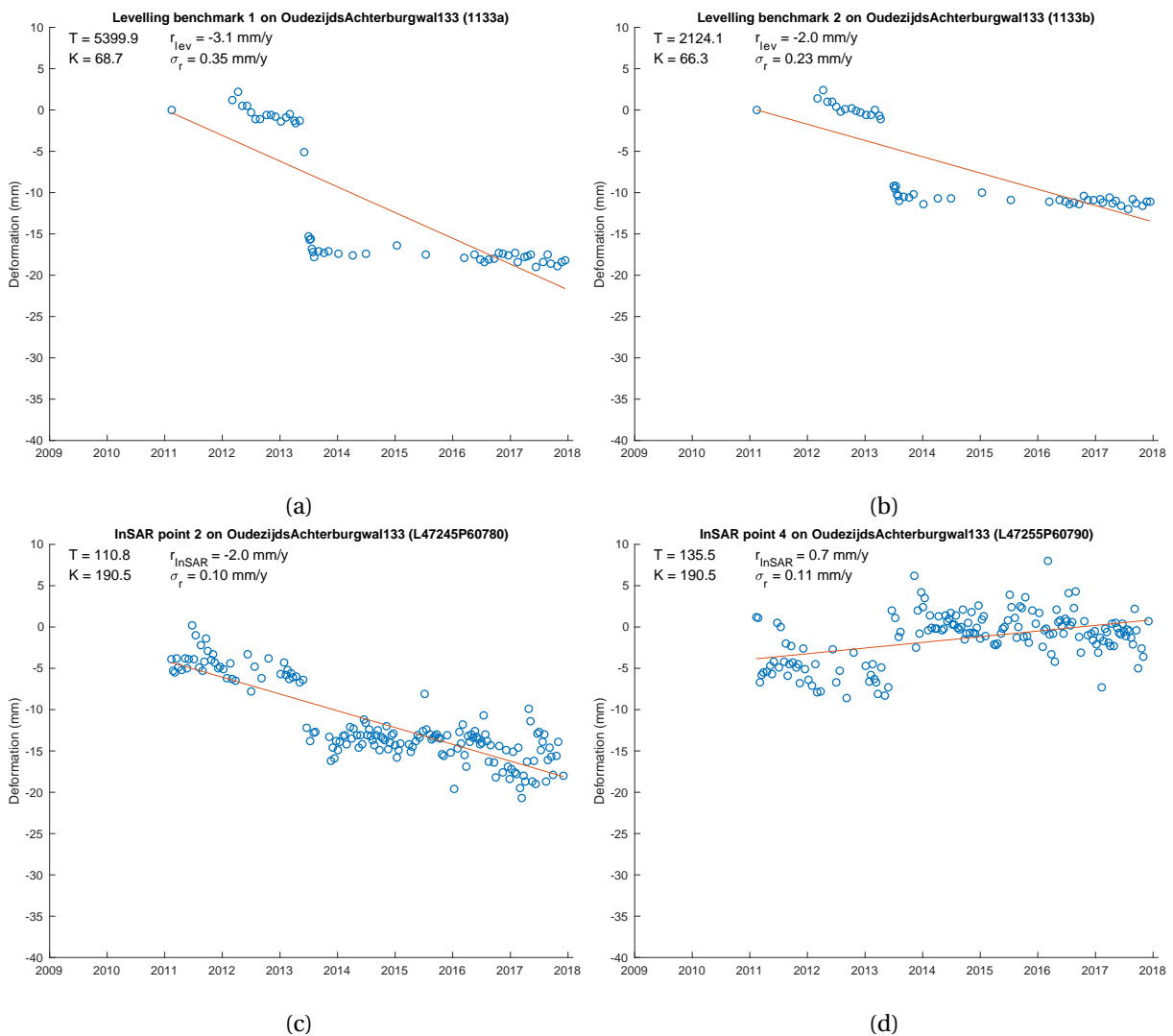
Figure 5.24: Deformations of two levelling benchmark (top left and right) and two InSAR points (bottom left and right) located on Oudezijds Achterburgwal 133

Oudezijds Achterburgwal 149 (Phase 2)

Four levelling benchmarks are installed on this building. Two of these benchmarks are shown in figure 5.25a and 5.25b. Very small deformations are observed for this building. This is also visible in the InSAR data. On this building, 27 InSAR points are present. Two InSAR points are shown in figure 5.25c and 5.25d. The linear deformation model is accepted for all four time series. Similar deformation rates are obtained from the levelling and InSAR data.
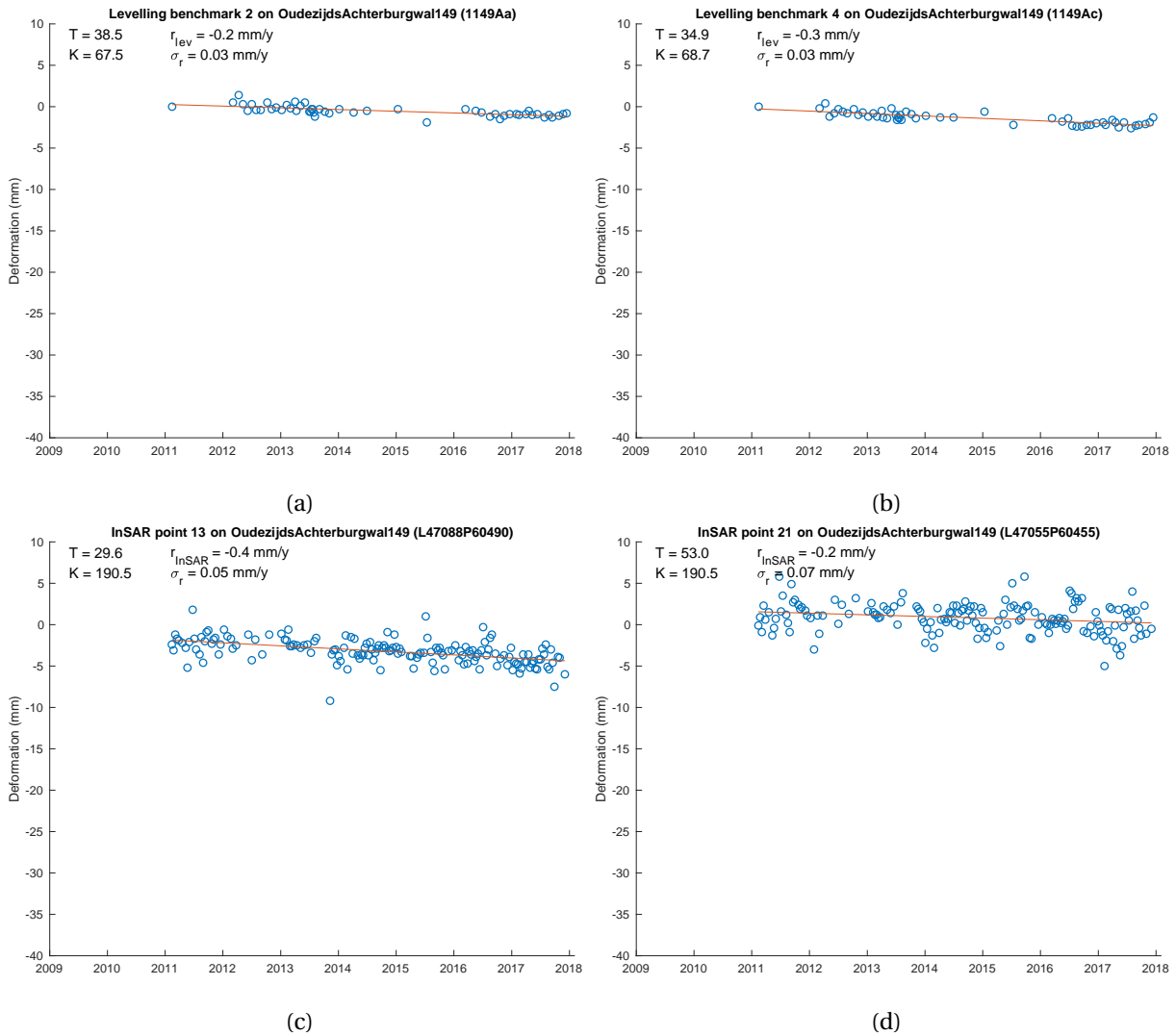
Figure 5.25: Deformations of the two levelling benchmark (top left and right) and two InSAR points (bottom left and right) located on Oudezijds Achterburgwal 149

5.3.2.2   Overall model test

An overall model test is performed to test whether the deformation model fits the observations. As the deformation time series in the previous section showed, the linear deformation model needs to be rejected in some cases. The results of the overall model test for the levelling and InSAR datasets are shown in table 5.5. A conservative measurement variance $\sigma^2_{y,a-priori}$ of 0.5^2 and 3^2 is used for the levelling and InSAR data respectively. Furthermore, a critical value K corresponding to a confidence level of 95%, is used.

The results show that the linear deformation model needs to be rejected for many levelling benchmarks. For buildings in phase 1 and phase 2, 59% and 61% of the levelling benchmarks is rejected, respectively. The corresponding InSAR data shows 26% and 22% of the InSAR points must be rejected in phase 1 and phase 2, respectively.

Table 5.5: Results of the overall model test for the Oudezijds Achterburgwal

Dataset	Area	Measurement variance $\sigma^2_{y,a-priori}$	Total number of points	Number of points rejected	Percentage of points rejected
Levelling	Phase 1	0.5^2	29	17	59%
InSAR asc_9y	Phase 1	3^2	80	21	26%
Levelling	Phase 2	0.5^2	36	22	61%
InSAR asc_9y	Phase 2	3^2	140	31	22%

5.3.2.3   A-posteriori precision analysis

After the linear deformation model is accepted according to the overall model test, the InSAR measurement variance is calculated. The a-posteriori variance calculation is described in section 5.1.1.3.

The calculated standard deviation of the InSAR points located on the buildings in phase 1 and phase 2, are shown in figure 5.26a and figure 5.26b respectively. The average standard deviation for both areas is roughly 2.4 millimeter. All standard deviations are between 1 millimeter and 3.5 millimeter.

(a)   (b)
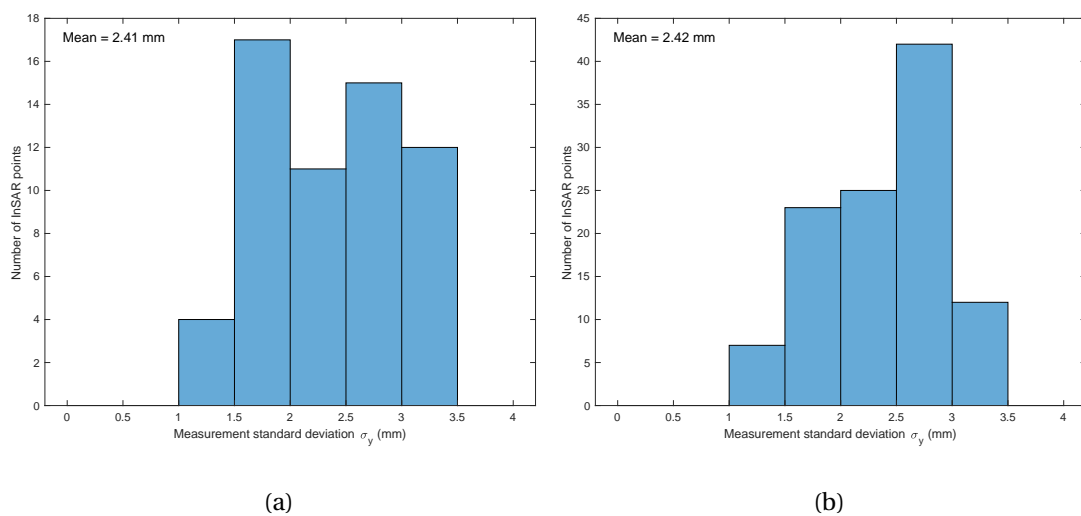
Figure 5.26: Histograms of the measurement variance of the InSAR points on the considered building along the Oudezijds Achterburgwal, for buildings in phase 1 (left) and buildings in phase 2 (right)

5.3.2.4 Building deformation map

Due to performed overall model test, only time series with linear deformation are left. The selection of these deformation time series allows for comparison of levelling and InSAR deformation rates. The calculated levelling and InSAR deformation rates are averaged for each building. To quantify the difference between the levelling and InSAR deformation rates, the mean absolute error (MAE) is calculated. It provides a measure of the average magnitude of the difference between the calculated values. It is calculated by

$$MAE = \frac{1}{n} \sum_{j=1}^{n} |r_{InSAR,average,j} - r_{lev,average,j}|, \tag{5.14}$$

where n is the number of buildings and $r_{InSAR,average}$ and $r_{lev,average}$ are the average deformation rates of each building derived from InSAR data and levelling data respectively.

Figure 5.27 and figure 5.28 shows the results of phase 1 and phase 2, obtained from levelling and InSAR data. The results are combined in one graph in figure 5.29. This graph depicts the difference between the two monitoring methods. Due to the rejectance of many levelling benchmarks with the overall model test, no deformation rate is calculated for many of the buildings. In total, for 21 of the 43 considered buildings, no deformation rate is calculated with levelling. With the InSAR data, no deformation rate was calculated for six of the 43 buildings. Largest deformation rates are calculated for buildings in phase 1. Some buildings show more than 1 mm/y difference between levelling and InSAR.
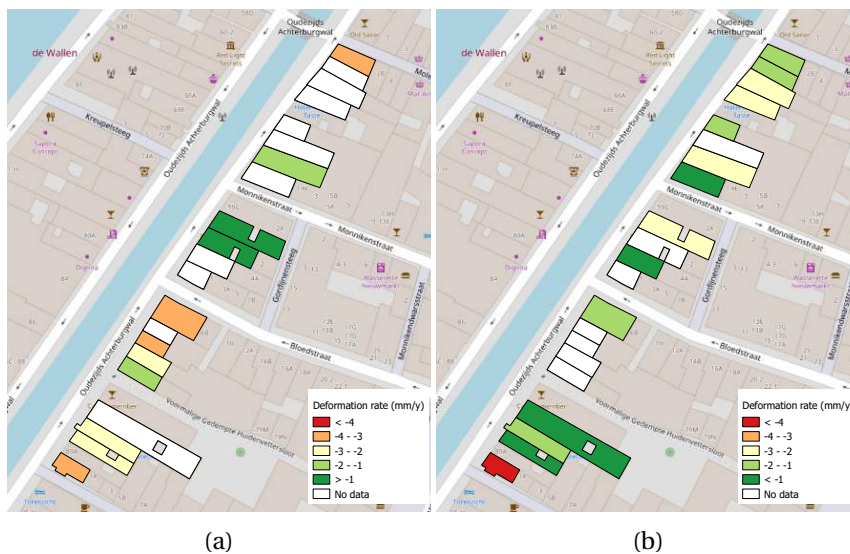
Figure 5.27: Average building deformation rate for buildings in phase 1 along the Oudezijds Achterburgwal from levelling data (left) and InSAR data (asc_9y)(right), between February 2011 and April 2014
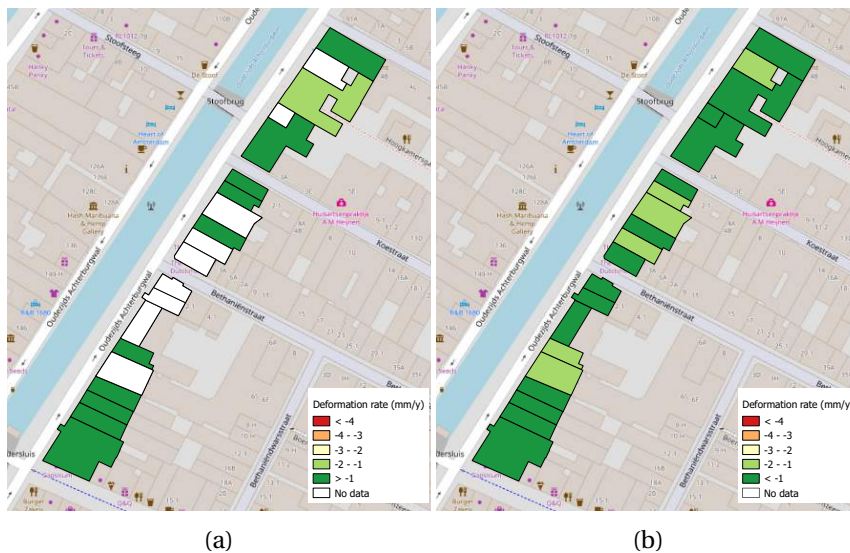
Figure 5.28: Average building deformation rate for buildings in phase 2 along the Oudezijds Achterburgwal from levelling data (left) and InSAR data (asc_9y)(right), between February 2011 and December 2017
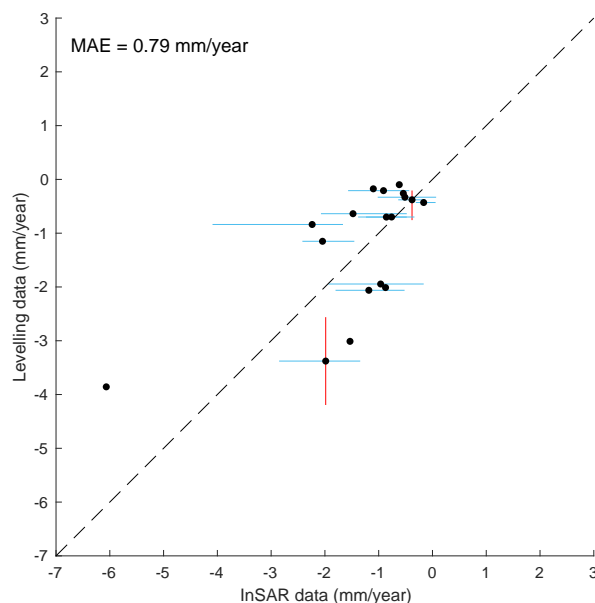
Figure 5.29: Graph of calculated deformation rates from the levelling data and the InSAR data (asc_9y) for the buildings in phase 1 and phase 2 of the Oudezijds Achterburgwal

5.3.2.5   Probability Map

In this section, the probability maps are shown for InSAR points located on the considered buildings in phase 1 and phase 2. This is shown in figure 5.30. The map only shows InSAR points for which the linear deformation model is accepted with the overall model test. The method to obtain this probability from the deformation time series is described in section 5.1.1.5. The probability is calculated for a deformation rate of -2 mm/y, which is used as threshold for moderate building movement in the building protocol, as described in 2.3.

Many of the InSAR points in phase 1 show a probability of more than 5% for a true deformation rate

of -2 mm/y. The probability map of phase 2 shows, in general, low probabilities. On one or two buildings, several red points are located.
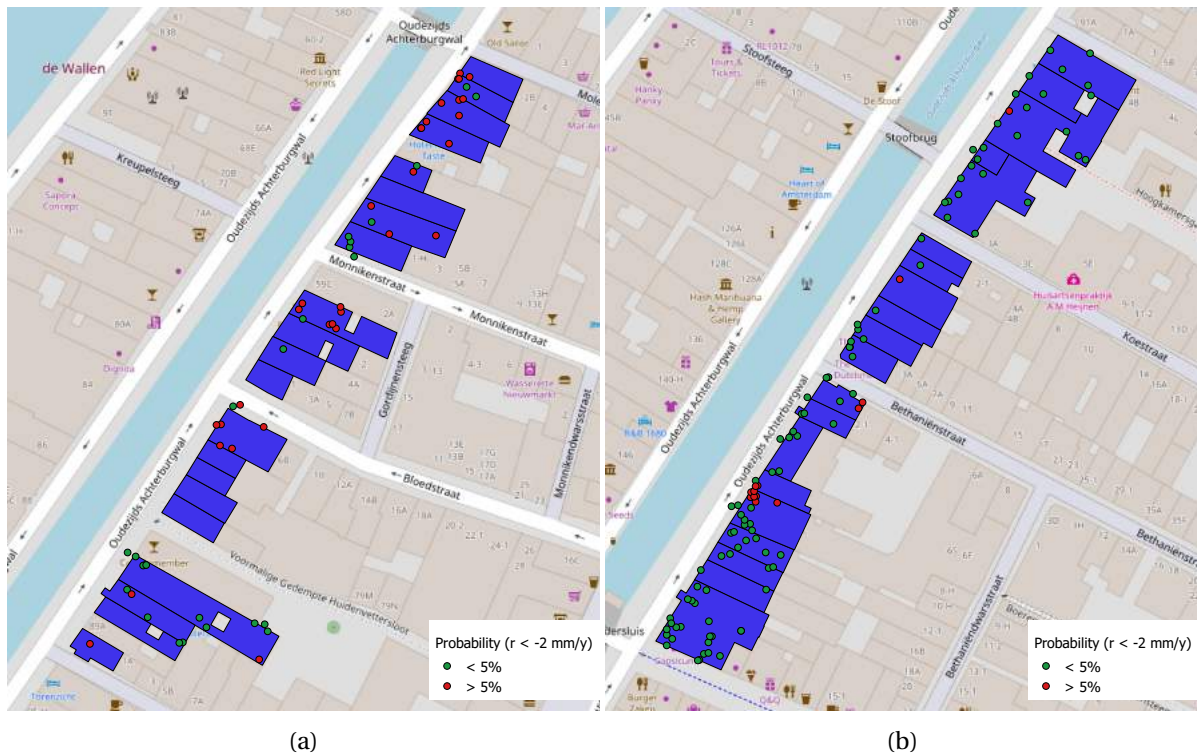
Figure 5.30: Probability of a deformation rate of more than -2 mm/y based on the calculated σ_r for each InSAR point of buildings in phase 1 (left) and phase 2 (right)

5.3.3   Discussion and Conclusion

A large amount of levelling data is available for this area. The area is subdivided in two phases. In phase 1, the buildings are monitored more than three years. The buildings in phase 2 are monitored almost eight years. Accordingly, InSAR data is selected covering the same time span as the levelling data.

Some of the levelling benchmarks in this area show a increased downward deformation deformation between 2011 and 2013. This is visible for Oudezijds Achterburgwal 65 and 133. This is suggested to be related to the construction activities in this period. The sudden downward deformation present in the levelling data sometimes appears in the InSAR data as an upward deformation, as can be seen for Oudezijds Achterburgwal 133. This upward deformation can be attributed to the phase unwrapping procedure during processing of the InSAR observations. The deformations depicted from halfway 2013 onwards, should therefore be shifted, at least, half a wave length (15.5 millimeter) downwards. The deformation shift indicates a large deformation is present and should be seen as a large deformation warning.

The results of Oudezijds Achterburgwal 65 show that not all InSAR points provide valuable information. A large variation of roughly 15 millimeter is present between 2011 and halfway 2012. This indicates incoherent observations and should therefore be disregarded. Probably, no stable scatterer was present in this time span.

Due to the construction activity, a linear deformation model is rejected for many levelling benchmarks. In the overall model test about 60% of the present benchmarks is rejected. For the InSAR data, roughly 25% of the InSAR points is rejected. This is related to the relatively large measurement variance present in the InSAR data. As the deformation time series of Oudezijds Achterburgwal 133

showed, the linear deformation model is accepted despite the deformation shift present in the data. This indicates that a visual assessment of the InSAR data is essential to detect these deformation shifts. For the accepted InSAR points according to the overall model test, an average measurement variance of 2.4^2mm^2 is calculated.

The average deformation rate is calculated for each building. Differences up to 2 mm/y are calculated between the levelling and InSAR data. The average difference is 0.79 mm/y. The largest deformation rate is calculated for Oudezijds Achterburgwal 91. A deformation rate of -3.9 mm/year is calculated with levelling while a deformation rate of -6.1 mm/y is obtained with InSAR. This is most likely the result of non-uniform building settlement. Non-uniform settlement behaviour can also be observed for Oudezijds Achterburgwal 133. For the levelling benchmarks on this building a deformation difference of several millimeters was observed.

In general, the InSAR data provides valuable information about the deformation behaviour of the buildings which is consistent with the levelling data. The detection of large sudden deformation is problematic in the current InSAR dataset. This is related to the phase unwrapping procedure during processing of the InSAR data. As a result, the presented deformation rate can be incorrect. However, these phase unwrapping errors can be seen in the InSAR deformation time series.

6

Case Spoorsingel Delft

On the east side of the Spoorsingel an underground underground parking facility has been constructed between 2015 and 2018. The underground parking facility is located close to the buildings along the Spoorsingel. Several techniques are used to analyse the occurring deformations of these buildings before and during construction. Levelling benchmarks have been installed on the façades of the buildings several years before construction started. During construction, the movement of buildings is also monitored with manual measurements of prisms installed on the buildings. In addition, InSAR data is available for analysing the deformations.

Using the abovementioned monitoring techniques, the deformation mechanism of the buildings along the Spoorsingel is assessed in section 6.2. Afterwards, the analysis of InSAR data of the Spoorsingel will be extended by calculation of the three-dimensional deformations. This is described in section 6.3. In section 6.4, the damage due to construction of the underground parking facility is evaluated. For this, the building damage of five buildings along the Spoorsingel is reported. The discussion and conclusions are treated in each section separately.

Figure 6.1: Project area for the Spoorsingel underground parking facility

6.1   Underground Parking Facility Construction

The Spoorzone project in the Delft municipality consists of the construction of a new railway tunnel, the new design of the public space and the redevelopment of free space acquired by underground construction of the public transportation [35]. As part of the Spoorzone project a new underground underground parking facility has been realised. Figure 6.1 shows the project area where the underground parking facility has been constructed.

Preparative works were carried out in 2014 [16]. The construction started halfway 2015 [17]. Diaphragm walls were installed to a depth of 24 m [17]. The underground parking facility is in use since the 5th of may 2018 [32]. The garage consists of two levels and provides 650 parking spots [32]. A small canal now covers the underground parking facility. The underground parking facility has been called the Prinsenhofgarage.

6.2   Monitoring data

This section is subdivided in five parts. Section 6.2.1, 6.2.2, 6.2.3 describe the available data and results from levelling, mini prisms and InSAR data respectively. A discussion of the results and the main conclusions are given in section 6.2.5.

6.2.1   Levelling data

Levelling benchmarks have been installed on some buildings along the Spoorsingel at around 30 cm from the ground. The benchmarks are installed on buildings in the northern part of the project area and are shown in figure 6.2. The baseline measurement was made in March 2010. The next measurements were conducted in February 2015, 2016 and 2017.

Figure 6.2: Positions of the levelling benchmarks

Results

An overview of the measured deformations is given in figure 6.3. The measurements are ordered based on the distance of the levelling benchmarks to the underground parking facility. Generally, the observed deformation between 2010 and 2015 is small with less than 5 millimeter settlement for most benchmarks. The observed deformation between 2010 and 2015 is expected to be a caused by autonomous settlement. Between February 2015 and February 2016 the deformation increases

significantly for most levelling benchmarks. Between February 2016 and February 2017 comparable deformations as the year before are observed. Most benchmarks within 15 meter distance of the underground parking facility show deformations between 15 and 20 millimeter. The deformation of Spoorsingel 98 and 99 (SS9900, SS9800, SS9801) is exceptionally large with deformations up to 45 millimeter. These buildings are located on the northernmost part of the project area. Furthermore, with increasing distance to the underground parking facility, the levelling benchmarks on the right side of the figure show much smaller deformation between February 2015 and February 2017.

Figure 6.3: Deformations of the levelling benchmarks and the distance of the levelling benchmarks to the underground parking facility

To further analyse the deformation behaviour, we zoom in on two adjacent buildings, Spoorsingel 78 and 79. Multiple levelling benchmarks are installed on these buildings. Figure 6.4 shows Spoorsingel 78 and 79 and the levelling benchmarks positions. The corresponding levelling data is shown in Figure 6.5. The deformations are largest on the northeast side of the buildings, closest to the underground parking facility. Significantly larger vertical deformations are measured at levelling benchmarks SS7903, SS7904 and SS7800 compared to the deformations at levelling benchmarks SS7902 and 7801. As expected, the deformations as indicated by the levelling data are related to the distance to the garage. This results in differential settlement of the buildings along the Spoorsingel.

Figure 6.4: Location of the levelling benchmarks on Spoorsingel 78 and 79
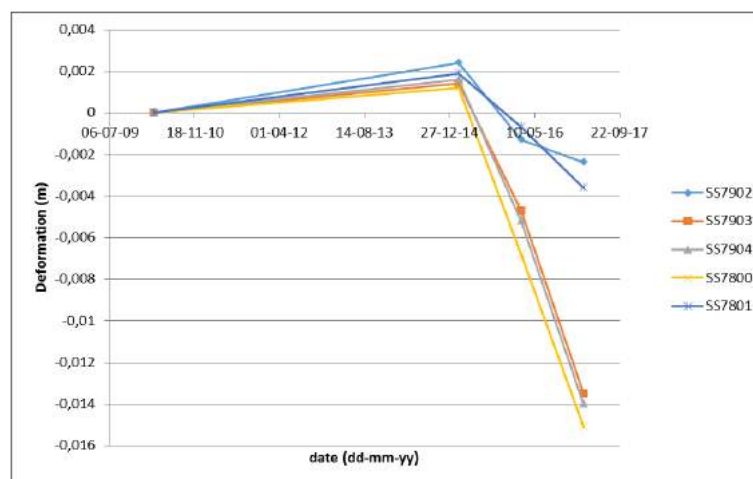
Figure 6.5: Deformations observed at the levelling benchmarks indicated in figure 6.4 on Spoorsingel 78 and 79

6.2.2 Mini prisms

During construction, the position of mini prisms installed on the building walls was manually measured. Buildings were subdivided into several compartments for a staged construction and the related monitoring. The measurements are made at predefined discrete moments of the construction works. Five measurement moments have been defined during construction of the underground parking facility:

- Before construction

- After Installation of diaphragm walls

- After excavation to roof of the garage

- After excavation to struts halfway

- After excavation to deepest level

The dates at which these measurements are conducted differs per compartment. The buildings along the Spoorsingel are located in two compartments. For building Spoorsingel 78 and 79, the mini prisms

were monitored on: 10-03-2015, 13-10-2015, 13-01-2016, 23-02-2016 and 10-05-2016. The location of the mini prisms is shown in figure 6.6.
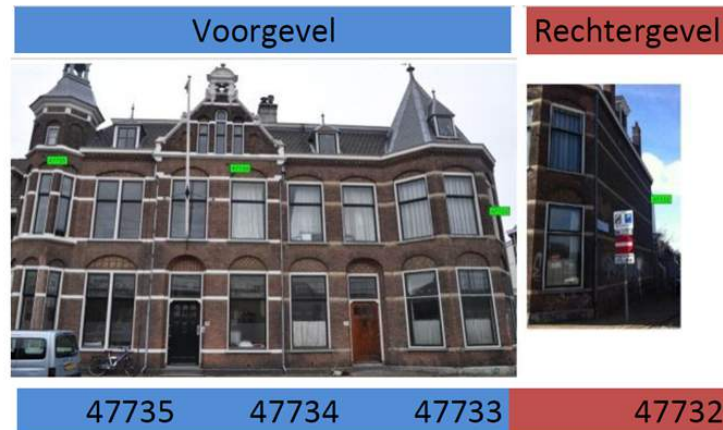
Figure 6.6: Position of the mini prisms (green rectangles) on the walls of Spoorsingel 78 and 79

Results

The measured deformations of the prisms are shown in figure 6.7. Over a period of 14 months, a vertical deformation between roughly 8 and 10 mm is observed on the front of the building (prisms 47735, 47734, 47733). The prism on the side wall (prism 47732) of Spoorsingel 79 shows less than 3 mm vertical deformation. The difference in deformation of the prisms on the front wall and the side wall suggests tilting of the buildings towards the underground parking facility.
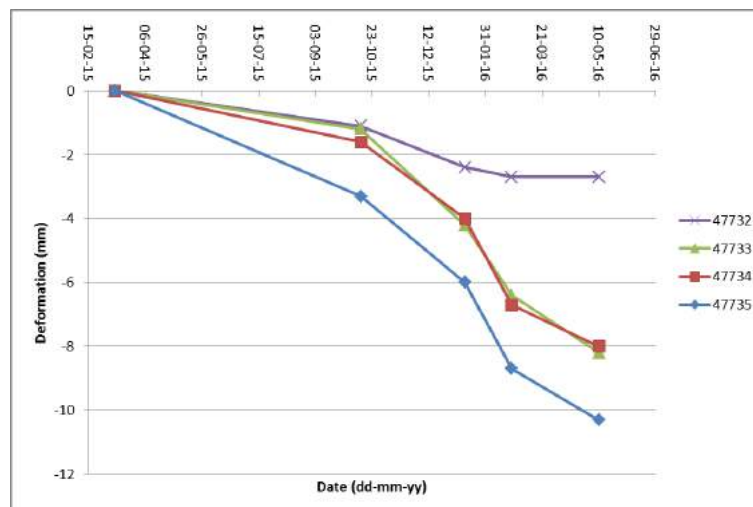
Figure 6.7: Vertical deformation of the mini prisms located on Spoorsingel 78 and 79

6.2.3 InSAR data

The InSAR data of this area contains four datasets with TerraSAR-X observations. Two datasets, from an ascending and descending track, span the time period 2009-2017 and two datasets, from an ascending and descending track, span the time period 2015-2017. Each dataset consists of four subsets: PS high points, PS low points, DS high points and DS low points. PS and DS stand for persistent scatterer and distributed scatterer respectively. Only PS high point subsets are used in the analysis. The specifications of the four datasets are given in table 6.1. All datasets give vertical deformations which have been calculated using the incidence angle and assuming no horizontal deformations.

Table 6.1: Specifications of the available InSAR datasets

Name	Acquisition period	Number of observations	Heading angle	Incidence angle
asc_9y	06-04-2009 19-12-2017	190	350°	39.3°
dsc_9y	08-04-2009 01-01-2018	250	192°	24.1°
asc_2y	15-01-2016 19-12-2017	64	350°	39.3°
dsc_2y	06-01-2016 01-01-2018	64	192°	24.1°

Results

An overview of the available InSAR data of 9 years (dataset asc_9y and dsc_9y) and of 2 years (dataset asc_2y and dsc_2y) is shown in figure 6.8. The 9 year InSAR data shows low deformation rates; Deformation rates between -1 and -2 mm/year are observed. The 2 year InSAR data shows relatively high deformation rates on the west side of the underground parking facility, especially at the northern part of the area.
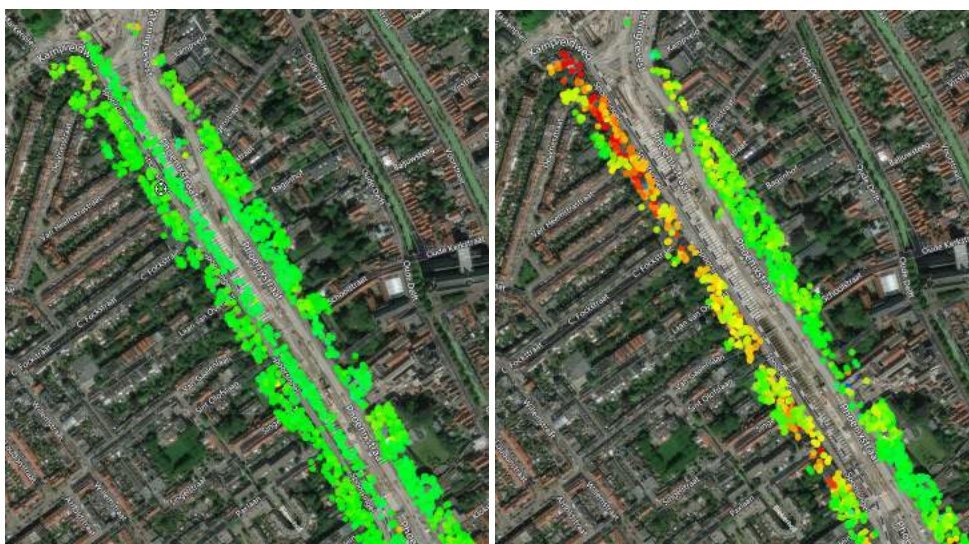
Figure 6.8: Deformation rates close to the underground parking facility of the 9 year InSAR data (left) and the 2 year data (right) of the ascending and descending tracks. Green, yellow, orange and red points indicate deformation rates higher than 0, 3, 5 and 8 mm/year respectively.

To analyse the difference between the 9 year and 2 year data, one point is selected in the dsc_9y and dsc_2y datasets as shown in figure 6.9. As the figure shows, the position of the points in both datasets is almost the same. Therefore it is likely that both points represent the same scatterer. The deformations of these points is shown in figure 6.10. The 2 year dataset, figure 6.10b, shows a constant deformation in 2016 and 2017 with, in total, about 19 mm of deformations. The deformation in this dataset is increasing, which is expected, due to the construction activity. In figure 6.10, the 9 year dataset shows an abrupt change in deformation. This upward shift can be attributed to the phase ambiguity of the InSAR data. The deformation rate, which is based on the line fitted through the observations, is consequently incorrect. Considering the 15 mm phase shift (half a wave length) in the 9 year dataset, similar deformations can be derived from both InSAR datasets. The 2 year dataset is used for further analysis.

Figure 6.9: InSAR data points in the northern part of the project area of the descending track of both the 2 year and 9 year dataset. A data point is indicated in both datasets which has almost exactly the same position.

(a)

(b)
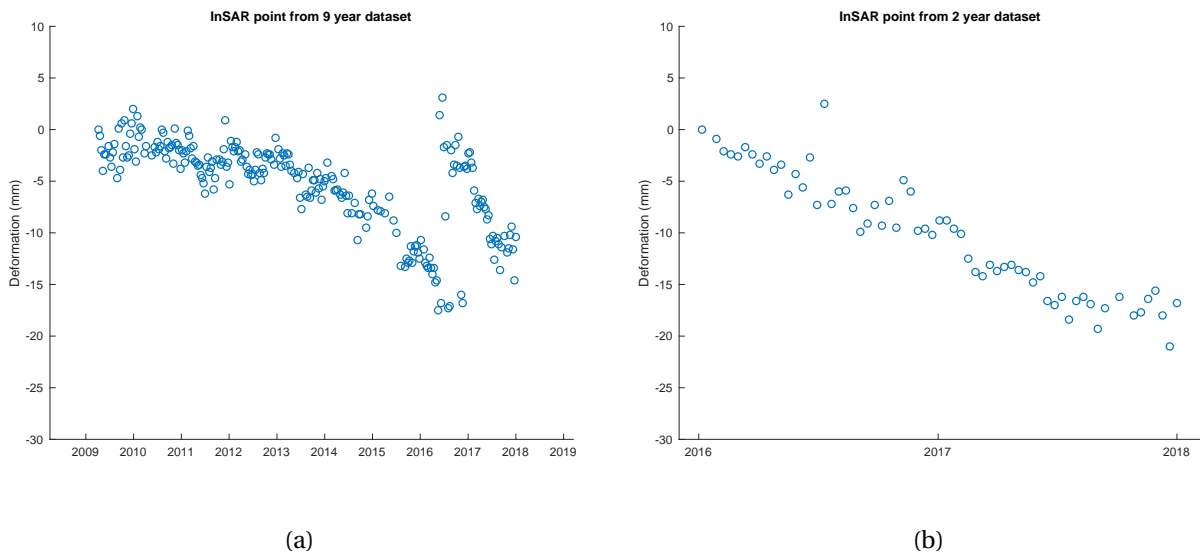
Figure 6.10: Deformation time series of two InSAR points which is likely to be the same scatterer in both datasets. Note the difference in time interval of the two datasets, the 9 year time series is shown on the left and the 2 year dataset is shown on the right.

The northern part of the ascending and descending track of the 2 year dataset is shown in figure 6.11a and figure 6.11b respectively. Due to the right-looking characteristic and the almost polar orbit of the TerraSAR-X satellite, the ascending dataset contains reflection points located mainly on the southwest side of the buildings and the descending dataset contains reflection points located on the northeast side. The figures clearly show larger deformation rates for the ascending track than for the descending track. The difference between the ascending and descending track is also clearly visible when looking at building Spoorsingel 78 and 79 specifically, as shown in figure 6.12.

This difference can be explained based on the viewing geometry of the two tracks as shown in figure 6.13. The ascending track records larger deformations due to tilting of the buildings in the direction away from the line of sight. The descending track however measures smaller deformations due to the deformation in the direction of the descending track line of sight.

(a)   (b)
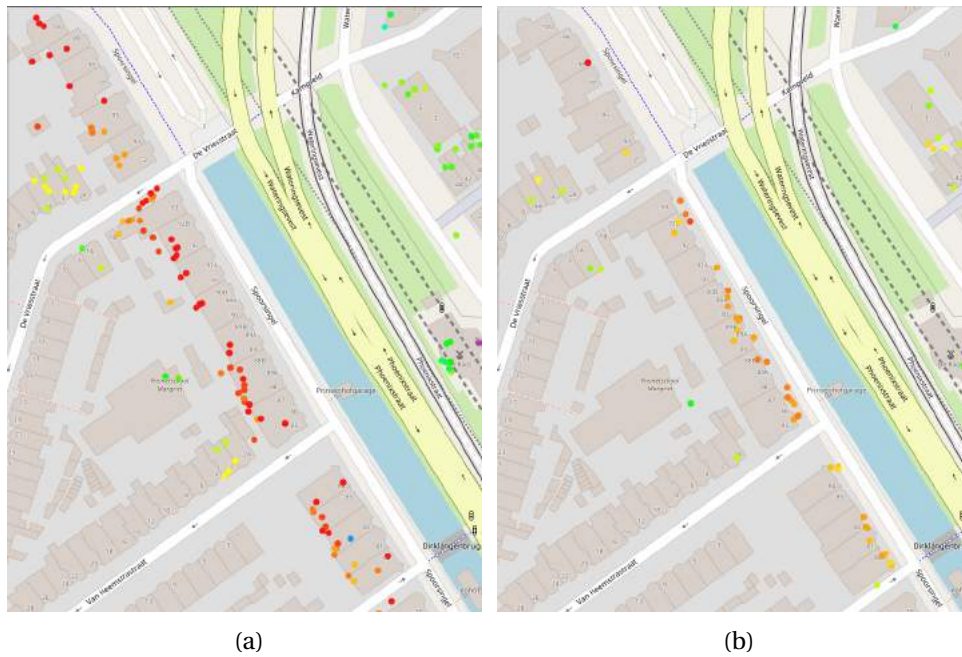
Figure 6.11: The northern part of the project area indicating the InSAR data points of the ascending (left) and descending (right) track. Green, yellow, orange and red points indicate deformation rates higher than 0, 3, 5 and 8 mm/year respectively.

Figure 6.12: InSAR points on buildings Spoorsingel 78 and 79 of the ascending (left) and descending (right) track
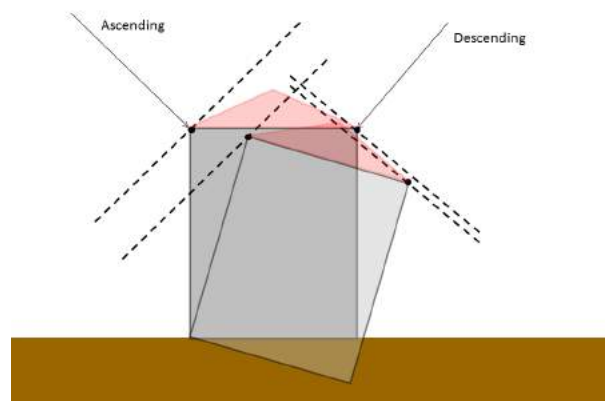
Figure 6.13: Effect of viewing geometry on line of sight measurements of the ascending and descending satellite track

6.2.4   Comparison of results

The different monitoring period of the monitoring techniques makes a comparison of observed displacements of the three monitoring techniques impossible. Only the levelling data has a significant

overlapping monitoring period with the 2 year InSAR dataset. Therefore only levelling and InSAR are compared.

For the comparison, the displacements are used between February 2016 and February 2017. A linear line is fitted through the observed deformations from levelling and InSAR. Figure 6.14a and figure 6.14b show an example of the linear model fitted through the deformations from levelling and InSAR respectively. This way a deformation rate is obtained which can be easily compared. When multiple levelling or InSAR points are located on one building, an average deformation rate is calculated. For the InSAR data, all data points within a 2 m radius of the buildings are selected, to account for the location precision of InSAR. The ascending and descending track are considered separately due to the large difference between the two, as mentioned before.

To compare the determined deformation rates from levelling data and InSAR data, the mean absolute error (MAE) is calculated. This value provides a measure of the average magnitude of the difference between the calculated values. It is calculated as follows:

$$MAE = \frac{1}{n} \sum_{j=1}^{n} |r_{sat,j} - r_{lev,j}| \tag{6.1}$$

Where r_{sat} and r_{lev} are the deformation rates derived from InSAR data and levelling data respectively.

(a)   (b)
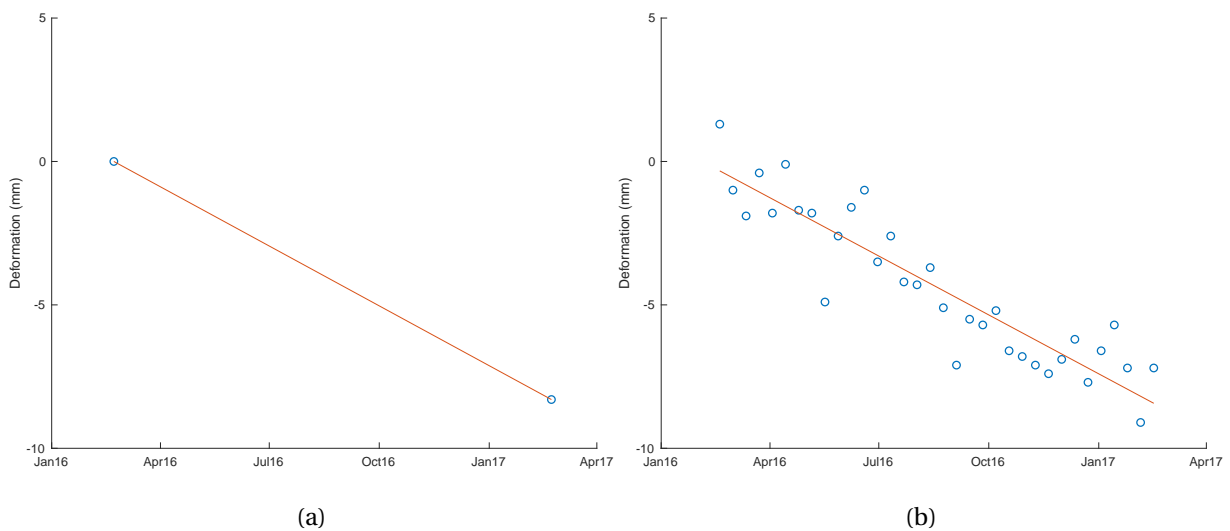
Figure 6.14: Deformations of a levelling point (left) and an InSAR point (right) and the linear line fitted through the data using least-squares

The comparison between the deformation rates obtained from levelling and the ascending and descending track is shown in figure 6.15 and 6.16. The lines through the points indicate the variation of the obtained deformation rates of each building. A fairly large mean absolute difference between the levelling data and the ascending track of 5.10 millimeter/year is observed. The descending track shows larger resemblance with the levelling as the ascending track. Between the levelling and descending track a mean difference of 3.14 millimeter/year is calculated.

The difference between the InSAR data and the levelling data is largest for Spoorsingel 98 and 99. The levelling benchmarks on these two buildings provide deformations of roughly -26 and -32 millimeter between February 2016 and February 2017. Spoorsingel 99 is not visible in figure 6.16 because no InSAR point was present on this building in the descending dataset.
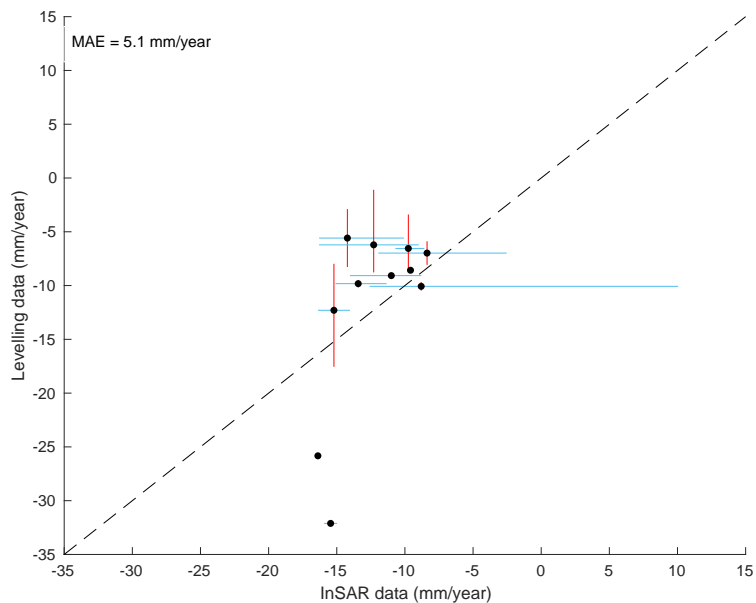
Figure 6.15: Graph of calculated deformation rates from the levelling data (left) and the ascending track of the InSAR data (right) (asc_2y), between February 2016 and February 2017
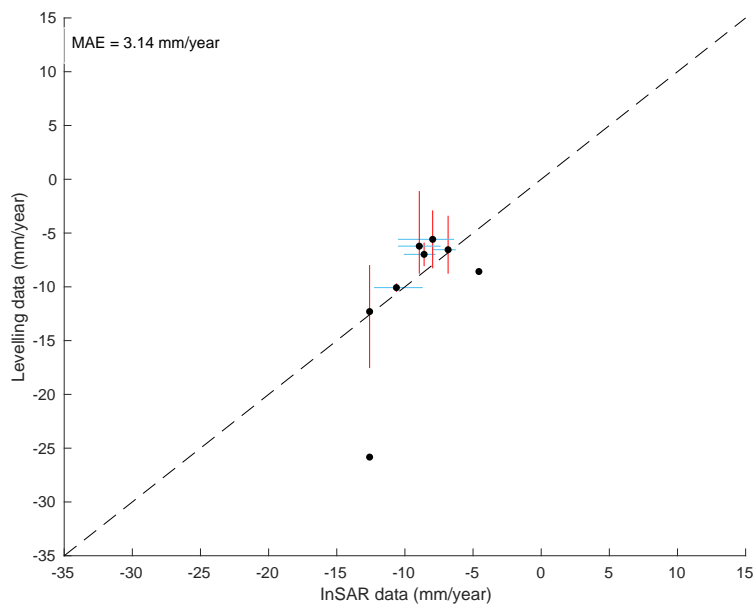
Figure 6.16: Graph of calculated deformation rates from the levelling data (left) and the descending track of the InSAR data (right) (dsc_2y), between February 2016 and February 2017

6.2.5 Discussion and Conclusion

Comparison of the 2 year and 9 year InSAR dataset shows the significance of the time interval of the InSAR data on the processing of the time series and the resulting deformations. When the deformation behaviour changes within the processed time period, errors can occur during processing of the InSAR data, in the phase unwrapping procedure.

The analysis of Spoorsingel 78 and 79 shows a comparable deformation mechanisms for the three monitoring techniques. For all three methods, differential settlement of these buildings is observed. The vertical deformations are largest on the side of the building closest to the new underground parking facility. Significantly smaller deformations are observed on the side of the building farthest away from the garage. This indicates tilting of the buildings along the Spoorsingel towards the underground parking facility. The tilting can be explained based on the construction. A large building pit was realized using diaphragm walls. The horizontal deformation of the diaphragm wall causes stress changes in the soil nearby and results in soil movement. Deformations decrease with increasing distance to the underground parking facility. The observed differential settlement is an important indicator for damage occurring to a building. Therefore the building damage due to the construction of the underground parking facility is assessed in section 6.4.

The comparison between levelling and the 2 year ascending and descending track show large differences (a mean absolute difference of 5.10 and 3.34 mm/year respectively). There are several reasons for this difference. First of all, the difference between levelling and InSAR is partially caused by the conversion from the line of sight deformations to vertical deformations. To calculate the vertical deformations from the line of sight deformations, it is assumed the horizontal deformations are negligible. However, as was observed in monitoring data, considerable horizontal deformations have occurred. For horizontal building deformation away from the line-of-sight (the ascending track) the vertical deformation is overestimated. For horizontal building deformation towards the line-of-sight (the descending track) the vertical deformation is underestimated. Besides, the rotation of the building results in varying vertical deformation depending on the location and height of the measurement point. This may result in larger and smaller vertical deformation of the InSAR point with respect to the levelling benchmark.

6.3 Three-dimensional deformations

The InSAR line of sight deformations are often directly converted to vertical deformations using the incidence angle. This assumes the horizontal deformations are neglible. However, in some situations the deformation might be three-dimensional. For example, a building might deform significantly in both vertical and horizontal direction next to a quay wall or next to a large excavation, as shown in section 6.2. Following the geometric sensitivity analysis of Chang et al. [11], a method is devised to allow for the calculation of 3D deformations and the analysis of sensitivity. This is specifically meant for buildings alongside excavations or other objects causing horizontal deformations.

The abovementioned situation of a row of houses along an excavation is shown in figure 6.17, with a global reference system in East, North and Up direction. To determine the 3D deformation of a building, an assumption must be made about the direction of deformation, as mentioned in section 4.6. For simplicity, it can be assumed that the excavation or quay wall has an infinite length. This results in a plane strain situation with no deformation in longitudinal direction.
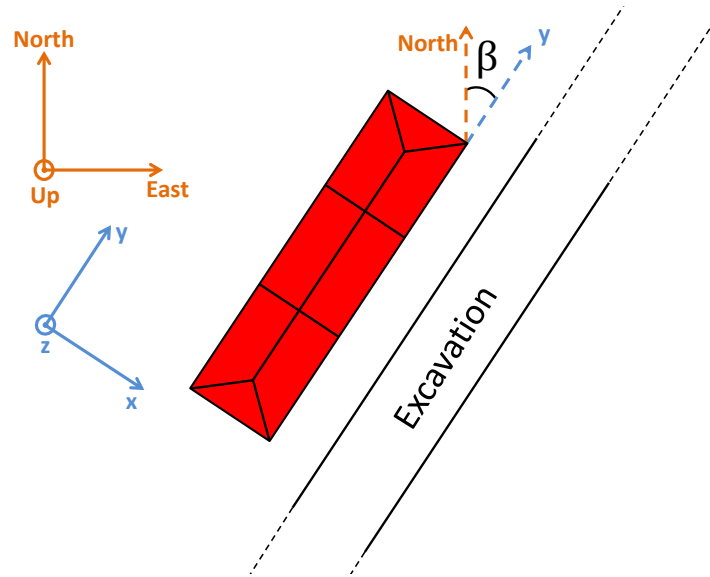
Figure 6.17: Top view of a row a houses along an excavation,

To distinguish this assumed direction of horizontal deformation, the global reference system (East, North, Up) must be rotated to a local reference system of the particular building (x, y, z) as shown in figure 6.17. This requires a rotation around the vertical axis and can be achieved using rotation matrix R_1:

$$R_1 = \begin{bmatrix} cos\beta & sin\beta & 0 \\ -sin\beta & cos\beta & 0 \\ 0 & 0 & 1 \end{bmatrix} \tag{6.2}$$

In this equation β is defined as the smallest angle of the longitudinal direction of the excavation with respect to the north.

Also, the line of sight measurements need to be projected on the global coordinate system (East, North, Up). For this, a projection vector p is used:

$$p = \begin{bmatrix} -sin\theta cos\alpha \\ sin\theta sin\alpha \\ cos\theta \end{bmatrix} \tag{6.3}$$

In this equation θ is the incidence angle and α is the heading of the satellite track.

The line of sight deformation d_{LOS} can now be obtained using:

$$d_{LOS} = p^T R_1 d_{building} \tag{6.4}$$

In this equation the deformation of the building is defined as $d_{building} = [d_x \ d_y \ d_z]^T$.

Then, by using two different viewing geometries (ascending and descending track) and the assumed zero deformation in y-direction, formula 6.4 can be written as a system of equations:

$$\begin{bmatrix} d_{LOS,asc} \\ d_{LOS,dsc} \\ d_y \end{bmatrix} = \begin{bmatrix} p_{1,asc} & p_{2,asc} & p_{3,asc} \\ p_{1,dsc} & p_{2,dsc} & p_{3,dsc} \\ 0 & 1 & 0 \end{bmatrix} \begin{bmatrix} d_x \\ d_y \\ d_z \end{bmatrix} \tag{6.5}$$

In this equation $p_{1,asc}$ is the first entry of the projection vector of the ascending track. This formula allows for the calculation of 3D deformation of buildings in plane strain situations.

Sensitivity

The method described in section 6.3 enables the calculation of the line of sight deformation sensitivity. The LOS unit vector can be projected onto the local reference system (x,y,z). The length of the projection onto the local reference system in a certain direction can be seen as a measure of observability of the deformation. This is called the sensitivity. The sensitivity analysis is performed for two TerraSAR-X tracks as shown in table 6.2. Two situations are considered: the longitudinal direction of the excavation northwards $\beta = 0°$ and the longitudinal direction of the excavation eastwards, $\beta = 90°$.

Table 6.2: Specifications of the used satellite tracks

Track	Heading angle	Incidence angle
TSX, ascending	349°	31.1°
TSX, descending	191°	35.4°

The results are shown in figure 6.18b and figure 6.19b. The angle indicated in the figures is the direction of deformation in the East,Up-plane and North,Up-plane respectively. Because of symmetry, only half a circle is drawn. Both figures show high sensitivity, larger than 0.8, for vertical deformations. For a standard deviation of 1 mm in line-of-sight direction, a sensitivity value of 0.86 in vertical direction translates to a standard deviation of 1.16 mm. Figure 6.18b shows the horizontal deformation in east- and west-direction is decreased by almost half. Figure 6.19b shows a reduction in sensitivity to roughly 0.1 in north- and south-direction. This indicates a very inaccurate estimation of the deformation of horizontal deformations in north and south direction, which was also mentioned in section 4.7. This is caused by the almost polar orbit of the satellite and the right-looking viewing geometry.

(a)

(b)
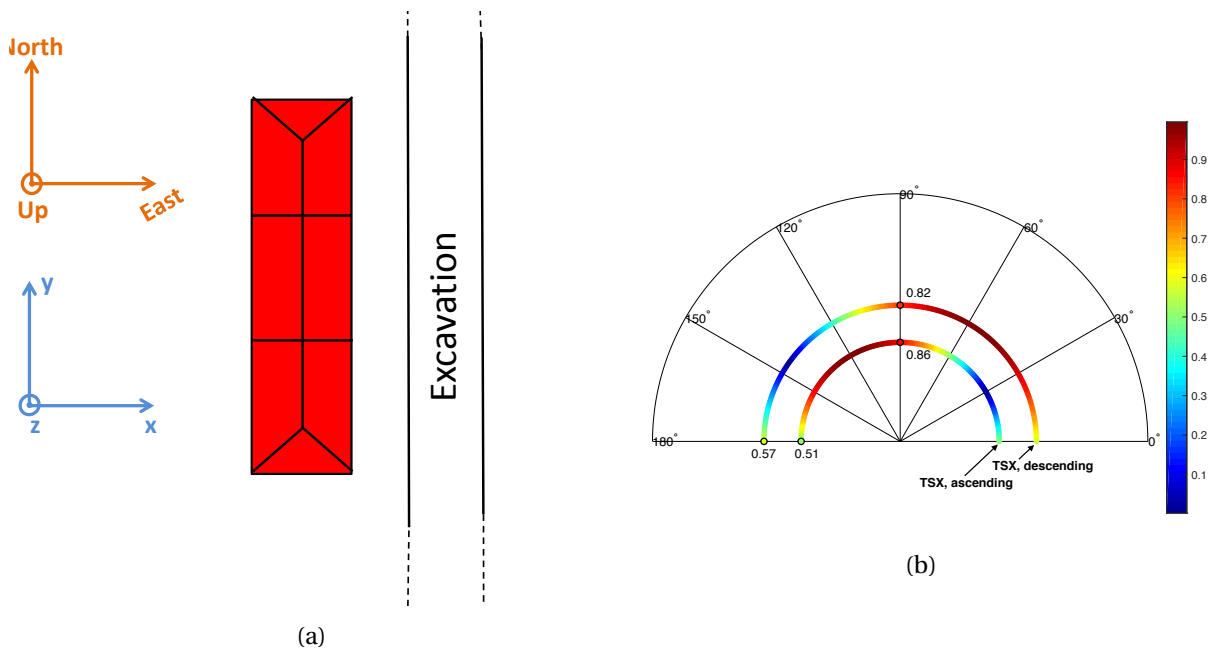
Figure 6.18: Row of houses for $\beta = 0°$ and the corresponding sensitivity circle (right), in the East,Up-plane

(a)

(b)
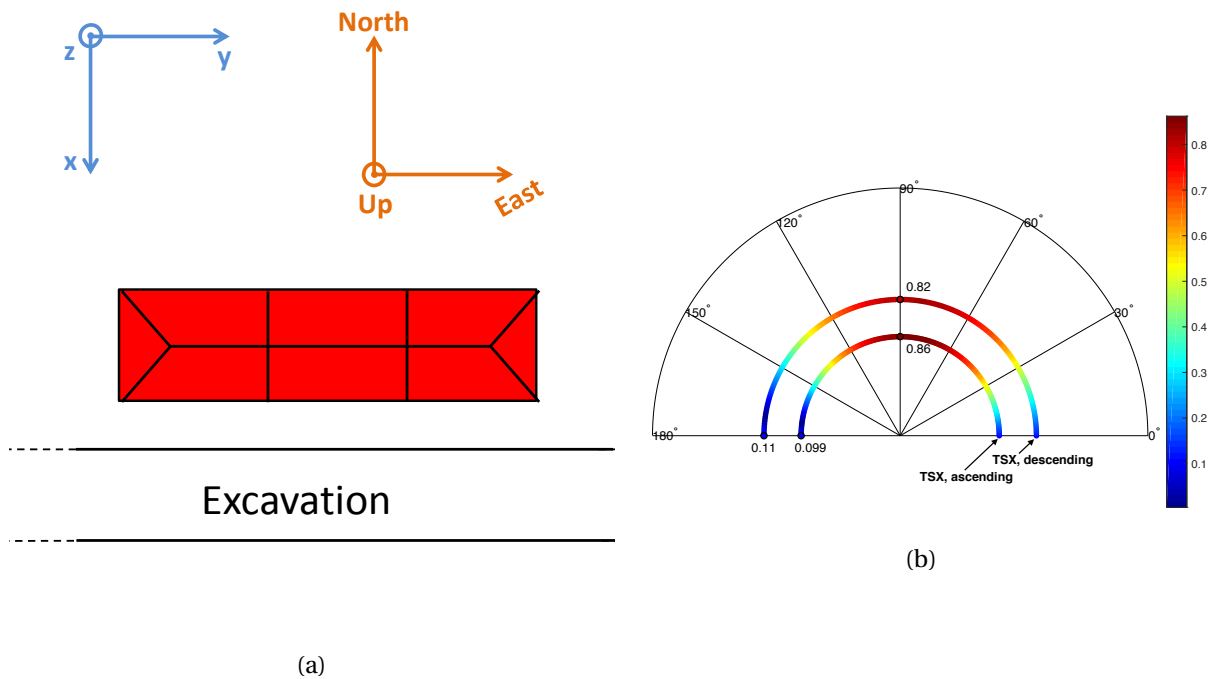
Figure 6.19: Row of houses for $\beta = 90°$ and the corresponding sensitivity circle (right), in the North,Up-plane

6.3.1   Discussion and Conclusion

The three dimensional deformation of a building can be determined using the InSAR ascending and descending track, and knowledge about the horizontal direction of deformation. This is the case in a plain-strain situation, i.e. for buildings next to an excavation or quay wall. However, for the InSAR data in the Spoorsingel area, the ascending points are mainly located on the southwest side of the buildings while the descending points are located on the northeast side of the buildings. The InSAR points of the two tracks are not on the same location. This prevents the calculation of the building three dimensional deformation. Due to the rotation of the buildings, as observed in the monitoring results, the three dimensional deformation of a building depends on the height and location of the measurement point on the building. Therefore the InSAR point of the ascending and descending track must be on the same position, to derive the three dimensional deformation at this particular point.

The sensitivity analysis shows to which extent the measurement precision is affected by the viewing geometry of InSAR. In vertical direction a sensitivity higher than 0.8 is achieved. In horizontal direction the sensitivity reduces to roughly 0.5 in east and west direction and it is reduced to roughly 0.1 in north east direction. In other words, the InSAR can't be used to measure horizontal directions in north and south direction.

6.4   Building damage

As described in section 6.2, significant deformations were observed during construction of the underground parking facility. As mentioned before, the differential settlement of the buildings can cause damage to the buildings. In the last few years, multiple habitants of the Spoorsingel area have reported damage to their house. In this section, it is investigated whether the deformations caused by construction of the underground parking facility has resulted in building damage. For this end, building damage of five buildings along the Spoorsingel is assessed.

First, the expected outcome of the building damage assessment is discussed in section 6.4.1. By con-

sidering the observed building settlement and structural building behaviour, the resulting formation and orientation of cracks in buildings can be estimated. Then, the building damage of five buildings in the affected area is observed and documented in section 6.4.2.

6.4.1 Expected results

The expected settlement profile next to an excavation is shown in figure 6.20. The amount of deformation and the exact shape of settlement profile depend on the stiffness of the diaphragm wall, the present soil type, the excavation depth and the soil-structure interaction. The settlement profile only indicates a rough estimation of the deformations due to the excavation. This figure also indicates two different zones: a hogging and a sagging zone. If a building is located in the hogging zone, the settlement profile is concave and the sides of the buildings settle more than average [28]. A building in the sagging zone settles most in the center of the building [28], the deformation profile is then convex.

The buildings along the Spoorsingel might be located in the sagging or the hogging zone. The monitoring results, as presented in section 6.2, indicate largest deformation on the side of the building closest to the underground parking facility. This means that, in figure 6.20, the building is located in the hogging zone or on the right side of the sagging zone. The expected damage can be based on the settlement profile in these areas. It is assumed all buildings have a shallow foundation.

Due to a plane strain situation, only damage is expected in the transversal plane. Figure 6.21 shows the deformation mechanisms of a building in the sagging and hogging zone respectively. Based on the work of Burland and Wroth [9], two types of cracks are likely to occur in this situation. The formation of bending cracks due to direct tensile strain and the formation of shear cracks due to diagonal tensile strain [9]. The shear cracks have an angle of roughly 45° with respect to the vertical. The vertical bending cracks can be located on top or on the bottom of the building, depending on the bending direction of the building (concave or convex). Although, the exact location of the cracks can not be predicted, an indication of the expected crack patterns is given in figure 6.21. If building damage is caused by construction of the underground parking facility, damage as shown in figure 6.21 can be expected.
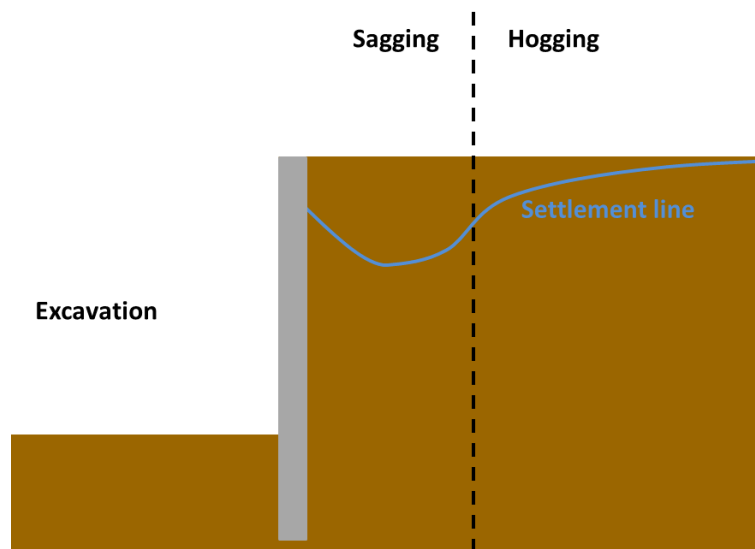
Figure 6.20: Expected settlement profile near the excavation
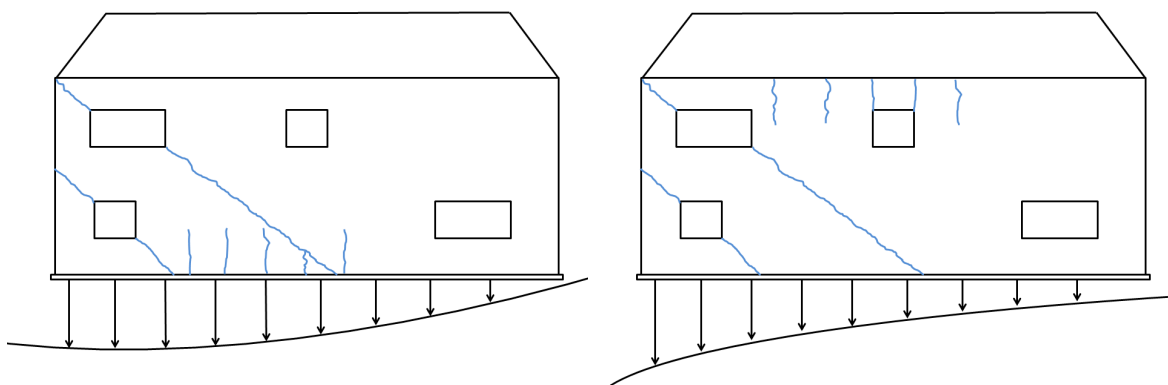
Figure 6.21: Side view of a building in a sagging zone (left) and a hogging zone (right). Vertical cracks and diagonal cracks due to bending and shear deformation are indicated in blue.

6.4.2 Results

The damage of the five buildings indicated in figure 6.22 is surveyed. The location, orientation and size of each crack is documented along with a picture. All the results of the building damage survey are shown in Appendix A. Of all the observed cracks, 19 cracks are located on the walls in longitudinal direction and 31 cracks are located on the walls transverse to the underground parking facility. The cracks in the transversal walls are depicted in figure 6.24, as these cracks are potentially the result of the underground parking facility construction. Many small cracks are observed for Spoorsingel 75 and 79. While Spoorsingel 78 and 79 are located next to each other, the amount of damage observed for Spoorsingel 78 is very limited. The age of each crack, according to the habitants, is documented as well. For the habitants, it was often hard to tell when a crack has formed or when certain damage has occurred. Therefore it is only possible to give a certain time frame in which the damage has occurred. The age of the cracks is subdivided into three classes: less than 5 years old, less than 15 years old and more than 15 years old. Almost all cracks for Spoorsingel 75 have formed in the last five years. A few of the cracks observed for Spoorsingel 99 and De Vriesstraat 2 also have formed in the last 6 years. Most cracks for Spoorsingel 78 and 79 have formed in the last 15 years.

Figure 6.22: Buildings for which a damage survey has been performed
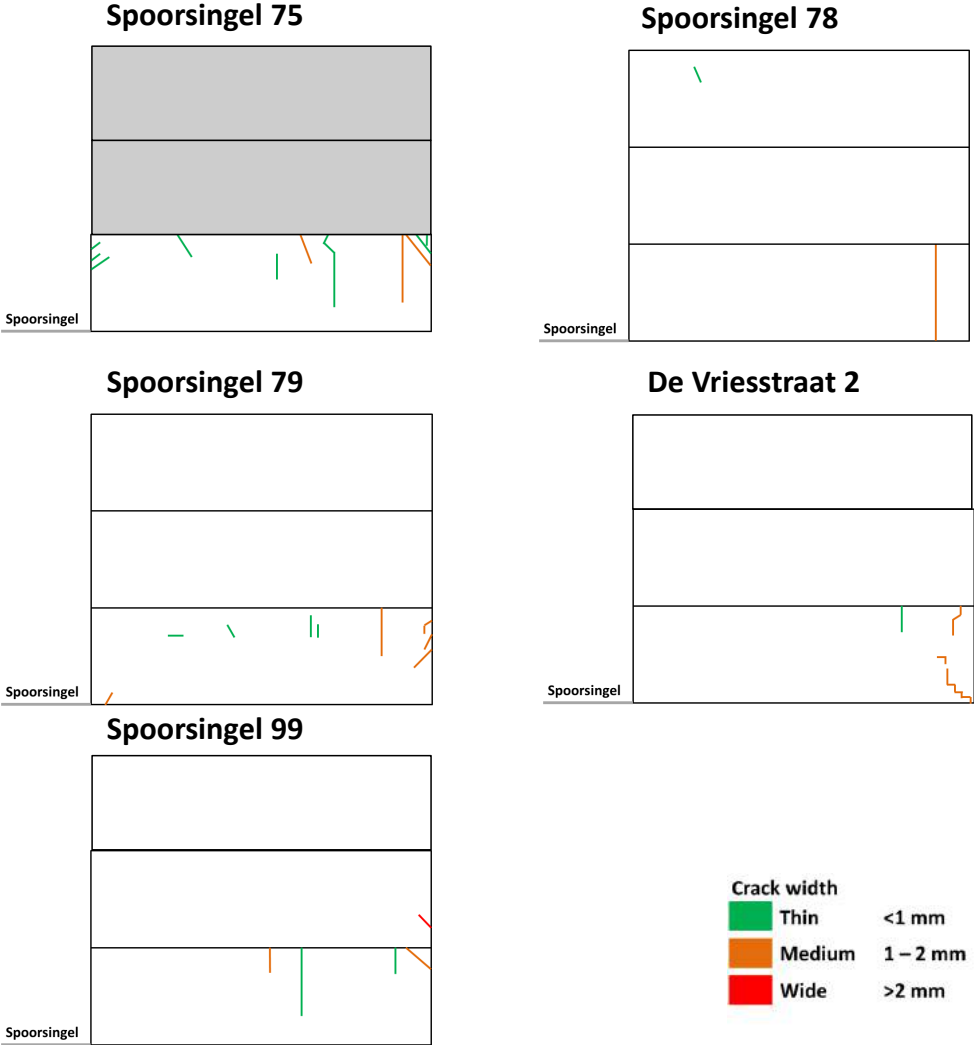
Figure 6.23: Overview of the observed cracks in all walls perpendicular to the underground parking facility, of the five buildings along the Spoorsingel
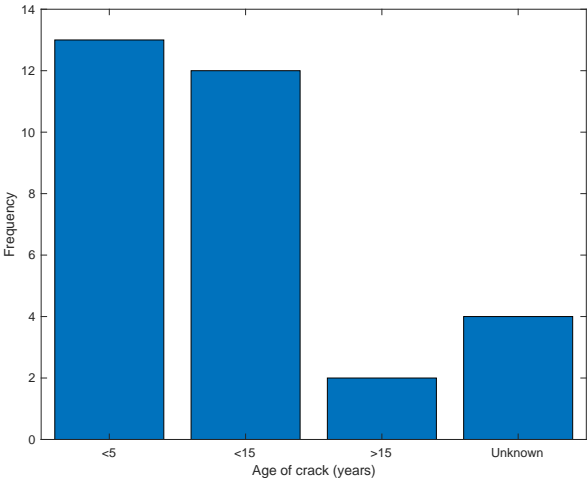
Figure 6.24: Age of the observed cracks on the walls transverse to the underground parking facility

6.4.3   Discussion and Conclusion

From the results it is obvious that many cracks in the walls transverse to the underground parking facility have formed in the last 15 years. Only for Spoorsingel 75, it was certain that almost all cracks have formed in the last 5 years. Most damage was observed on the backside of the buildings, where deformation related to the underground parking facility construction is smallest. No clear pattern can be distinguished in the direction of the diagonal cracks. The vertical cracks present could indicate bending movement of the buildings. The amount of cracks was largest for Spoorsingel 75 and 79. The damage for Spoorsingel 78 was minimal. The formation of cracks might be related to the age and maintenance of the building. All in all, the results are not considered to be convincing. The damage is not clearly related to the deformations caused by the underground parking facility construction.

Damage might be related to the vibrations during construction as well. Besides, other construction activities may be the cause of damage. Many construction activities have occurred in the last 15 years. This includes the demolishment of the nearby railway viaduct and other local construction works such as sewage repairs.

7

Conclusion and Recommendations

This chapter consists of two parts. In section 7.1 the conclusion of this research is given. The recommendations are presented in section 7.2.

7.1 Conclusion

To answer the main research question, the sub-questions are answered first:

1. How are quay walls in an urban environment managed and replaced?
Currently, the management of urban quay walls is mainly reactive. Measures are taken once large deformation are observed or once cracks in the quay wall appear. This means repairs are performed or a new quay wall is placed. Due to the large amount of replacements necessary in the city of Amsterdam, innovative solutions are sought. The use of a combi-wall for quay wall replacement has recently been developed. Compared to the traditional replacement method, the concrete L-wall, this method is faster and does not require a temporary building pit. Besides, the risk of damage is considered to be lower for this type of replacement.

2. How can deformation measurements be obtained using the InSAR technique?
The Synthetic Aperture Radar (SAR) transmits microwaves towards the earth's surface. By processing the backscattered energy, an image of the earth's surface can be obtained. Two images can be combined to obtain an interferogram. This interferogram contains phase differences between the two images. By careful analysis of the phase difference contributions, a phase difference due to deformation can be derived. The calculated deformation has occurred between the acquisitions of the two SAR images. Interferometric Synthetic Aperture Radar (InSAR) is a series of processing techniques to obtain deformations from SAR data. The SAR has a right-looking geometry and therefore measures line-of-sight deformation. InSAR points are locations on the earth's surface which provide stable reflections. Thus the measurement locations can not be predetermined.

3. To which extent can the displacements observed by InSAR be explained from actual physical driving mechanisms?
Using the InSAR deformations, the deformation behaviour of a building can be recognized. Differences between the ascending and descending InSAR track can be caused by rotating building movement. This was observed for the Spoorsingel in Delft between January 2016 and December 2017. For this, rigid building behaviour was assumed. The building rotation was caused by the construction of an underground parking facility nearby. Tilting of the Spoorsingel buildings was also observed with levelling benchmarks and total stations. Thus, the InSAR data enables the identification of occurring deformation mechanisms.

4. To which extent does the estimated displacement time series from the SAR data depend on the applied processing methodology?
One of the main factors affecting the estimation of the time series, is the a-priori deformation model

used for processing. Due to the repetitive nature of the InSAR phase observations, a deformation model is required to estimate the deformation time series. When the deformation behaviour is not known a-priori, the deformation model is, by default, set to steady-state deformation. This is the most likely type of deformation. When a sudden deformation of several millimeters occurs, this can be interpreted as both an upward and a downward deformation.

Another factor affecting the displacement time series is the processed time span. This is related to the deformation model. When the deformation pattern changes considerably within the processed time span, the displacement time series might not show this properly. To analyze short term deformations it is therefore useful to process, for example, only the last two years of SAR data.

Furthermore, as InSAR is a set processing techniques, it can be tuned to specific needs. Settings and thresholds can be adapted. The size of the processed area is of influence on the results. For a large area, the SAR data is processed in such a way that the overall results are good. However, optimization is possible when a small area is processed. This means more InSAR points are obtained and the quality of the InSAR points is higher.

Main research question: How and under what conditions can the InSAR data contribute to monitoring of buildings adjacent to quay walls?
InSAR data can provide complementary information about the deformation behaviour of buildings. For linear deformation in time, similar deformation rates are obtained from InSAR and levelling. Differences between the two monitoring methods are suggested to be the result of non-uniform building movement.

The quality of the deformation time series varies among the InSAR points. Using an overall model test, it can be tested whether a predefined deformation variance and a fitted deformation model can explain the present noise in the displacement time series. The quality of the displacement time series and the number of InSAR points can be further enhanced by processing only the area of interest. For a small area, the processing can be optimized.

Nevertheless, a visual assessment of the InSAR displacement time series is still valuable. This way, a possible phase shift or the presence of incoherent observations can be detected. A phase shift can be present in the data when a deformation of more than 7.5 millimeter has occurred between two observations. Also, some displacement time series can contain observations originating from unstable scatterers. Usually, these observations are filtered out during processing of the SAR data. However, when only part of the time series contains incoherent observations, the overall quality might still be considered as sufficient. In this case, the time series can still be present in the provided dataset. Incoherent observations can be recognized by a 15 millimeter deformation range.

One of the main advantages of InSAR is the long time period of available deformation measurements. For the TerraSAR-X satellite, already about 9 years of deformation data is available. Thus, the InSAR can provide a long deformation history. However, it can be of added value to process only the last few years of SAR data. This way, it can be observed whether the deformation behaviour has changed in the last years. This was clearly observed for the Spoorsingel dataset.

To assess the foundation quality of a building, one is mainly interested in buildings with high deformation rates. Often a deformation rate is stipulated above which the condition of the foundation is considered to be alarming. In this thesis a deformation rate threshold of 2 mm/y is used. In the presented probability map, the calculated deformation rate is combined with the variance of that estimate. Using this information, the probability of a 2 mm/y deformation rate can be calculated. The map shows InSAR points in red when this probability is more than 5%. The probabilistic approach is especially useful when using short InSAR time series. For one or two years of INSAR data, the variance of the deformation rate estimate is significant.

Furthermore, the location precision of the InSAR points needs to be considered when using InSAR

for building monitoring. For the TerraSAR-X satellite a location precision of one or two meters can be expected. Also, due to the right-looking geometry of the SAR satellite, the horizontal displacements should be minimal to convert the line-of-sight deformations to vertical deformations.

All in all, InSAR provides valuable information regarding building movement. When using InSAR for this purpose, factors such as the quality, the line-of-sight measurement, the location precision and variance of the deformation rate estimate should be taken into account. The recommended approach with regard to post-processing of InSAR data to analyze building movement, is described in a flow chart in the next section.

7.2   Recommendations

For both InSAR and levelling, a probabilistic approach is advisable with regard to determined deformation rates from the data. For InSAR, this is especially relevant when only a few years of InSAR data is used, due to measurement variance of InSAR. For levelling this is mainly due to the low amount of measurements. Generally, levelling is carried out only several times a year.

For users of InSAR data, the InSAR technology might be viewed as a black box. This idea can be partially removed by a thorough understanding of the InSAR technology. Also, by understanding the workings of InSAR, the user knows what can be expected from the InSAR data and how the displacement time series should be interpreted. It is therefore advised to have at least a basic understanding of the InSAR technology before using this data.

The use of InSAR for monitoring purposes is not merely a scientific matter but also an emotional question regarding the confidence in this monitoring method. This thesis does not only aim to assess the performance of InSAR but also to give more feeling for the InSAR results. This is achieved through comparison with conventional levelling.

In addition, the placement of several artificial corner reflectors in the city centre of Amsterdam could add to the acceptance of InSAR as monitoring technique. These corner reflectors provide a stable reflection of which the location is well known. By monitoring these corner reflectors with levelling as well, it can be assured the two monitoring techniques measure exactly the same object.

In the analyzed Amsterdam cases most buildings showed small settlement. Only for some of the buildings along the Oudezijds Achterburgwal a large deformation was observed. For many buildings, this was an abrupt change in deformation due to the construction activity. For only a handful of buildings a large gradual deformation was observed which allowed for comparison between InSAR and levelling. Large deformations were also observed for the buildings along the Spoorsingel in Delft. However, due the horizontal movement of these buildings, no direct comparison of deformations was possible. Therefore it is advised to search for more buildings with relatively large gradual displacements for comparison with levelling benchmarks. These buildings are of main interest concerning their foundation quality.

Flowchart for use of InSAR in building monitoring

To evaluate the use of InSAR data for building monitoring, a flow chart is constructed in figure 7.1. To use the InSAR data , the following questions need to be answered:

1. Are InSAR points located on the building?

To select only InSAR points located on buildings, it is advised to use only high points from the InSAR dataset. These points are located at least two meter above ground level. Furthermore, due to location precision, high points within two meter distance are likely to be reflections originating from the buildings. Therefore these InSAR points should be considered as well.

2. Does the time series of the InSAR point show homogeneous deformations?

On some occasions, the InSAR deformation time series does not show homogeneous variance. In this case, the time series may contain incoherent observations. This is likely to be the case, when a

deformation variance of roughly 15 millimeter is present in (part of) the time series. This is about half a wavelength for the TerraSAR-X satellite (31 mm wavelength). This means no stable scatterer was present within this timeframe. Therefore, in case of roughly 15 mm deformation variance, (this part of) the deformation time series needs to be disregarded. No valuable information can be derived from the data then.

3. Does the time series contain deformation shifts?
In case a sudden deformation shift is present within the processed timespan, the InSAR deformation time series should be handled with extra care. This phenomenon is related to the repetitive nature of the InSAR phase observations and indicates an abrupt change in deformation has occurred between two observations. In this case, no deformation rate can be derived from the displacement time series and the building has settled significantly.

4. Is the deformation linear in time?
For most buildings the deformation in time is roughly linear. This allows for a simple deformation model fit and deformation rate calculation as was performed in this thesis. In case, a different deformation pattern is observed, for example a quadratic function or deformation model with breakpoints, such a deformation model should be applied.

5. Do the defined deformation variance and deformation model explain the observations?
To answer this question, an overall model test needs to be performed. By considering the number of observations, the number of unknowns and a level of significance, a critical value K can be determined. Next, a test statistic T is calculated, which depends on the predefined measurement variance and the residuals. When the test statistic T exceeds the critical value K, the deformation model is unlikely to fit the observations. If not, the deformation rate r and the variance of this estimate σ_r can be calculated.

6. Is a deformation rate of more than 2 mm/y likely?
Subsequently, it is advised to calculate the probability of 2 mm/y deformation or more. This is currently used as threshold for moderate building deformation. With such a deformation rate, additional measures are required before construction activities are carried out nearby. For these buildings, additional investigation is required concerning their foundation. In the flow chart, a probability less than 5% is considered unlikely. However, any significance level can be chosen here. This is mainly a decision the asset manager should make.

7. Do more InSAR points on this building show possible large deformation?
When the InSAR point indicates possible large deformation, other InSAR points on the building should be considered. As said earlier, the location precision of the InSAR points needs to be taken into account as well. When the InSAR point is located close to the adjacent building, the reflection could be originating from this building as well. Also, the reflection could be be originating from other high scatters, such as a street light pole close to the building. When multiple InSAR points on the building show possible large deformation, a reasonable chance exists that the building foundations requires further investigation.

Building deformation monitoring
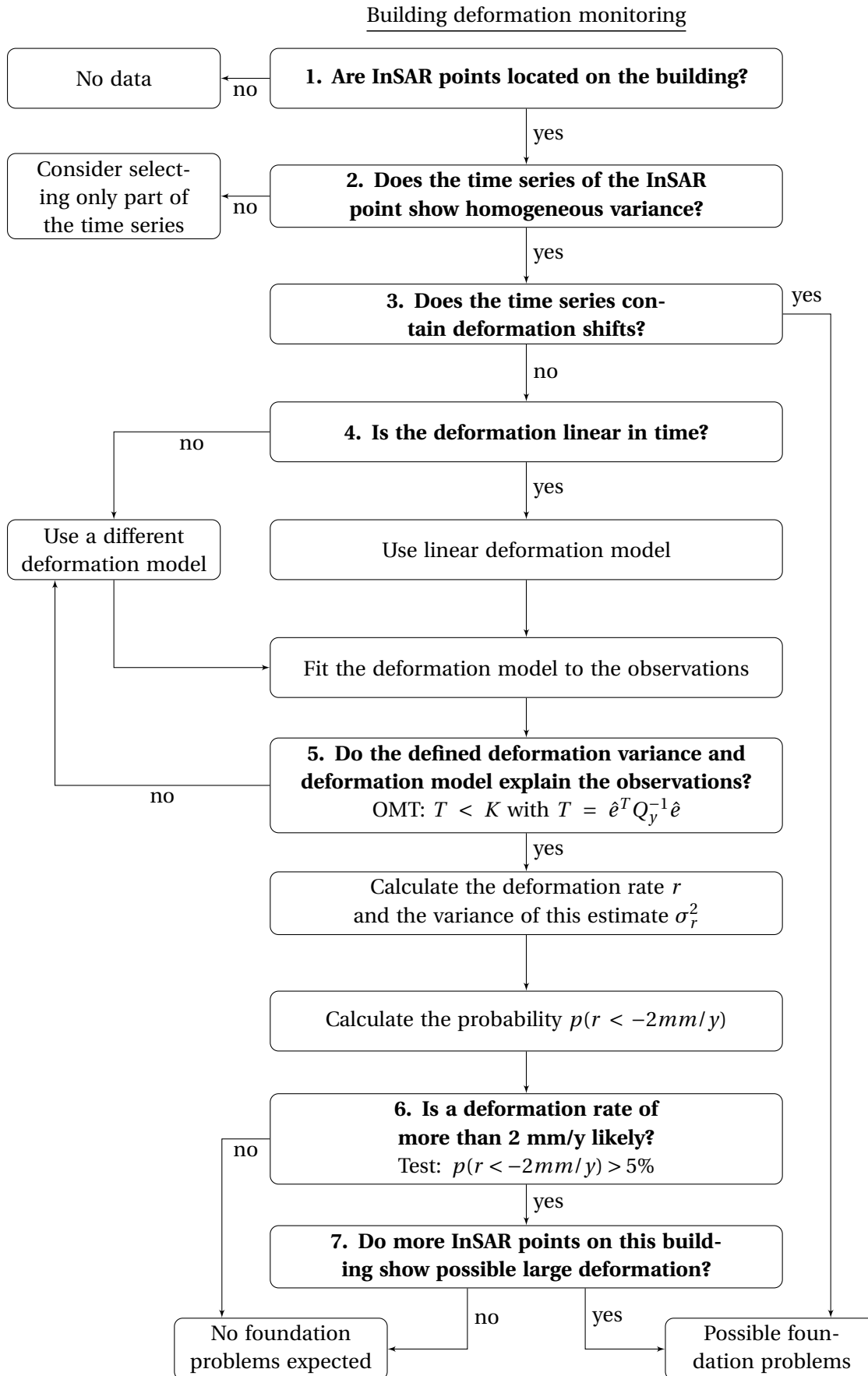
Figure 7.1: Recommended flowchart for use of InSAR in building monitoring

Bibliography

[1]   European Space Agency. *InSAR Principles. Guidelines for SAR Interferometry Processing and Interpretation*. ESA Publications, 2007.

[2]   Ingenieursbureau gemeente Amsterdam. *19e bouwvergadering Oudezijds Achterburgwal*. Tech. rep. 2013.

[3]   Ingenieursbureau gemeente Amsterdam. *Concept inkoopstrategie - Innovatiepartnerschap Kademuren*. Tech. rep. Gemeente Amsterdam, Mar. 2018.

[4]   Ingenieursbureau gemeente Amsterdam. *Concept probleemanalyse kademuurvervangingen*. Tech. rep. Gemeente Amsterdam, Apr. 2018.

[5]   Ingenieursbureau gemeente Amsterdam. *Herinrichtingsvoorstel Oudezijds Achterburgwal oneven zijde*. Tech. rep. 2009.

[6]   Ingenieursbureau gemeente Amsterdam. *Opschorten 2e fase walmuurvernieuwing Oudezijds Achterburgwal*. Tech. rep. 2012.

[7]   Ingenieursbureau gemeente Amsterdam. *Walmuurvernieuwing Herengracht*. Tech. rep. 2016.

[8]   *Basisregistratie Adressen en Gebouwen (BAG) - Nationaal Georegister (NGR)*. URL: `https://geodata.nationaalgeoregister.nl/bag/wfs?` (visited on 09/14/2018).

[9]   J.B. Burland and C.P. Wroth. "Settlement of Buildings and Associated Damage". In: (1974).

[10]   CRUX Engineering BV. *Bouwprotocol. Richtlijnen en stappenplan voor Geotechnisch Risicomanagement van bouwprojecten*. Tech. rep. 2014.

[11]   L. Chang, R.P.B.J. Dollevoet, and F. Hanssen. "Monitoring Line-Infrastructure With Multisensor SAR Interferometry: Products and Performance Assessment Metrics". In: *IEEE Journal of Selected Topics in Applied Earth Observations and Remote Sensing* 11.5 (2018), pp. 1593–1605.

[12]   L. Chang and F. Hanssen. "A Probabilistic Approach for InSAR Time-Series Postprocessing". In: *IEEE Transactions on Geoscience and Remote Sensing* 54.1 (2016).

[13]   D. Cook. "Robotic Total Stations and Remote Data Capture: Challenges in Construction". In: *Geotechnical Instrumentation News* (2006).

[14]   R. van de Crommert. *Amsterdamse kades dreigen in te storten*. URL: `https://www.telegraaf.nl/nieuws/1585245/amsterdamse-kades-dreigen-in-te-storten` (visited on 07/09/2018).

[15]   CUR. *Handbook Quay Walls*. 2005.

[16]   Spoorzone Delft. *Spoorsingel*. URL: `https://www.spoorzonedelft.nl/locatie/spoorsingel/`.

[17]   Spoorzone Delft. *Start bouw diepwanden Spoorsingel*. URL: `https://www.spoorzonedelft.nl/actueel/nieuwsberichten/start_bouw_diepwanden_spoorsingel`.

[18]   I.M. Elhassan and A.S. Ali. "Comparative study of accuracy in distance measurement using: Optical and digital levels". In: *Journal of King Saud University* (2009).

[19]   A. Ferretti, G. Savio, R. Barzaghi, A. Borghi, S. Musazzi, F. Novali, C. Prati, and F. Rocca. "Sub-millimeter accuracy of InSAR time series: experimental validation". In: *IEEE Transactions on Geoscience and Remote Sensing* 45.5 (2007), pp. 1142–1153.

[20]   *Glossary of Meteorology - radar resolution*. URL: `http://glossary.ametsoc.org/wiki/Radar_resolution`.

[21]   R.F. Hanssen. *Radar Interferometry. Data Interpretation and Error Analysis*. Dordrecht, The Netherlands: Kluwer Academic Publishers, 2001.

[22]   A.J. Hooper. "Persistent scatter radar interferometry for crustal deformation studies and modeling of volcanic deformation". PhD thesis. Stanford University, 2006.

[23]   D. Inaudi. "Overview of 40 bridge structural health monitoring projects". In: *International Bridge Conference* (2009).

[24]   *Kademuur bij Nassaukade ingestort; lek waterleiding weer gedicht.* URL: http://www.at5.nl/
        artikelen/179152/kademuur-bij-nassaukade-ingestort (visited on 07/09/2018).

[25]   G. Ketelaar, F. van Leijen, P. Marinkovic, and R. Hanssen. "Multi-track PS-InSAR datum con-
        nection". In: *International Geoscience and Remote Sensing Symposium, Barcelona, Spain, 23-27
        July 2007* (2007).

[26]   V.B.H. Ketelaar. *Satellite Radar Interferometry. Subsidence Monitoring Techniques.* Springer, 2009.

[27]   V.B.H. Ketelaar, R.F. Hanssen, A.P.E.M. Houtenbos, and R.C. Lindenbergh. "Idealization preci-
        sion of points scatterers for deformation modeling". In: *4th International Symposium on Re-
        trieval of Bio- and Geophysical Parameters from SAR Data for Land Applications, Innsbruck,
        Austria, 16-19 Nov. 2004* (2004).

[28]   M. Korff. "Response of piled buildings to the construction of deep excavations". PhD thesis.
        University of Cambridge, 2013.

[29]   F.J. van Leijen. "Persistent Scatterer Interferometry based on geodetic estimation theory". PhD
        thesis. Delft University of Technology, 2014.

[30]   A. Lepadatu and C. Tiberius. "GPS for structural health monitoring - case study on the Basarab
        overpass cable-stayed bridge". In: *Journal of Applied Geodesy* 8.1 (2014), pp. 65–85.

[31]   P. Marinkovic, G. Ketelaar, F. van Leijen, and R. Hanssen. "InSAR Quality Control: Analysis of
        five years of corner reflector time series". In: ().

[32]   Mobilis. *Prinsenhofgarage opgeleverd aan Parkeren Delft.* URL: https://www.mobilis.nl/
        nl/prinsenhofgarage-opgeleverd-aan-parkeren-delft.

[33]   *Monitoring in de praktijk. Ervaringen grote infraprojecten.* Tech. rep. Nederlands kenniscen-
        trum voor ondergronds bouwen en ondergronds ruimtegebruik (COB).

[34]   *Noodmaatregel kademuur Singel Amsterdam.* URL: https://movares.nl/projecten/noodmaatregel-
        kademuur-singel-amsterdam/ (visited on 07/09/2018).

[35]   *Ontwerpbestemmingsplan Parkeergarage Spoorsingel.* Tech. rep. Gemeente Delft, 2014.

[36]   D. Peduto, G. Nicodemo, J. Maccabiani, and S. Ferlisi. "Multi-scale analysis of settlement-induced
        building damaage using damage surveys and DInSAR data: a case study in The Netherlands".
        In: *Engineering Geology* (2017), pp. 117–133.

[37]   J. Piersma. *Deel Marnixstraat nog een week dicht na sinkhole.* URL: https://www.parool.
        nl/amsterdam/deel-marnixstraat-nog-een-week-dicht-na-sinkhole~a4527868/
        (visited on 07/09/2018).

[38]   W.G. Rees. *Physical Principles of Remote Sensing.* Cambridge University Press, 2012.

[39]   Paul A Rosen. *Principles and Theory of Radar Interferometry.* 2014. URL: https://www.unavco.
        org/education/professional-development/short-courses/course-materials/
        insar/2014-insar-isce-course-materials/InSARPrinciplesTheory_UNAVCO_14.
        pdf.

[40]   SBRCURnet. *Binnenstedelijke kademuren.* 2014.

[41]   SkyGeo. *InSAR Technical Background.* URL: https://skygeo.com/insar-technical-
        background/ (visited on 08/28/2018).

[42]   *TU Delft OpenCourseWare - Observation Theory: Estimating the unknown.* URL: https://ocw.
        tudelft.nl/course-readings/6-1-summary/?course_id=20741 (visited on 11/12/2018).

[43]   H.W. van Waning. "A feasibility study of building monitoring and forensic engineering with In-
        terferometric Synthetic Aperture Radar". Master's thesis. Delft University of Technology, 2014.

[44]   Witteveen+Bos. *Startoverleg werkzaamheden walmuurvervanging Oudezijds Achterburgwal o.e.z.
        stabilisatieconstructie 2e fase.* Tech. rep. 2013.

[45]   Witteveen+Bos. *Vervangen walmuur Krom Boomssloot - Inschrijvingsleidraad.* Tech. rep. 2015.

[46]   K. Yang, L. Yan, G. Huang, C. Chen, and Z. Wu. "Monitoring Building Deformation with InSAR:
        Experiments and Validation". In: *Sensors* 16.2182 (2016).

A
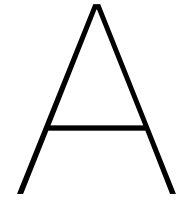
Building damage survey

This appendix contains damage surveys of five buildings along the Spoorsingel in Delft. The damage of Spoorsingel 75, 78, 79, 99 and De Vriesstraat 2 is described. The location of these buildings is shown in figure A.1. The damage survey of each building gives a general description and the observed damage of the building. It contains pictures of the observed damage and the properties of the cracks, including the location, the orientation, the size and the formation and development of the crack over time. The orientation is defined as the smallest angle with respect to the horizontal. The development of the crack is defined as a time frame in which the crack is expected to have formed.

Figure A.1: Locations of the buildings in the building damage survey

A.1 Spoorsingel 75

Figure A.2 shows Spoorsingel 75. The damage survey was conducted on 24-08-2018. The house was built in 1930 [8]. Spoorsingel 75 is located on the ground floor of this building. The location of the damage is shown in figure A.3. Pictures and specifications of the damage are shown in the next few pages. A lot of cracks were observed for this building. Almost all cracks have formed in the last five years. The cracks in the walls orthogonal to the parking garage are shown in figure A.13.

Figure A.2: Spoorsingel 75
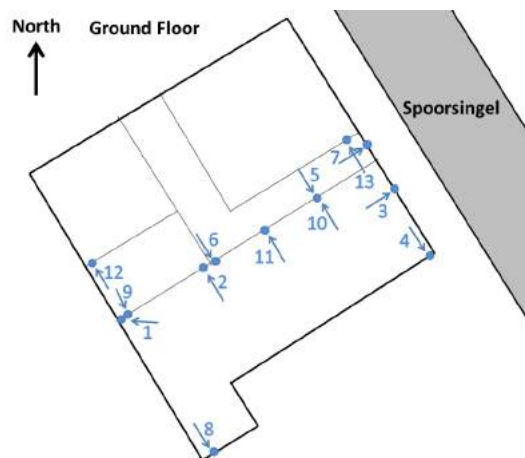
Figure A.3: Location of the observed damage
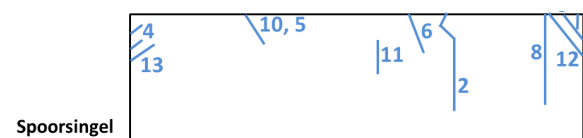
Figure A.4: Indication of cracks in the walls orthogonal to the parking garage

Location 1
Orientation of the wall w.r.t. the north: 60°
Angle w.r.t. the horizontal: 90°
Size: <1 mm
Development: At most 5 years old
Additional information: -

Location 2
Orientation of the wall w.r.t. the north: 60°
Angle w.r.t. the horizontal: 90°
Size: <1 mm
Development: At most 5 years old
Additional information: -

Location 3
Orientation of the wall w.r.t. the north: -30°
Angle w.r.t. the horizontal: 0°
Size: 1 mm
Development: At most 5 years old
Additional information: -

Location 4
Orientation of the wall w.r.t. the north: 60°
Angle w.r.t. the horizontal: 40°
Size: <1 mm
Development: At most 5 years old
Additional information: -

Location 5
Orientation of the wall w.r.t. the north: 60°
Angle w.r.t. the horizontal: 50°
Size: <1 mm
Development: At most 5 years old
Additional information: -

Location 6
Orientation of the wall w.r.t. the north: 60°
Angle w.r.t. the horizontal: 70°
Size: 1 mm
Development: At most 5 years old
Additional information: -

Location 7
Orientation of the wall w.r.t. the north: -30°
Angle w.r.t. the horizontal: 0°
Size: <1 mm
Development: At most 5 years old
Additional information: -
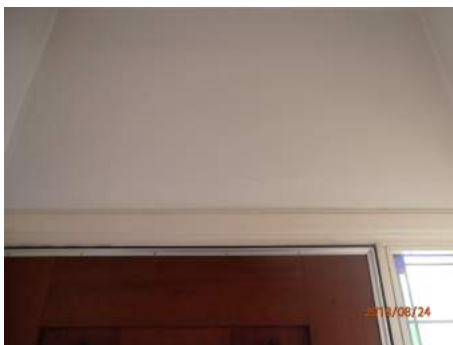
Location 8
Orientation of the wall w.r.t. the north: 60°
Angle w.r.t. the horizontal: 90°
Size: 2 mm
Development: At most 15 years old
Additional information: -

Location 9
Orientation of the wall w.r.t. the north: 60°
Angle w.r.t. the horizontal: 50°
Size: <1 mm
Development: At most 5 years old
Additional information: -

Location 10
Orientation of the wall w.r.t. the north: 60°
Angle w.r.t. the horizontal: 50°
Size: <1 mm
Development: At most 5 years old
Additional information: -

Location 11
Orientation of the wall w.r.t. the north: 60°
Angle w.r.t. the horizontal: 90°
Size: <1 mm
Development: At most 5 years old
Additional information: Photo is missing

Location 12
Orientation of the wall w.r.t. the north: 60°
Angle w.r.t. the horizontal: 40°
Size: 1 mm
Development: At most 5 years old
Additional information: -

Location 13
Orientation of the wall w.r.t. the north: 60°
Angle w.r.t. the horizontal: 60°
Size: <1 mm
Development: At most 5 years old
Additional information: -

A.2 Spoorsingel 78

Figure A.5 shows Spoorsingel 78. The damage survey was conducted on 24-08-2018. The house was built in 1895 [8]. The location of the damage is shown in figure A.6. Pictures and specifications of the damage are shown in the next few pages. The building has been renovated and plastered almost completely 15 years ago. In general, the building seems to be well maintained in the last 15 years with regular repairs and small renovations. The observed damage is very limited. A few doors are jamming since approximately 2 years. The residents indicate that a lot of construction activities have occurred in the last few years. The sewage system was replaced roughly two years ago and the nearby railway viaduct has been demolished. The cracks in the walls orthogonal to the parking garage are shown in figure A.7.

Figure A.5: Spoorsingel 78
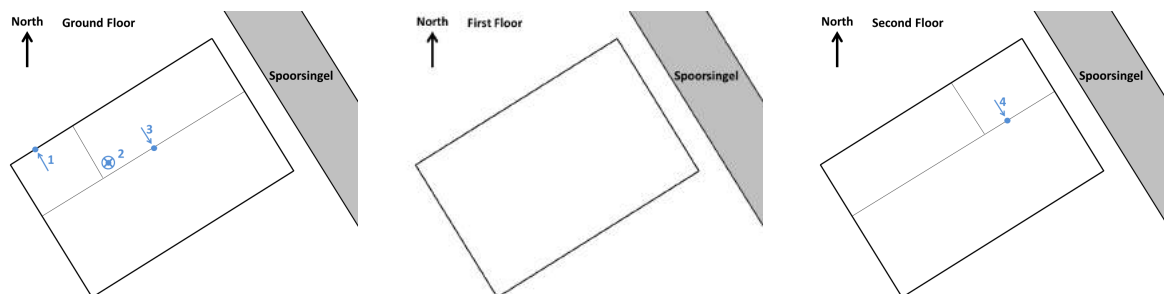
Figure A.6: Location of the observed damage on the ground floor (left), first floor (middle) and second floor (right)
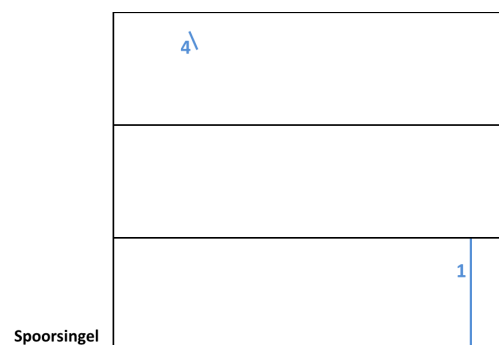
Figure A.7: Indication of cracks in the walls orthogonal to the parking garage

Location 1
Orientation of the wall w.r.t. the north: 60°
Angle w.r.t. the horizontal: 90°
Size: 1 mm
Development: More than 15 years old
Additional information: Crack over the whole height of the wall and continues on the floor. Crack has lengthened and widened in the last 15 years.

Location 2
Size: 2 mm
Development: More than 15 years old
Additional information: Cracks are located on the floor

Location 3
Orientation of the wall w.r.t. the north: 60°
Development: At most 5 years old
Additional information: Tiles have come off the wall

Location 4
Orientation of the wall w.r.t. the north: 60°
Angle w.r.t. the horizontal: 70°
Size: <1 mm
Development: At most 15 years old
Additional information: Only room that wasn't replastered 15 years ago

A.3 Spoorsingel 79

Figure A.10 shows Spoorsingel 79. The damage survey was conducted on 26-07-2018. The house was built in 1895 [8]. The location of the damage is shown in figure A.9. Pictures and specifications of the damage are shown in the next few pages. A lot of damage was observed. Most of the cracks are really small. A lot of cracks were visible at corners of the plaster and near connections with doorposts. The residents indicate that a lot of construction activities have taken place in the last 10 years. The demolition of the railway viaduct caused a lot of vibrations. The sewage system in front of the house was replaced in recent years. Also, a gas pipe, entering the house at the front of the building, broke four or five years ago. In the last five years some doors on the ground floor have started to jam. The cracks in the walls orthogonal to the parking garage are shown in figure A.10.

Figure A.8: Spoorsingel 79
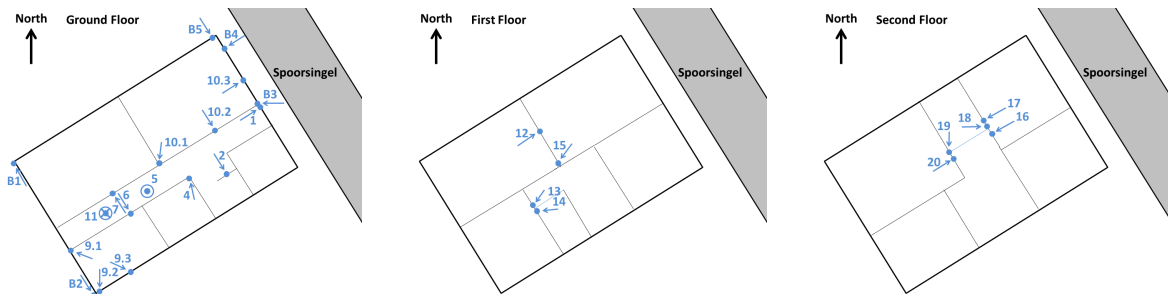
Figure A.9: Location of the observed damage on the ground floor (left), first floor (middle) and second floor (right)
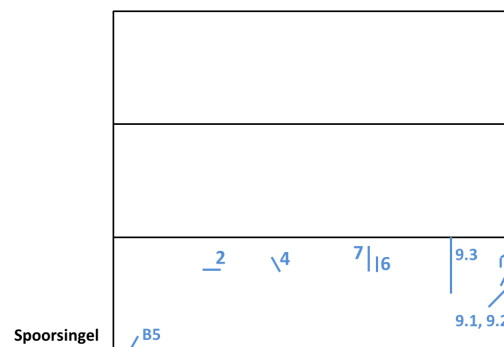
Figure A.10: Indication of cracks in the walls orthogonal to the parking garage

Location 1
Orientation of the wall w.r.t. the north: -30°
Angle w.r.t. the horizontal: 90°
Size: <1 mm
Development: At most 15 years old
Additional information: -

Location 2
Orientation of the wall w.r.t. the north: 60°
Angle w.r.t. the horizontal: 0°
Size: <1 mm
Development: At most 15 years old
Additional information: -

Location 4
Orientation of the wall w.r.t. the north: 60°
Angle w.r.t. the horizontal: 70°
Size: <1 mm
Development: At most 15 years old
Additional information: -

Location 5
Size: <1 mm
Development: At most 15 years old
Additional information: Crack is located on the
ceiling.

Location 6
Orientation of the wall w.r.t. the north: 60°
Angle w.r.t. the horizontal: 90°
Size: <1 mm
Development: At most 15 years old
Additional information: -

Location 7
Orientation of the wall w.r.t. the north: 60°
Angle w.r.t. the horizontal: 90°
Size: <1 mm
Development: At most 15 years old
Additional information: -

Location 9.1
Orientation of the wall w.r.t. the north: 60°
Angle w.r.t. the horizontal: 70°
Size: 2 mm
Development: At most 15 years old
Additional information: -

Location 9.2
Orientation of the wall w.r.t. the north: 60°
Angle w.r.t. the horizontal: 70°
Size: 2 mm
Development: At most 15 years old
Additional information: -
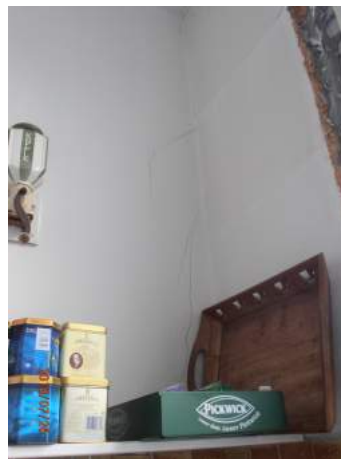
Location 9.3
Orientation of the wall w.r.t. the north: 60°
Angle w.r.t. the horizontal: 90°
Size: 2 mm
Development: More than 15 years old
Additional information: -

Location 10.2
Orientation of the wall w.r.t. the north: 60°
Angle w.r.t. the horizontal: 90°
Size: <1 mm
Development: At most 15 years old
Additional information: -

Location 10.1
Orientation of the wall w.r.t. the north: 60°
Angle w.r.t. the horizontal: 90°
Size: <1 mm
Development: At most 15 years old
Additional information: -

Location 10.3
Orientation of the wall w.r.t. the north: -30°
Angle w.r.t. the horizontal: 90°
Size: 2 mm
Development: At most 15 years old
Additional information: -

Location 11
Size: 3 mm
Development: More than 15 years old
Additional information: Cracks are located on the floor. The floor has become more uneven in the last few years

Location 12
Orientation of the wall w.r.t. the north: -30°
Angle w.r.t. the horizontal: 50°
Size: 1 mm
Development: At most 15 years old
Additional information: -

Location 13
Orientation of the wall w.r.t. the north: -30°
Angle w.r.t. the horizontal: 10°
Size: <1 mm
Development: At most 15 years old
Additional information: -

Location 14
Orientation of the wall w.r.t. the north: -30°
Angle w.r.t. the horizontal: 10°
Size: <1 mm
Development: At most 15 years old
Additional information: -
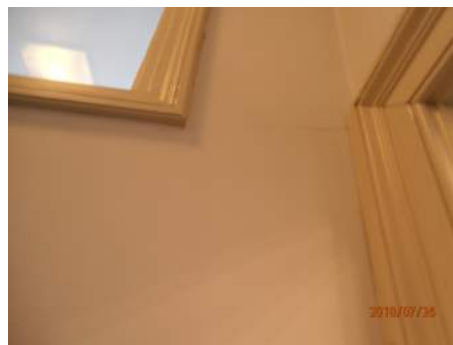
Location 15
Orientation of the wall w.r.t. the north: -30°
Angle w.r.t. the horizontal: 10°
Size: <1 mm
Development: At most 15 years old
Additional information: -

Location 16
Orientation of the wall w.r.t. the north: -30°
Angle w.r.t. the horizontal: 10°
Size: 1 mm
Development: At most 15 years old
Additional information: -

Location 17
Orientation of the wall w.r.t. the north: -30°
Angle w.r.t. the horizontal: 0°
Size: 1 mm
Development: At most 15 years old
Additional information: -

Location 18
Orientation of the wall w.r.t. the north: -30°
Angle w.r.t. the horizontal: 10°
Size: 1 mm
Development: At most 15 years old
Additional information: -

Location 19
Orientation of the wall w.r.t. the north: -30°
Angle w.r.t. the horizontal: 90°
Size: <1 mm
Development: At most 15 years old
Additional information: -

Location 20
Orientation of the wall w.r.t. the north: -30°
Angle w.r.t. the horizontal: 70°
Size: 2 mm
Development: At most 15 years old
Additional information: -

Location B1
Orientation of the wall w.r.t. the north: 60°
Development: At most 15 years old
Additional information: -

Location B2
Orientation of the wall w.r.t. the north: 60°
Development: At most 15 years old
Additional information: -

Location B3
Orientation of the wall w.r.t. the north: -30°
Angle w.r.t. the horizontal: 40°
Size: 1 mm
Development: At most 15 years old
Additional information: -

Location B4
Orientation of the wall w.r.t. the north: -30°
Angle w.r.t. the horizontal: 50°
Size: 3 mm
Development: At most 15 years old
Additional information: -

Location B5
Orientation of the wall w.r.t. the north: 60°
Angle w.r.t. the horizontal: 60°
Size: 1 mm
Development: At most 15 years old
Additional information: -

A.4   De Vriesstraat 2

Figure A.11 shows De Vriesstraat 2. The damage survey was conducted on 30-07-2018. The house was built in 1933 [8]. The location of the damage is shown in figure A.12. Pictures and specifications of the damage are shown in the next few pages. A few cracks have formed in the last five years. The age of several cracks was unknown. The cracks in the walls orthogonal to the parking garage are shown in figure A.13.

Figure A.11: De Vriesstraat 2
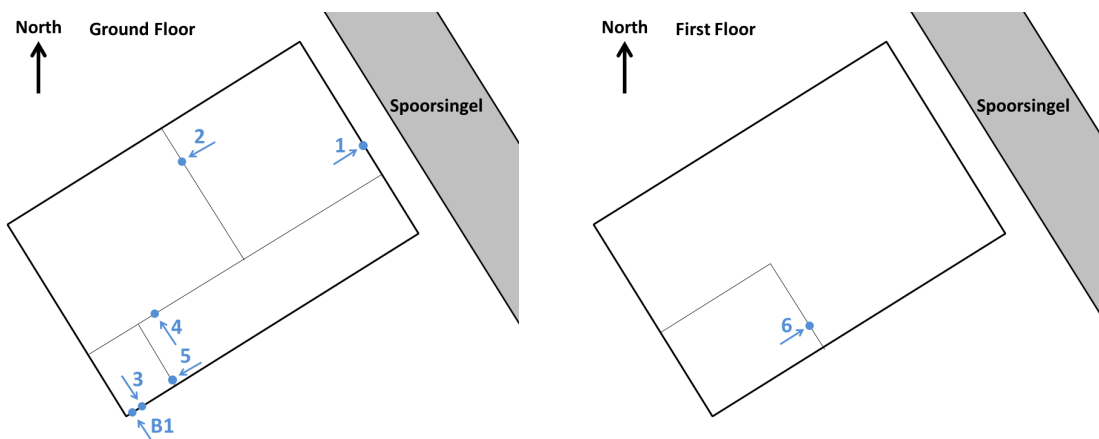
Figure A.12: Location of the observed damage on the ground floor (left) and first floor (right)
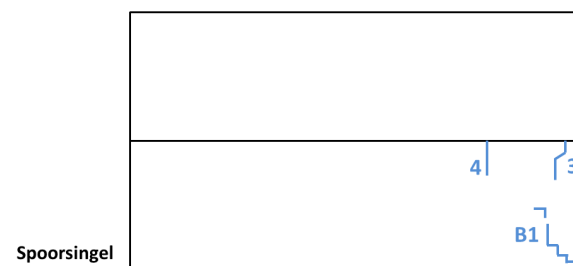
Figure A.13: Indication of cracks in the walls orthogonal to the parking garage

Location 1
Orientation of the wall w.r.t. the north: -30°
Angle w.r.t. the horizontal: 90°
Size: 1 mm
Development: At most 5 years old
Additional information: -

Location 2
Orientation of the wall w.r.t. the north: -30°
Angle w.r.t. the horizontal: 80°
Size: 1 mm
Development: At most 10 years old
Additional information: -

Location 3
Orientation of the wall w.r.t. the north: 60°
Angle w.r.t. the horizontal: 90°
Size: 1 mm
Development: At most 5 years old
Additional information: -

Location 4
Orientation of the wall w.r.t. the north: 60°
Angle w.r.t. the horizontal: 90°
Size: <1 mm
Development: At most 15 years old
Additional information: -

Location 5
Orientation of the wall w.r.t. the north: -30°
Angle w.r.t. the horizontal: 0°
Size: 1 mm
Development: Unknown
Additional information: Crack at the corner of the ceiling with the wall

Location 6
Orientation of the wall w.r.t. the north: -30°
Angle w.r.t. the horizontal: 80°
Size: <1 mm
Development: Unknown
Additional information: -

Location B1
Orientation of the wall w.r.t. the north: 60°
Angle w.r.t. the horizontal: 40°
Size: 2 mm
Development: Unknown
Additional information: The crack is indicated in red in the picture

A.5   Spoorsingel 99

Figure A.14 shows Spoorsingel 99. The damage survey was conducted on 25-07-2018. The house was built in 1933 [8]. The location of the damage is shown in figure A.15. Pictures and specifications of the damage are shown in the next few pages. The cracks in the walls orthogonal to the parking garage are shown in figure A.16. The age of several cracks is unknown. Several damages have occurred in the last five years. Most damage is found in the back part of the building. The damage at location 5 is most likely caused by large vibrations during demolition of the railway viaduct.

Figure A.14: Spoorsingel 99
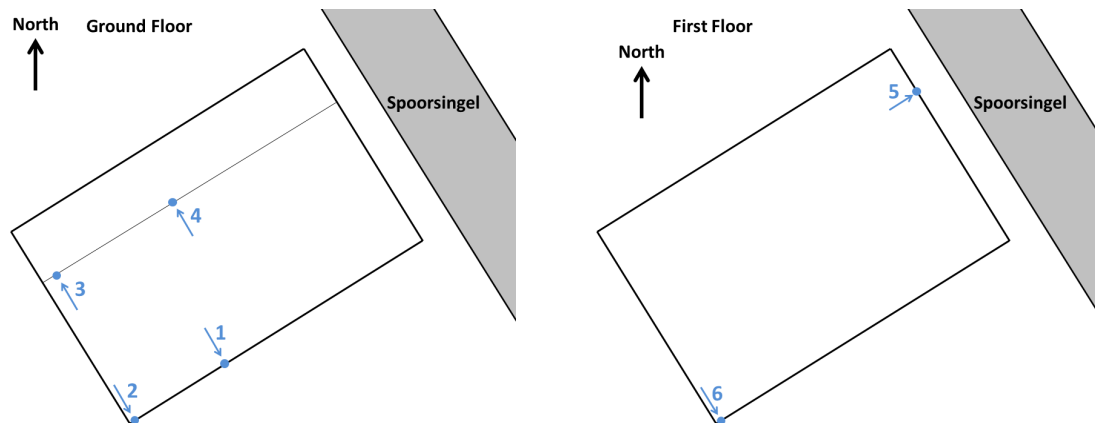
Figure A.15: Location of the observed damage on the ground floor (left) and first floor (right)
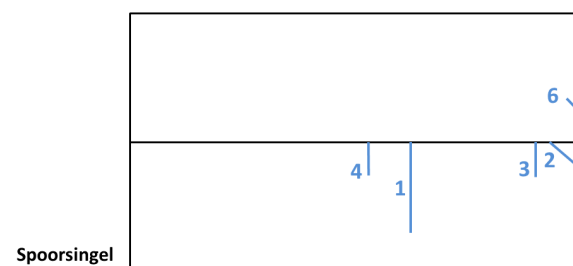
Figure A.16: Indication of cracks in the walls orthogonal to the parking garage

Location 1
Orientation of the wall w.r.t. the north: 60°
Angle w.r.t. the horizontal: 90°
Size: <1 mm
Development: Unknown
Additional information: Crack has
lengthened in the last 5 years.

Location 2
Orientation of the wall w.r.t. the north: 60°
Angle w.r.t. the horizontal: 50°
Size: 2 mm
Development: Unknown
Additional information: Crack has widened
in the last 5 years
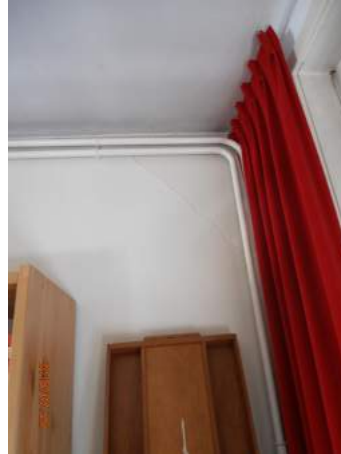
Location 3
Orientation of the wall w.r.t. the north: 60°
Angle w.r.t. the horizontal: 90°
Size: <1 mm
Development: Unknown
Additional information: -

Location 4
Orientation of the wall w.r.t. the north: 60°
Angle w.r.t. the horizontal: 90°
Size: 1 mm
Development: At most 5 years old
Additional information: Crack has widened
in the last 5 years
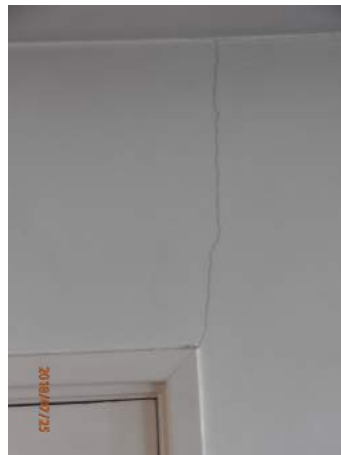
Location 5
Orientation of the wall w.r.t. the north: -30°
Additional information: The curtain rail
and part of the wall broke off on the day
a nearby pillar of the former railway
viaduct was removed (2015). The wall and
the curtain rail have been repaired.

Location 6
Orientation of the wall w.r.t. the north: 60°
Angle w.r.t. the horizontal: 50°
Size: 4 mm
Development: At most 5 years old
Additional information: -